Electrochemical generation-collection sensors for bioanalysis

Parinya Seelanan

A thesis submitted for the degree of Doctor of Philosophy and the Diploma of Imperial College London

Department of Bioengineering
Imperial College London
SW7 2AZ

I hereby declare that the work presented in this thesis is my own under supervision of Dr. Danny O'Hare and Professor Tony Cass. The material herein is original and has not been submitted for a degree or diploma at any other university.

Parinya Seelanan

Abstract

Electrochemical generation-collection devices have potential for application in a wide range of analytical devices, both as free standing sensor systems and as components in analytical systems such as high performance liquid chromatography (HPLC) or flow injection analysis (FIA). The underlying principle is that an electrochemical reaction on one element is used to generate some chemical species which is then transported by diffusion or diffusion and convection to a second electrode where the electrochemical reaction is reversed. The fraction collected is a function of device geometry, operating conditions, any reaction of the generated species in bulk solution and mass transport.

This thesis describes the construction of generation-collection sensors comprising coplanar inlaid microelectrodes of different size and shape: ring-disc and disc-disc in sizes ranging from 10 μm to 100 μm. Fabrication techniques including sputter-coating and embedding of wires were developed and are described.

The sensors were characterised using scanning electron microscopy and their electrochemical characterisation was achieved using reversible outer sphere redox couples including ferrocene derivatives, ruthenium hexaammine (III/II) and ferro/ferricyanide. Experimental data are given for the effects of geometry, size and generator current density, particularly where this would affect the uniformity of the flux. Tests were also undertaken in specially built flow cells to assess their viability for application in FIA and LC detection. Where possible, performance in both the steady state and transient mode were compared with numerical and analytical models.

Three specific bioanalytical applications were investigated and are described: (i) detection of peptides and amino acids using electrochemically generated bromine/ hypobromite (ii) electrochemical biuret detection and (iii) determination of titratable acidity and alkalinity (buffer capacity). Results for (i) showed more complex behaviour with the Pt-Pt dual microelectrode than that has been reported for macroelectrodes under similar system. Voltammetric results are reported. Electrochemical biuret systems showed less improvement in sensitivity with the generation-collection mode to

small peptide molecules. For the buffer capacity sensor, both disc-disc and ring-disc geometries were investigated in a range of sizes 25 to 75 μm for the disc and approximately 1 μm for the ring. A pH sensitive surface was prepared by the deposition of hydrated iridium oxide on gold. Local pH changes were effect by electrolysis of the buffer solution. Experimental works emphasised the importance of controlling the current density to ensure that buffer capacity was not exceeded. An analytical model was of great use in optimising the device. Results are reported for various buffer systems comparing experiments with steady-state theory.

ACKNOWLEDGEMENTS

First of all, I would like to express my gratitude to Dr Danny O'Hare, my thesis supervisor, for his professionalism, guidance, forbearance, motivation and devotion toward my research. My special thanks extends to Professor Tony Cass, my co-supervisor, for his valuable comments. Besides, I wish to thank the Institute of Biomedical Engineering and Department of Bioengineering for all facilities and supports. I am appreciated and thankful for Professor Edmond Magner and Dr Sylvain Ladame for the discussion, comments and contribution on my PhD viva. Moreover, I am much indebted to the Royal Thai Government for the opportunity, funding and help from the start till the end.

I am grateful to all members of the e-Sensors group for their cooperation and helps. Thanks to Dr Severine Harvey, Dr Bhavik A. Patel, Dr Eleni Bitziou, Dr Beinn Muir, Dr Hong Zoua, Dr Arun Arora, Dr Christopher Bell, Professor Peter Knox and Professor Martyn Boutelle for keeping me leveled up in this challenging work. In addition, I would like to thank Dr Yoko Kikuchi, Dr Raphael Toullion, Dr Michelle Roger, Dr Pei Ling Leow, Dr Jin Young Kim, Dr Agnes Cheung and Dr Tempest Van Scheik for the work, trips, laugh, drinks, complaints and funs we have been sharing during my time here. In particular, thanks Dr Monphichar Srisa-art for her care and encouragement, I am truly appreciated. Thanks to members of the Thai society for our memorable activities which usually come in a perfect time after all my long and hard days. My gratitude is also extended to everyone who has contributed a suggestion and support throughout this research. Without each single piece of the puzzle, there will never be an accomplishment for the perfect picture.

I wish to bless and thank Ms Krongrat Trisatayapan, my beloved aunt, for her unconditional love, pray and support through to the end. Finally, I am eternally grateful to my parents and the rest of my family members for their endless love and warmth, the greatest things in my life I have ever had.

Content

Chapter 1: Introduction 9
1. Aim 10
1.1 Bioanalysis 10
1.1.1 Sample Preparation 12
1.1.2 Analyte Concentration 13
1.2 Trends in bioanalytical and biomedical research 13
1.2.1 Biomolecules 14
1.2.2 pH monitoring and its application 15
1.3 Analytical tools and techniques 15
1.4 Electrochemical methods 18
1.4.1 Background and theory 18
1.4.2 Electrode reaction 19
1.4.3 Mass transport 20
1.5 Mode of detection 23
1.5.1 Voltammetry 23
1.5.2 Amperometry 27
1.5.3 Potentiometry 27
1.6 Choices of working electrode 28
1.6.1 Single electrode 28
1.6.2 Dual electrode 31
1.6.3 Multisensor 31
1.7 Application of the generation – collection device 32
1.7.1 Scope of this work 32
Chapter 2: Electrochemical Generation-Collection Devices 36
2. The generator – collector system 37
2.1 Introduction of fabrication methods 37
2.2 Types of sensor 40
2.2.1 Ring – disc electrode 40
2.2.2 Dual disc electrode 44
2.3 Sensor Characterisation 45
2.3.1 Pt/Pt ring-disc electrode characterisation 46
2.3.2 C/C ring – disc electrode characterisation 52

2.3.3 Dual disc electrode characterisation 54
2.4 Generation – Collection Characterisation 57
2.4.1 Pt/Pt ring-disc electrode under generation–collection 57
2.4.2 C/C ring – disc electrode under generation – collection process 64
2.4.3 Dual disc electrode generation–collection experiments 65
2.5 Conclusion 67
Chapter 3: Electrochemical Methods for Biomolecule Detection 70
3. Biomolecule detection 71
3.1 General approaches for amino acid, peptide and protein 71
3.2 Amino acid detection with electrochemical methods 72
3.3 Generation –collection detection 74
3.4 Indirect detection of amino acid 75
3.4.1 Ring – disc titration 75
3.4.2 Mode of titration 76
3.4.3 Sensor fouling 80
3.5 Permanganate titration with generation-collection process 83
3.6 Electrochemical detection of peptides 86
3.6.1 Peptide-biuret complex detection 86
3.6.2 Study of peptide-biuret complex with platinum and carbon electrodes 88
3.6.3 Generation-collection detection of peptide 92
3.7 Conclusion 95
Chapter 4: Measurement of Buffer Capacity using Generation – Collection Sensor 99
4. Measurement of Buffer Capacity using Generation – Collection Sensor 100
4.1 Overview of buffer and buffer capacity 100
4.2 pH in physiological fluid 102
4.2.1 Control of pH in human blood 103
4.2.2 Acidosis 104
4.2.3 Alkalosis 105
4.3 pH measurement using electrochemical based technique 106
4.3.1 Relationship between pH and potential 106
4.3.2 pH sensor 109
4.3.2.1 Glass membrane pH electrode 109
4.3.2.2 ISFET 110
4.3.2.3 Metal oxide electrode 111

4.4 Iridium oxide (IrOx) pH sensor 112
4.4.1 Electrodeposition of IrOx 113
4.4.2 pH sensor calibration 115
4.5 Generation-collection sensor for buffer capacity measurement 117
4.5.1 Titratable acidity sensor 117
4.5.2 Titratable acidity under HEPES buffer 118
4.5.3 Steady state measurement 122
4.5.4 Test with bicarbonate (HCO_3^-) system 123
4.6 Conclusion 126
Chapter 5: Generation-Collection Processes for Dual Electrode System 128
5. Generation – Collection Processes for Dual Electrode System 129
5.1 Overview of Generation-Collection Electrode System 129
5.2 Dual Disc Electrode 133
5.3 Electrode Behaviour of Single Electrode on Inlaid Dual Disc 134
5.4 Generation-Collection Detection on Dual Disc Sensor 138
5.4.1 Constant Current Generation – Passive Collection System 138
5.4.2 Constant Potential Generation – Constant Potential Collection System 143
5.5 Conclusion 149
Chapter 6: Summary and Future Work 154
6. Summary and Future Work 155
- Appendix 158
a. List of Figures 158
b. List of Tables 163

Chapter 1: Introduction

1. Aim

The aim of this work is to develop an electrochemical sensor for bioanalytical and biomedical applications. The fabricated sensor is designed for generation – collection operation and capable of measuring the generated species and/or product of the reaction. Change of biomolecule concentration and pH in biological fluid will be monitored and verified by means of different electrode geometries and modes of detection. The fabricated device can be used as free standing sensor and as part of an analytical system. Applications of the sensor in clinical diagnosis or as an alternative healthcare device are of interest.

1.1 Bioanalysis

Bioanalysis relates to the investigation, identification and quantification of biological substances and their environments. Diseases can be frequently characterized or diagnosed from a change in chemical, biochemical species or metabolism [1]. Biological measurement presents unique challenges and problems due to sample heterogeneity which exists on several length scales, time-varying composition on time scales ranging from sub millisecond to decades, and complexity [2]. In comparison with food, environmental and pharmaceutical research, biological processes are much more complicated. Samples such as blood, urine and other biological fluids contain many compounds or have a complex and active matrix [3]. Some compounds present in a large concentration and the concentrations of some compounds change dynamically, that can effect sensor performance and make the tested results hard to interpret. For example; human blood consists of three main parts, white blood cells, red blood cells and plasma, as shown in figure 1.1. When determining a particular protein in the plasma, other proteins or interferences could lead to an error or false detection. Analysis of specific parts of the blood component offers less heterogeneity and complexity for the measurement.

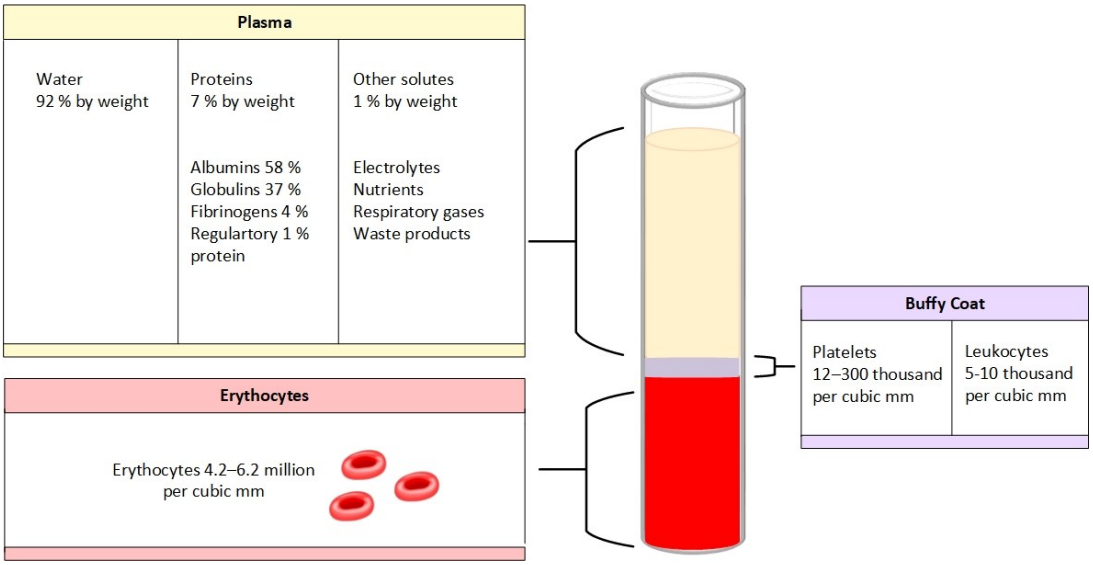

Figure 1.1 A schematic picture of human blood composition, a common biological sample, adapted from Raven PH et al. [4].

Size of sample is another important factor. Unlike environmental research, biological samples such as blood are obviously limited in size and frequency of collection [5]. Determination of the analyte in a small amount of sample increases the need for of high-throughput measurement. In addition, sampling method and duration can directly effect the measurement. For the determination of degradable samples, time of analysis is potentially a source of error. Single time point measurements in extracted samples, such as blood, urine, tissue etc, inevitably lose dynamic information such as time courses, rapid excursions, and typical concentration ranges, i.e. variance or range which are of substantial biological significance. Furthermore, sample preservation, losses during preparation can reduce the value of such measurements unless there is a well-established relationship between the biomeasurement and the disease state, such as diabetes or blood lipid levels. Continuous analysis *in vivo* measurement is the alternative but presents its own significant scientific and engineering challenges. Since the *in vivo* experiment is done in a living organism where biochemical processes are maintained, the understanding of biological mechanism can be accelerated [6]. The best established and most widely used *in vivo* analysis in basic biological studies is the monitoring of neurotransmitters. Normally, the neurotransmitter is released rapidly in a highly localized manner over a subsecond timescale and leads to the excitement or inhibition of a human symptom after synapse [7]. A possible way of understanding a

human disease relies on monitoring within neural tissue. And the capability of *in vivo* measurement is well suited for a study of dynamics of symptom. A number of works on rapid chemical communication have been reviewed [8]. There are both non-invasive and invasive methods which are able to capture a fast chemical signal [9].

Although several approaches can be achieved, real time monitoring of a patient in clinic is even more challenging due to ethical constraints and, from the measurement perspective, optimum instrument configurations can clash with clinical imperatives and can be disturbed by surrounding environment or random interruption such as a physical movement. Long term investigation can be problematic especially when patients are examined using invasive techniques due to fouling and foreign body responses amongst other thing [10, 11]. In this case, *ex situ* measurement, where sample is taken out and tested externally from the living source may be the best option. Urine, saliva, mucus and blood are most common samples taken for *ex situ* test in clinic. One advantage of *ex situ* measurement is it allows sample preparation prior to analysis. A typical example is blood testing, where the blood sample is centrifuged and plasma is analysed instead of blood cells or whole blood, greatly simplifying the matrix and removing significant heterogeneity.

1.1.1 Sample Preparation

In most analytical techniques, sample preparation plays an important role in the whole step of measurement. Many techniques are not responsive to the analyte in its native form and the results are often distorted by interfering species. Sample preparation will maintain the species of interest while decreasing of matrix interference [12, 13]. Methods of sample preparation involve filtering, dilution, dissolution, extraction or reaction with some chemical species. One step or a combination of sample preparation could apply in an analysis. After sample preparation, the analyte can be preconcentrated and the detected signal to noise ratio is thus enhanced. The benefit of preconcentration is particularly crucial in trace analysis.

1.1.2 Analyte Concentration

For each measurement, determination of analyte concentration is principally targeted: motivations include a known relationship between analyte levels and progression of disease, or more fundamental physiological or biochemical investigation. Multiple measurements can provide dynamic information, though sample size or invasiveness may be problematic and there is inevitably a delay between sampling and analytical results, which may militate against clinical usefulness. For bioanalysis, the concentration of chemical compounds such as amino acid, bicarbonate, lactate, etc., in human biological fluids can provide diagnostic information regarding serious illnesses or malfunction [14, 15]. For example, analysis of the amino acid composition can lead to determination of free amino acids in biological sample. Changes in an amino acid profile may occur in many diseases such as genetic defects, improper diet, digestion disorders, liver or kidney disease [16, 17].

1.2 Trends in bioanalytical and biomedical research

A particular biological fluid, such as blood, plays an important role in maintaining human health, comfort and well-being. Its properties provide a clue in recognition of disease states. With a practical and reliable method, diseases can be diagnosed and suitable interventions can begin as early as possible. Clinical diagnosis and biochemical pathology are involved and modelled in biomedical applications. Much bioanalytical research focuses on investigation of biomolecules; for example, DNA, circulating nucleic acids and protein biomarkers that have either a statistical or mechanistic relationship with disease. Direct measurement of disease biomarkers is preferred [18, 19]. Monitoring of blood pressure, tissue perfusion, oxygen, glucose and pH are some of examples which are achieved clinically [3, 6, 14, 15]. The obtained information could indicate the risk of a serious condition to allow enough time for the treatment.

This work, is particularly interested in detection of biomolecules such as amino acids and the measurement of pH and titratable alkalinity. Each application will be briefly reviewed along with an introduction of key experimental techniques, instrumentation and the approaches exploited.

1.2.1 Biomolecules

Biomolecules primarily consist of carbon and hydrogen, along with nitrogen, oxygen, phosphorus and sulfur. Other elements are sometimes incorporated. Groups of interesting biomolecules include amino acids, peptides and proteins. An amino acid is a molecule that contains both a carboxylic and an amine group. Twenty essential amino acids can be categorised by the organic substituent (R) [20], as shown in figure 1.2. Amino acids are the basic structural unit of proteins.

Each amino acid molecule can form a peptide bond, a covalent bonding between nitrogen atoms of an amine group to the carbonyl group of another amino acid. By polymerisation, the amino acid molecules joined with a peptide bond arrange in a linear chain, at least in functional peptides in higher animals, and then create a protein. Consider protein molecules, their three-dimensional function can be different based on different chemical properties of the side chains of the amino acids. The chemical properties for one protein might not be similar to others. Since amino acids are the primary unit of peptides and proteins, the information obtained from amino acid detection can be applied and used for peptide and protein detection further. Moreover, detection of specific proteins; for example, neuropeptides and protein markers, can lead to an information for some diseases [21]. This facilitates confident diagnoses and appropriate medical treatment to the patient; detection of biomolecules therefore necessitates achieving challenging figures of merit.

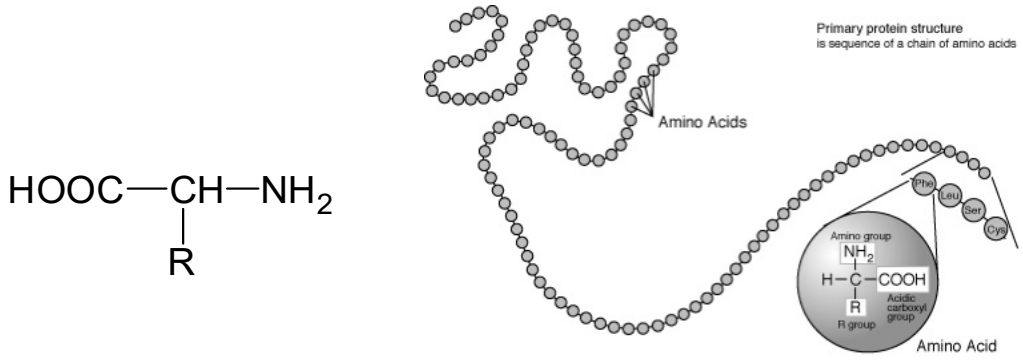

Figure 1.2 Chemical structure of amino acid (left) where R is the substituent group and primary protein structure (right), adapted from [22].

1.2.2 pH monitoring and its application

In most bioanalytical and biomedical measurements, physiological acid-base chemistry is involved and plays important role to human health control. pH monitoring is the basic approach to indicate the change in chemical species related to some pathological symptoms. If the proton (H^+) concentration change occurs in the mechanism of organ failure or disorder, tracing change in pH will be important as one of key in physiological measurements. The most common application is the measuring of blood pH [14]. Both respiratory and metabolic disorders lead to severe health problem and these may be most easily detected from a change in blood pH. In clinical diagnosis, the blood will be taken out from the patient and sent for testing in the lab. The blood pH can be found; however, no clear information of the human resistant to pH change is elucidated. Consider of clinical test, there is a time delay from sample transportation which can lead to an error due to dissolved CO_2 in blood. A precise method of buffer capacity measurement is essential [23]. The idea of determining more meaningful parameter, buffer capacity and real time monitoring is challenging and proposed. More details and approaches will be discussed in Chapter 4.

1.3 Analytical tools and techniques

The methods of analysis are essential to obtain the meaningful data. In each experiment, the observed response is normally accumulated with background signal and targeted molecule. The signal from targeted molecule is generally proportional to its concentration; whereas the background signal comes from the interference of sample and other source such as temperature or sample preparation which can effect to an increase or decrease in the observed response. For a mixture of analytes where a non-selective response to particular compound is achieved, a separation method is required. Separation methods usually combine sample preparation with qualitative and quantitative analysis. The most widely-used method is high performance liquid chromatography (HPLC). Separation is based on differential migration in a flowing medium due to different partitioning between the mobile phase and stationary phase [24]. This is a characteristic property of the analyte and can enable identification by comparison with reference materials or standards. Once the multiple components have been separated and identified by retention time (by comparison with external standards)

or my use of a mass detector on elution, subsequent quantification is possible using conventional detection methods. Chromatography is mainly classified into two types, planar and column chromatography. The latter is the most widely-used technique. Chromatographic methods are categorised based on the nature of mobile phase. For example, liquid chromatography is named of liquid mobile phase. There are also different modes of separation such as ion exchange, size exclusion or affinity that exploit physico-chemical properties of the analyte. These combined techniques have emerged as indispensable and almost universally applicable tools for biochemical analysis [25]. Some of works focus on determination of analyte in a trace amount and complex matrices [25-27]. Not only the successful separation is required for the analysis, a reliable and sensitive detection is also needed. Selection of the appropriate method with optimised conditions can improve the limit of detection of a technique. This enhances the detection sensitivity which is useful for a biological sample in a complicated matrix or with small amount of sampling [28].

Practical methods for the analyte detection can be categorised into a number of analytical measurements. In this Chapter, three categorised and widespread techniques are addressed which are molecular spectroscopy, ion spectroscopy and interfacial method.

- Molecular spectroscopy (UV-Visible and Fluorescence)
- Ion spectroscopy (Mass spectrometry)
- Interfacial method (Electrochemistry)
- Mass spectrometry

Some of the earliest biomolecule measurement involved the use of spectroscopy. For molecular spectroscopy, UV-Visible spectrometry is the most widely used and suitable for analytes that contain a chromophore. Whilst mass detectors are now growing in significance, UV detection was historically important, enabled rapid growth and application of this technology. Significant aspects of HPLC bioassays have been reviewed [29-31].

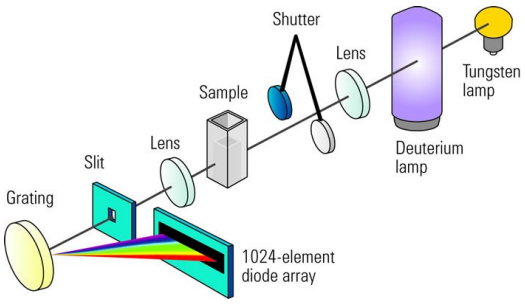

Figure 1.3 A schematic picture of spectrophotometer for UV detection using diode array detector, adapted from [24].

However, the sensitivity of this technique mainly depends on analyte concentration and the cell path length of the detection system, according to Lambert and Beer's law. With a small sample volume or miniaturised devices, UV-Visible spectroscopy can lack sensitivity for trace measurements; background absorption and scattering present serious problems. Fluorescence can usually offer a lower limit of detection. A large number of separation methods for biomolecule in a small device or micro total analysis system were equipped with fluorescence detection [32-34]. Although fluorescence provides sufficient sensitivity for biological samples, derivatisation is normally required for molecules which contain no fluorophore. This leads to a complicated process and could be troublesome for the measurement [35-37] from, e.g. band broadening due to increased dead volume, incomplete reactions or variable kinetics from matrix interference. Plus, fluorescence is costly and not applicable for all molecular systems- not all molecules can be derivatised and mobile phase composition is necessarily restricted [38]. Mass spectrometry is well-known as a powerful method

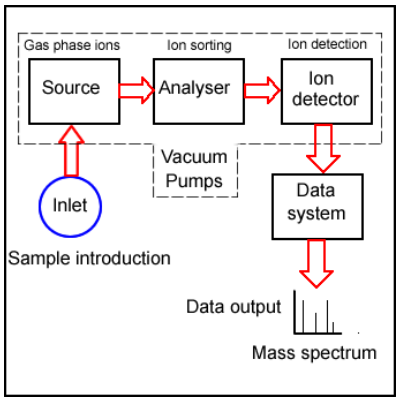

Figure 1.4 A schematic picture of mass spectrometric detection, adapted from [39].

for qualitative analysis and offers excellent sensitivity and is now more broadly applied as new, cheaper technology such as quadrupole or time-of-flight detection has become more widely available and more versatile sample introduction (notably MALDI) have been introduced [40]. Mass spectrometry provides positive identification and trace quantification of biomolecules in a complex mixture. The analyte is analysed and detected depending on a mass to charge ratio. Since the analyte needs to be ionised prior to the detector, a vacuum system is essential. Therefore, it is not practical for real time monitoring and point-of-care use [34].

An alternative method with relatively simple instrumentation, good sensitivity and fast analysis time is electrochemistry. Electrochemical detection is based on the electron transfer between solution and electrode surface from a chemical reaction. Basic aspects of processes at electrified interfaces, microelectrode properties and their application to detection methods will be further discussed.

1.4 Electrochemical methods

1.4.1 Background and theory

Electrochemical methods analyze and exploit current or potential and their relationships which arise from interfacial oxidation or reduction reactions. The current or potential measured during an electrochemical reaction is caused by faradaic and nonfaradaic processes from the change of reactions at the electrode-electrolyte interface [41]. In the faradaic process, current arises from electrolysis of one or more target species. The result of faradaic current contains qualitative and quantitative information about the analyte. For nonfaradaic processes, current arises from the changing ionic population at the electrode-electrolyte interface. The non-faradaic charging currents in dynamic electrochemistry are typically a source of interference (bias). It should be noted that a decrease in the absolute magnitude response and current-voltage relationship may reveal adsorption associated with a fouling of electrode or adsorption of spectator species such as proteins, peptides and thiols which can be presented in biological samples.

1.4.2 Electrode reaction

The reaction mechanism applicable to a simple electrochemical oxidation and reduction is simply written as

$$O + ne^- \rightarrow R \qquad (1.1)$$

where O and R represent as an oxidized and reduced species, respectively, n is the number of electrons (e^-) involved in the reaction. The pathway of a working electrode reaction can be illustrated in Figure 1.5. The reaction rate at the electrode surface can be controlled by any of these coupled steps and include the transport of O and R species to and from the working electrode vicinity and the applied potential through its effects on the electron transfer rate constant. Considering the reduction reaction, the O from bulk solution is transferred to the electrode surface by diffusion, at least for the last part of the journey, where chemical reactions, adsorption and desorption may also be involved prior to or following electron transfer [41].

The current of the electrochemical process is proportional to the rate of reaction and is proportional to the concentration of redox species. The rate of reaction depends on mass transfer, electron transfer, pre- or post-chemical reaction of electron transfer and surface reactions.

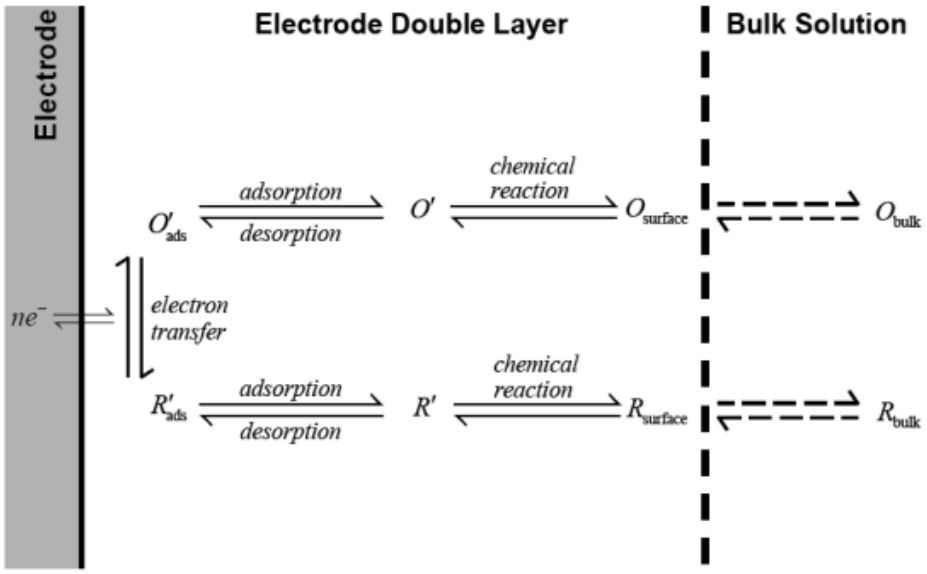

Figure 1.5 A general electrode reaction pathway, adapted from Bard A.J. [41]

1.4.3 Mass transport

Mass transport is categorized into three modes, migration, diffusion and convection. Migration is the movement of charged particles in an electrical potential gradient. Diffusion arises from Brownian motion is the movement and leads to net mass transport in the presence of concentration gradient. Convection is the movement from hydrodynamic transport or stirring and is described by the Navier-Stokes equations. From the Nernst-Planck equation, the mass transfer to the electrode for species *i* in one dimension along x-axis is expressed as

$$J_i(x) = -D_i \frac{\partial C_i(x)}{\partial x} - \frac{z_i F}{RT} D_i C_i \frac{\partial \phi(x)}{\partial x} + C_i v(x) \qquad (1.2)$$

where $J_i(x)$ is the flux of species *i* (mol s^{-1} cm^{-2}) at distance x from the surface, D_i is the diffusion coefficient (cm^2 s^{-1}), $\partial C_i(x)/\partial x$ is the concentration gradient at distance *x*, $\partial \phi(x)/\partial x$ is the potential gradient, z_i is the charge of species *i*, C_i is the concentration of species *i* (mol cm^{-3}), $v(x)$ is the velocity (cm s^{-1}). Diffusion and migration result from a gradient in electrochemical potential ($\bar{\mu}$, the partial molar free energy of charges species) while convection results from an imbalance of forces on the solution. Consider two points in the solution for a certain species (i), the difference of $\bar{\mu}_i$ between two points can arise over a distance due to difference of concentration or ϕ of species *i*. The flux of species *i* then occur and is proportional to the gradient of $\bar{\mu}_i$, expressed by

$$J_i \ \alpha \ \nabla \bar{\mu}_i \qquad (1.3)$$

where ∇ is called grad and is a vector operator. The gradient operator in three-dimensional Cartesian space is

$$\nabla = i\frac{\partial}{\partial x} + j\frac{\partial}{\partial y} + k\frac{\partial}{\partial z} \qquad (1.4)$$

For linear mass transfer in one dimension, equation 1.3 then becomes

$$J_i = -\left(\frac{C_i D_i}{RT}\right)\frac{\partial \overline{\mu}_i}{\partial x} \tag{1.5}$$

Therefore, the Nernst-Planck equation can be written in general as

$$J_i = -D_i \nabla C_i - \frac{z_i F}{RT} D_i C_i \nabla \phi + C_i v \tag{1.6}$$

The flux is determined by diffusion and migration of the species and changes at different positions in a solution at a given time. In general, the electroactive species will be transported by both diffusion and migration at the electrode surface.

Diffusion

Diffusion occurs with a random-walk process of one species in the solution. When one molecule moves, the probability distribution for one-dimension over the time (t) of the molecule can be estimated by the root-mean-square displacement, $\overline{\Delta}$, expressed as

$$\overline{\Delta} = \sqrt{2Dt} \tag{1.7}$$

where D is the diffusion coefficient. From equation 1.7, the diffusion velocity (v_d) can be defined as

$$v_d = \frac{\overline{\Delta}}{t} \tag{1.8}$$

For two- and three-dimensional random walks, $\overline{\Delta}$ can be treated as $(4Dt)^{1/2}$ and $(6Dt)^{1/2}$, respectively.

Fick's Laws of diffusion

To describe the flux of species and its concentration as a function of time and position, Fick's laws are generally used. In one-dimensional diffusion of O species, for example, the flux of O at a given location and time is proportional to the concentration gradient. Fick's first law can be expressed as

$$-J_O(x,t) = D_O \frac{\partial C_O(x,t)}{\partial x} \tag{1.9}$$

And Fick's second law is relevant to the change in concentration (C_O) with time for constant D_O, as shown in equation 1.10.

$$\frac{\partial C_O(x,t)}{\partial t} = D_O\left(\frac{\partial^2 C_O(x,t)}{\partial x^2}\right) \tag{1.10}$$

This $C_O(x,t)$ expresses concentration profiles. For any geometry, the general equation of Fick's second law becomes

$$\frac{\partial C_O}{\partial t} = D_O \nabla^2 C_O \tag{1.11}$$

where ∇^2 is the Laplacian operator. Table 1.1 shows the forms of ∇^2 for different type of electrode geometry.

Table 1.1 The ∇^2 forms for different types of electrode geometry, obtained from Bard A. J. [41]

Type	Variables	∇^2
Linear	x	$\partial^2/\partial x^2$
Spherical	r	$\partial^2/\partial r^2 + (2/r)(\partial/\partial r)$
Cylindrical	r	$\partial^2/\partial r^2 + (1/r)(\partial/\partial r)$
Disc	r, z	$\partial^2/\partial r^2 + (1/r)(\partial/\partial r) + \partial^2/\partial z^2$
Band	x, z	$\partial^2/\partial x^2 + \partial^2/\partial z^2$

Consider equation 1.1, the current obtained from the transport of *O* to the electrode with only diffusion is related to the flux of *O*, $J_O(0,t)$, at the electrode surface (x=0), given by:

$$-J_O(0,t) = \frac{i}{nFA} = D_O\left[\frac{\partial C_O(x,t)}{\partial x}\right]_{x=0} \qquad (1.12)$$

It should be noted from equation 1.12 that the total electrons transferred to the electrode must be proportional to the quantity of *O* reaching the electrode in a unit time. This highlights the relation between the changes in concentration profile near the electrode and the current flowing in an electrochemical system. In case of several electrochemical species present in the solution, the current can be assumed as the summation of their fluxes to electrode surface.

1.5 Mode of detection

In this work, three electrochemical methods will be discussed: potentiometry amperometry, and voltammetry. Potentiometry is used for measuring the potential related to concentration of electroactive species. Voltammetric methods are based on current measurement as a function of applied potential. Techniques used in voltammetry include linear sweep voltammetry (LSV), cyclic voltammetry (CV) and pulse voltammetry. Consider CV technique, the applied potential is a reversible linear scan while current is monitored. In the amperometry, the current detected is proportional to the amount of analyte generating the current. More details on electrode reactions involved in these methods will be discussed in next topic.

1.5.1 Voltammetry

The measurement of current as a function of the applied voltage can provide remarkable information of the interested reaction. The simplest approach to the measurement of current-voltage relationship involves the use of two electrodes, working and reference electrode [42]. The reaction of interest occurs at the working electrode (WE), whereas a stable and fixed potential is provided at the reference electrode (RE). When voltage (*E*) is applied, the drop in potential between WE and solution, $\phi_{\mathrm{WE}} - \phi_{\mathrm{S}}$, is defined which is the driving force for electrolysis at electrode surface. For larger electrode

surface, the E can split into 3 terms, i) $\phi_{WE} - \phi_S$, ii) voltage drop in solution (iR), iii) potential drop at RE/solution interface ($\phi_S - \phi_{RE}$), expressed as

$$E = (\phi_{WE} - \phi_S) + iR + (\phi_S - \phi_{RE}) \quad (1.13)$$

For microelectrode, iR drop can typically be neglected, since the current is small ($<10^{-7}$ A) and the usual electrolytes and cell geometries lead to a resistance of the order of ohms and thus an ohmic drop of significantly less than a microvolt. Since $\phi_S - \phi_{RE}$ is fixed by chemical composition of the RE, change in applied E is directly reflect in driving force. In general, a three electrodes system is set where an electrode with large surface area is called counter electrode [42]. Using a controlled electronic source, the current will flow only between counter and working electrode. No current passes through RE, and therefore no electrolysis occurs at the RE which maintains the chemical composition of RE and thus the $\phi_S - \phi_{RE}$ term.

Linear sweep voltammetry

Consider the reaction which undergoes with 1 electron transfer (n=1), the voltammetric behaviour is related with electrode kinetics, shown below

$$O(aq) + e^-(at\ WE) \xrightarrow{k} R(aq) \quad (1.14)$$

where k represents as the electrochemical rate constant. The mass transport of O to electrode surface can be expressed using equation

$$\frac{\partial[O]}{\partial t} = D_O \frac{\partial^2[O]}{\partial x^2} \quad (1.15)$$

When applied E is performed in a function of time, the current-voltage curve can be predicted as shown in Figure 1.6. The potential is swept from where no reaction occurs (E_1) to where electron transfer is driven and limited by mass transport (E_2). In the beginning, no current is passing because the applied E is not great enough to drive the

electron transfer. When more negative potential is swept, the reduction of *O* occurs as the *k* becomes greater which gives the rise of current. Current will reach the maximum value and become steady (for microelectrode) or start to fall off, where semi-infinite linear diffusion is a reasonable model. In case of Figure 1.6, the maximum current in the curve is defined as the peak current, i_p, controlled by the electrode kinetics and the mass transport properties. For any system, i_p is directly proportional to the concentration of *O* and also increases with the potential scan rate.

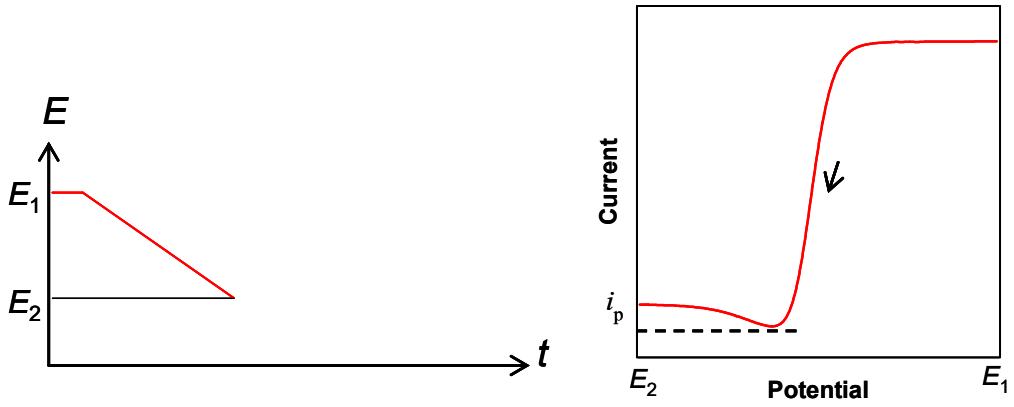

Figure 1.6 Potential waveform and cyclic voltammogram, where E_1 is initial potential, E_2 is final potential and i_p peak current, adapted from Fisher A. C. [42]

Cyclic voltammetry

Cyclic voltammetry (CV) is the most common technique used in various applications with the benefits about information of complicated electrode reaction. CV is an extension of the linear sweep method with reversal scan of voltage after reaching the maximum current [42]. Consider a reversible redox reaction, the potential scan profile and typical voltammogram can be presented in Figure 1.7. The peak potential (E_p) and the peak size of reversed scan can reflect both the thermodynamic and chemical reversibility of the reaction. In practical, the formal potential (E^0) of the redox couple can be approximated from

$$E^0 = \frac{E_p^{red} + E_p^{ox}}{2} \qquad (1.16)$$

where E_p^{red} and E_p^{ox} are the peak potentials of reduction and oxidation reactions, respectively, provided the diffusion coefficients of the reduced and oxidized species do not differ, and the reaction is thermodynamically reversible (the heterogeneous rate constant is effectively infinite). Unlike the $E_{p,}$ the absolute peak currents for both forward and reward scans depend on the voltage sweep rate (v). With Fick's second law of diffusion, the peak current (i_p) is described by the Randles-Sevcik equation,

$$i_p = 2.69 \times 10^5 n^{3/2} D^{1/2} C_{bulk} A v^{1/2} \qquad \text{at } 25°C \qquad (1.17)$$

where A in m^2, D in $m^2\ s^{-1}$, C_{bulk} in mol m^{-3} and v in V s^{-1}. A reversible process distributes information for both qualitative and quantitative analysis. CV can also provide more information on rates of electron transfer or reaction mechanism of different situations. Using of CV technique in the analysis of analyte will be discussed later in the context of the experimental results.

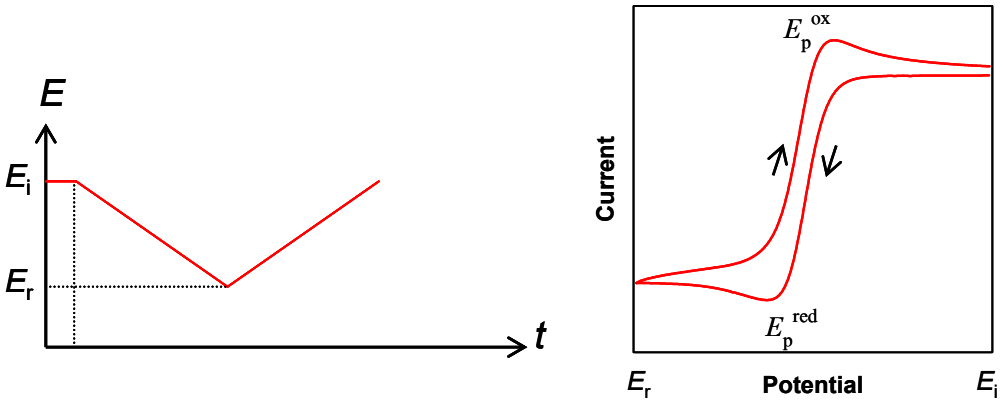

Figure 1.7 Potential waveform and cyclic voltammogram, where E_i is initial potential, E_r is reversible potential, E_p^{red} and E_p^{ox} are the peak potentials of reduction and oxidation reactions, adapted from Fisher A. C. [42]

1.5.2 Amperometry

Amperometry is used for current measurement and current monitoring including in clinical and biomedical applications. This technique is widely used for electrochemical sensor or biosensor for both flow and non-flow system. In this technique, a constant potential is applied which is enough to drive the electrochemical reaction at rates limited by mass transport [43]. The applied potential is normally obtained from current-voltage curve during initial scoping experiments. In quantitative analysis, the observed current is proportional to analyte concentrations.

1.5.3 Potentiometry

Potentiometry is based on thermodynamic relationships of electrochemical species, in particular with the Nernst equation [43]. Consider reduction reaction in Eq. 1.18, the Nernst equation represents the potential (E) established at the electrode under reaction equilibrium, expressed by

$$E = E^0 - \frac{RT}{nF} \ln \frac{[R]}{[O]} \tag{1.18}$$

where E^0 is standard potential, R is the gas constant, F is Faraday's constant, n is electron number and T is temperature. Although the reaction of electrochemical cell always involves two redox half reactions, it is more convenient to show only as a reduction. The potential in Eq. 1.18 is known as half-cell potential and related to the concentrations (strictly the activity) of redox species. To perform the measurement, the system contains a working electrode capable of monitoring the interested species, and a reference electrode providing constant and known half-cell potential that working electrode potential can refer to. Though the measurement is based on the redox couple in the system, the method can be applied to precipitation, ion complexation and acid-base processes. This can be achieved when either the oxidised or reduced conjugate of interested species is known and maintained at the electrode. In our work, potentiometry is used for pH detection in Chapter 4 using the pH-dependent redox equilibrium of hydrated oxide films of Ir(III)/ Ir(IV).

1.6 Choices of working electrode

The working electrode (WE) serves as a transducer responding to the excitation signal and the concentration of the investigated analyte in the solution. Current measured from WE is not only due to electrolysis of the redox species of interest (faradaic current), but also from some other sources of noises such as redox reactions of interfering species, adsorption or desorption and non-faradaic charging currents. The optimal WE choice depends on many factors such as applied potential range, stability in working condition, kinetics of electron transfer reaction. For industrial scale, macroelectrode or large metal rod for one reactor would be suitable to use. Again, when the biomedical application or *in vivo* experiments are concerned, a microelectrode is more applicable and of interest where reduced size and current limit the analyte consumption (and hence chemical perturbation of the system) and the small size (typically sub millimeter in the finished device) reduces tissue damage and occlusion of capillaries. Microelectrode properties are briefly discussed and types of sensor used in our work will be highlighted in the following sections.

Microelectrodes

A microelectrode is an electrochemical sensor which is fabricated to have a very small surface area [44]. It can be made with a carbon fibre or a metal wire (diameter 5 to 50 μm) connected to a conductive wire and embedded in an epoxy or a glass tube. The microelectrode dimension can be the diameter of a disc electrode or the thickness of a band or a ring electrode. Microelectrodes have unique properties and are different from macroelectrodes in terms of early transient and steady-state regimes. As the electrode radius becomes smaller, the cell time constant and the Ohmic (iR) drop decrease for early transient experiments [44, 45]. In steady-state experiments, mass transport enhancement occurs and the iR drop decreases. Another advantage associated with microelectrodes is due to the edge effect, where there is a larger ratio of faradaic current to the double layer charging current than there is in macroelectrodes, since for the convergent diffusion fields associated with microelectrodes, the faradaic current scales with linear dimension and the capacitive current scales with area. The current ranges from microampere (μA) to picoampere (pA) is usually found. Therefore, an extra sensitive current measurement instrument with low noise is required. In addition,

polishing and manipulation of the microelectrode are essential. Work with microelectrodes is mainly focused on disc geometry because it is well-characterised, easy to fabricate and commercially available. However, ring microelectrodes have the benefit of mass transport improvement, reduced capacitance and high current density which is useful to improve signal to noise ratio. Both disc and ring electrodes are chosen for electrochemical generation – collection device where their characters will be further discussed.

1.6.1 Single electrode

The disc microelectrode

In the vicinity of an electrode, one factor determining the electrode behaviour is mass transport. Consider a disc microelectrode; the three-dimensional diffusion with hemispherical mode is applied for mass transport whereas the semi-infinite planar diffusion occurs when using a macroelectrode [45]. From Figure 1.8, the slow scan quasi-steady cyclic voltammogram shows the value for the steady state current given by

$$i_{\text{disc}} = 4nFC_{\text{bulk}}Dr \qquad (1.19)$$

where n is the number of electron transferred in the reaction, D is the diffusion coefficient for the analyte and r is the electrode radius [41]. For a relatively low scan rate, a microelectrode exhibits a steady-state current shown in Figure 1.8. It should be noted that nonsteady-state regime becomes dominant when fast scan rate is carried out, resulting in the current response resembling in that of a macroelectrode. The important and defining scaling here is the relative magnitude of the diffusional length scale, $((2Dt)^{1/2})$ and the characteristic length scale of the microelectrode, in this case the radius.

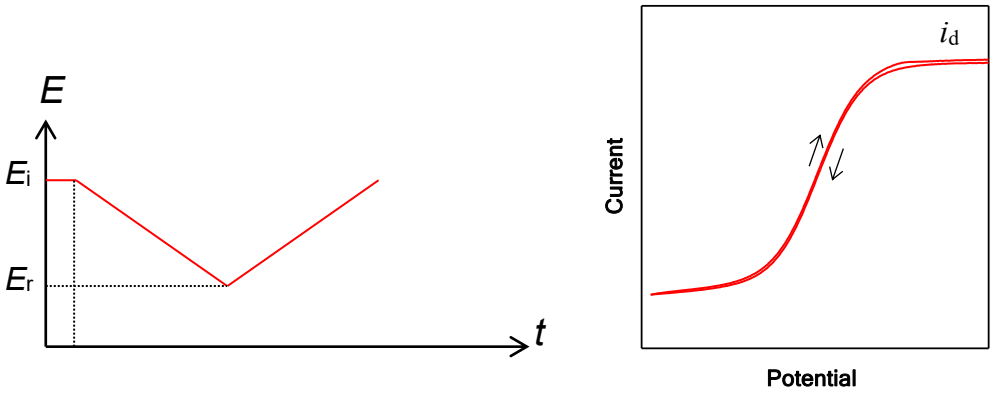

Figure 1.8 Potential waveform and current – voltage curve, where E_i is initial potential, E_r is reversible potential and i_d limited current, adapted from Zoski C. G. [45]

The ring microelectrode

The ring microelectrode has an attractive mass transport property related to surface area and thickness of the ring. The increase of current effected from inner and outer edge produces a high current density which can improve detection limits and allow the probing of reactions with fast kinetics. In the steady state diffusion-limited regime, the bulk of the flux occurs at the edges, so the value of the steady state current is similar to a disc of the same radius, but since the overall area is much reduced, the charging current is much smaller. Most of the time, ring microelectrodes have been manufactured using painting methods, deposition, evaporation or sputtered deposition of a metal layer, particularly from gold or platinum, onto a solid support such as a glass capillary or optical fibre [45, 46]. The methods of ring electrode fabrication will be briefly discussed in Chapter 2. Much work on the theory of diffusion controlled steady-state current at ring microelectrode has been published [47]. Theoretical steady-state current (i_{ring}) considered for thin ring electrode where the ratio of outer radii (b) to inner radii (a) is less than 1.1 can be calculated by

$$i_{ring} = nFC_{bulk}D\frac{\pi^2(a+b)}{\ln[16(b+a)/(b-a)]} \qquad (1.20)$$

where an infinite thickness of insulator is assumed [46].

1.6.2 Dual electrode

Dual electrode systems are mainly used for generation – collection process and have recently been reviewed by Compton's group [48]. Both electrodes can be fabricated in similar or different geometry. Similar electrode systems such as disc-disc, band-band and wire-wire configuration has been reported and mainly used with flow-based systems. For a system with different geometry, ring-disc electrode is the most popular configuration. It has also been widely used in electrochemical titration, dual analytes detection, end-column detection in flowing systems, and the study of reaction kinetics and hydrodynamic effects [43, 49]. The main benefits of the ring-disc electrode over other dual electrodes are the radial symmetry and the different shape of the two electrodes. These advantages allow the ring-disc sensor to operate with no preferred axis in the experiment and achieve different types of measurement due to the significant difference in the edge to area ratio between the disc and the ring. Moreover, with a relatively small size of microelectrode, a ring-disc sensor can be assembled as a small probe which is suitable for *in vivo* measurement.

1.6.3 Multisensor

Multisensors has become popular due to the ability to either provide real-time spatial variation in a single analyte or contemporaneous measurements of multiple analytes. Arrays of sensor from screen printed electrode or lithography are widely used. Each electrode can be modified to be a selective sensor or biosensor which allows simultaneous multi-detection of interested analytes. Sensor arrays can also be used to increase the sensitivity when overall signal is accumulated from each electrode. This gives an advantage especially when one electrode is fouled or malfunction and can extend the lifetime of an implanted device since not all sensors will fail at the same time in the same way- the array provides redundancy [50, 51].

1.7 Application of the generation – collection device

Much work on generation – collection sensor is focused on the post-electron transfer chemical reactions, typically occurring in the homogeneous phase. In particular, the ring-disc electrode was originally used for the study of unstable intermediates in electrode reactions [52]. The benefits of ring-disc electrode are inspiring and suited to a portable sensor which can be used for detection and monitoring of physiological substances, provided that suitable miniaturization is achieved. The dual disc sensor is also a useful geometry and good model of generation and collection process. The study of dual disc generation and collection under electrochemical reaction could lead to a better performance of sensor array.

1.7.1 Scope of this work

The generation – collection sensor will be developed for biomolecule detection, buffer capacity measurement and dual detection processes and compared with theoretical models. Current works are categorised in each chapter, detailed as

- In Chapter 2, fabrication methods of disc, ring and dual sensor are discussed. Sensor characterization is described in both flow and no flow system, supported by theoretical models of previous work of our group [53].
- Chapter 3 presents work on biomolecule detection, mainly focused on amino acids, peptide and proteins. The ring-disc sensor is used under the basic method of detection. Results and discussion are discussed.
- The development of a sensor for the measurement of buffer capacity using a ring-disc sensor configuration is described in Chapter 4. This includes work on a potentiometric metal oxide pH sensor fabrication and theoretical considerations for the experiment.
- The study of generation and collection using dual disc experiments is further investigated in Chapter 5. Numerical models have been introduced, tested and used to guide experimentation.
- Chapter 6 is the summary of what have been achieved so far. Principal achievements and limitations are highlighted, and experimental next steps are proposed.

References

1. Mathews CK, van Holde KE, Ahern KG: **Biochemistry**, 3rd edn: Benjamin Cummings; 2000.
2. Kirk PL, Duggan EL: **Biochemical Analysis**. *Analytical Chemistry* 1952, **24**(1):124-131.
3. Gaw A (ed.): **Clinical biochemistry : an illustrated colour text**, 4th edn. Edinburgh: Churchill Livingstone; 2008.
4. Raven PH, Johnson GB, Losos J, Singer S: **Biology**, 7th edn: McGraw-Hill Education; 2005.
5. Nicoll D, McPhee SJ, Pignone M: **Pocket guide to diagnostic tests** 4th edn. New York: McGraw-Hill; 2003.
6. Billingham MS, Wheeler MJ, Hall RA: **Biochemical function tests : a guide to specialised investigations in chemical pathology**. Oxford: Blackwell Scientific; 1987.
7. Kelly RB: **Biochemistry of neurotransmitter release**. *Annual Review of Neuroscience* 1979, **2**(1):399.
8. Robinson DL, Hermans A, Seipel AT, Wightman RM: **Monitoring rapid chemical communication in the brain**. *Chemical Reviews* 2008, **108**(7):2554-2584.
9. Garris PA: **Advancing neurochemical monitoring**. *Nature Methods* 2010, **7**(2):106-108.
10. Frost MC, Rudich SM, Zhang H, Maraschio MA, Meyerhoff ME: **In Vivo Biocompatibility and Analytical Performance of Intravascular Amperometric Oxygen Sensors Prepared with Improved Nitric Oxide-Releasing Silicone Rubber Coating**. *Analytical Chemistry* 2002, **74**(23):5942-5947.
11. Soto RJ, Privett BJ, Schoenfisch MH: **In Vivo Analytical Performance of Nitric Oxide-Releasing Glucose Biosensors**. *Analytical Chemistry* 2014, **86**(14):7141-7149.
12. Chen Y, Guo Z, Wang X, Qiu C: **Sample preparation**. *Journal of Chromatography A* 2008, **1184**(1-2):191-219.
13. Kole PL, Venkatesh G, Kotecha J, Sheshala R: **Recent advances in sample preparation techniques for effective bioanalytical methods**. *Biomedical Chromatography* 2010, **25**(1-2):199-217.
14. Kellum JA: **Determinants of blood pH in health and disease**. *Critical Care* 2000, **4**(1):6-14.
15. Jia W, Bandodkar AJ, Valdés-Ramírez G, Windmiller JR, Yang Z, Ramírez J, Chan G, Wang J: **Electrochemical Tattoo Biosensors for Real-Time Noninvasive Lactate Monitoring in Human Perspiration**. *Analytical Chemistry* 2013, **85**(14):6553-6560.
16. Zhao C, Zhang JC, Song JF: **Determination of L-cysteine in amino acid mixture and human urine by flow-injection analysis with a biamperometric detector**. *Analytical Biochemistry* 2001, **297**(2):170-176.
17. Herzog G, Arrigan DWM: **Electrochemical strategies for the label-free detection of amino acids, peptides and proteins**. *Analyst* 2007, **132**(7):615-632.
18. Naylor S: **Biomarkers: current perspectives and future prospects**. *Expert Review of Molecular Diagnostics* 2003, **3**(5):525-529.
19. Mayeux R: **Biomarkers: Potential Uses and Limitations**. *NeuroRx* 2004, **1**(2):182-188.
20. Barrett GC: **Chemistry and biochemistry of the amino acids**. London: Chapman and Hall; 1985.

21. Schrohl A-S, Wurtz S, Kohn E, Banks RE, Nielsen HJ, Sweep FCGJ, Brunner N: **Banking of Biological Fluids for Studies of Disease-associated Protein Biomarkers**. *Molecular & Cellular Proteomics* 2008, **7**(10):2061-2066.
22. David. H, Nigel. H: **Biochemistry**, 4th edn. New York ; London: Garland Science; 2011.
23. Gandhi SI: **Lab-on-a-chip device to quantify buffer capacity of blood**. In: *Bioengineering.* vol. PhD thesis: Imperial College London; 2015.
24. A. SD, M. WD, James. HF: **Analytical chemistry : an introduction**, 7th edn. Fort Worth ; London: Saunders College; 2000.
25. Anderson DJ: **High performance liquid chromatography in clinical analysis**. *Analytical Chemistry* 1999, **71**(12):314R-327R.
26. Schoneich C, Huhmer AFR, Rabel SR, Stobaugh JF, Jois SDS, Larive CK, Siahaan TJ, Squier TC, Bigelow DJ, Williams TD: **Separation and analysis of peptides and proteins**. *Analytical Chemistry* 1995, **67**(12):R155-R181.
27. Larive CK, Lunte SM, Zhong M, Perkins MD, Wilson GS, Gokulrangan G, Williams T, Afroz F, Schoneich C, Derrick TS *et al*: **Separation and analysis of peptides and proteins**. *Analytical Chemistry* 1999, **71**(12):389R-423R.
28. Lindsay AE, Greenbaum AR, O'Hare D: **Analytical techniques for cyanide in blood and published blood cyanide concentrations from healthy subjects and fire victims**. *Analytica Chimica Acta* 2004, **511**(2):185-195.
29. Sandberg M, Weber SG: **Techniques for neuropeptide determination**. *Trac-Trends in Analytical Chemistry* 2003, **22**(9):522-527.
30. Chen JG, Logman M, Weber SG: **Effect of peptide primary sequence on biuret complex formation and properties**. *Electroanalysis* 1999, **11**(5):331-336.
31. Shi F, Woltman SJ, Weber SG: **Kinetics of the post-column complexation reaction of Cu(II) with N-formylmethionyl chemoattractant and chemotactic peptides**. *Analytica Chimica Acta* 2002, **474**(1-2):1-9.
32. Khandurina J, Guttman A: **Bioanalysis in microfluidic devices**. *Journal of Chromatography A* 2002, **943**(2):159-183.
33. Banks PR: **Fluorescent derivatization for low concentration protein analysis by capillary electrophoresis**. *Trac-Trends in Analytical Chemistry* 1998, **17**(10):612-622.
34. Huikko K, Kostiainen R, Kotiaho T: **Introduction to micro-analytical systems: bioanalytical and pharmaceutical applications**. *Eur J Pharm Sci* 2003, **20**(2):149-171.
35. Boppana VK, MillerStein C: **High-performance liquid chromatographic determination of peptide drugs in biological fluids by means of pre- and post-column fluorescence derivatization techniques**. *Analytica Chimica Acta* 1997, **352**(1-3):61-69.
36. Lindroth P, Mopper K: **High-performance liquid chromatographic determination of subpicomole amounts of amino acids by precolumn fluorescence derivatization with ortho-phthaldialdehyde**. *Analytical Chemistry* 1979, **51**(11):1667-1674.
37. Krull IS, Strong R, Sosic Z, Cho BY, Beale SC, Wang CC, Cohen S: **Labeling reactions applicable to chromatography and electrophoresis of minute amounts of proteins**. *J Chromatogr B* 1997, **699**(1-2):173-208.
38. Jakeway SC, de Mello AJ, Russell EL: **Miniaturized total analysis systems for biological analysis**. *Fresenius J Anal Chem* 2000, **366**(6-7):525-539.
39. A. SD, James. HF, R. CS: **Principles of instrumental analysis**, 6th edn. Pacific Grove, Calif. : Brooks/Cole ; London: Thomson Learning; 2007.

40. Beavis RC, Chait BT: **Rapid, sensitive analysis of protein mixtures by mass spectrometry**. *Proceedings of the National Academy of Sciences of the United States of America* 1990, **87**(17):6873-6877.
41. Bard AJ, Faulkner LR: **Electrochemical Methods: Fundamentals and Applications**, 2nd edn. New York; Chichester Wiley; 2000.
42. Fisher AC: **Electrode dynamics**. Oxford: Oxford University Press; 1996.
43. Sawyer DT, Sobkowiak A, Roberts JL: **Electrochemistry for chemists**, 2nd edn. New York: Wiley; 1995.
44. Bond AM: **Past, present, and future contributations of microelectrodes to analytical studies employing voltammetric detection - A review**. *Analyst* 1994, **119**(11):R1-R21.
45. Zoski CG: **Ultramicroelectrodes: Design, fabrication, and characterization**. *Electroanalysis* 2002, **14**(15-16):1041-1051.
46. Bitziou E, Rudd NC, Unwin PR: **Microjet ring electrode (MJRE): Development, modelling and experimental characterisation**. *Journal of Electroanalytical Chemistry* 2007, **602**(2):263-274.
47. Bell CG, Seelanan P, O'Hare D: **Microelectrode generator-collector systems for electrolytic titration: theoretical and practical considerations**. *Analyst* 2017, **142**(21):4048-4057.
48. Barnes EO, Lewis GE, Dale SE, Marken F, Compton RG: **Generator-collector double electrode systems: a review**. *Analyst* 2012, **137**(5):1068-1081.
49. Pletcher D: **A first course in electrode processes**. Romsey: Electrochemical Consultancy; 1991.
50. Menshykau D, O'Mahony AM, Javier del Campo F, Munz FX, Compton RG: **Microarrays of Ring-Recessed Disk Electrodes in Transient Generator-Collector Mode: Theory and Experiment**. *Analytical Chemistry* 2009, **81**(22):9372.
51. Niwa O, Morita M: **Carbon film-based interdigitated ring array electrodes as detectors in radial flow cells**. *Analytical Chemistry* 1996, **68**(2):355-359.
52. Frumkin A, Nekrasov L, Levich B, Ivanov J: **Die anwendung der rotierenden scheibenelektrode mit einem ringe zur untersuchung von zwischenprodukten elektrochemischer reaktionen**. *Journal of Electroanalytical Chemistry* 1959, **1**(1):84-90.
53. Harvey SLR, Parker KH, O'Hare D: **Theoretical evaluation of the collection efficiency at ring-disc microelectrodes**. *Journal of Electroanalytical Chemistry* 2007, **610**(2):122-130.

Chapter 2:

Electrochemical Generation–Collection Devices

2. The generator – collector system

An electrochemical generation–collection sensor is comprised of two working electrodes with reciprocal or coupled electrochemical reactions. In this work, a dual sensor with different geometry was assembled using ring and disc electrodes. The dual disc sensor is also of interest for the working electrodes with similar geometry applied to our analysis. Methods of fabrication will be briefly reviewed. The practical methods used for each sensor are described and evaluated. Selected methods for fabrication of our ring-disc sensor are discussed.

2.1 Introduction of fabrication methods

The ring-disc electrode is generally used for study of reaction mechanism which is related to redox species in electrochemical processes [1]. The ring-disc electrode is available commercially in macro size, typically 4-7 mm disc diameter, for operation under controlled hydrodynamic conditions such as the widely-use rotating ring disc electrode, the wall-jet flow-through electrode and titration sensors. However, a commercial ring–disc microelectrode has not been reported to date. In this work, a small sensor suitable for application in biomedical experiments is of interest. For *in vivo* application in humans this would restrict the maximum dimension to around 0.7 mm, around the dimension of a 21G hypodermic needle.

A general approach to the fabrication of ring-disc devices uses a single insulated wire metal to which is applied an extra band of ring surface concentric with the longitudinal axis of the wire. Methods for controlling space, thickness and uniformity for the ring are required. For a disc made from commercial metal wire, fabrication of the ring electrode is the most challenging aspect and the principal focus here. Practical methods of ring fabrication include lithography, physical vapour deposition (PVD) and chemical vapour deposition (CVD). Each method will be briefly described and the final fabrication process used for our ring – disc fabrication is elaborated.

Lithography

Lithography was originally developed as a printing technology with simple chemical processes to create an image on the surface of interest. Photolithography is a microfabrication technique which is applied to make integrated circuits and microelectromechanical systems [2]. With photolithography, a photo mask with desired geometric pattern is transferred to a light-sensitive chemical photoresist on the substrate. It should be noted that there are two modes of photoresist called positive or negative resist. After a series of chemical treatments, the desired pattern will be engraved or deposited on the substrate material. Photolithography for fabrication of carbon ring electrodes has been reported [3-5]. The ring – disc electrode can be well fabricated and introduced to generation – collection application. However, in conventional lithographic processing, one or more of the common issue will be electrodes recessed or protruding which will dramatically affect the local diffusional mass transport [6, 7]. Unless the complex process of using vias between backside connections and the working electrodes (which presents major alignment problems and at least two additional process steps), the essential 2-D nature of photolithographic patterning inevitably results in incomplete or non-continuous ring electrodes to enable passage of the disc electrode hook-up or connector [4]. This will affect the current density at the electrode; depending on the precise dimensions, such a ring could behave more like a band electrode. This is not ideal for evaluating the validity or experimental utility of the semi-analytical asymptotic methods used to describe these experiments mathematically and which can otherwise be used to identify key parameters for development.

Chemical vapour deposition

Chemical vapour deposition (CVD) is operated with chemical process to produce high-purity solid materials. The process involves flowing of precursor gas to a heated surface in the chamber. Reaction is commonly initiated by heat or plasma. The chemical reaction of vapour precursor will result in formation and conformal deposition of a thin film onto the substrate. A high purity metal deposit can be obtained with fast deposition rates. Disadvantages of CVD are based on the requirement to use toxic precursors and the mechanical instability of the deposited film. Ring–disc electrodes fabricated by

CVD have been reported with a few materials. Zhao's group has reported the fabrication of carbon/carbon ring-disc microelectrodes using carbon fibre disc electrode with carbon ring electrode separated by a silica layer [8]. This method shows good uniformity and radial symmetry of the layer of the electrode. However, the deposition process is complicated and reproducibility is very low. Metallic ring-disc electrodes were also fabricated using the CVD method [9]. However, choices of materials used are limited. Physical vapour deposition (PVD) has been introduced as an alternative method for metal ring fabrication. The fundamentals of PVD will be discussed in the next section.

Physical vapour deposition

Physical vapour deposition (PVD) is the method for a film deposition under vacuum condition. In PVD, the condensation of a vaporized form of the material leads to deposition on to various surfaces. The deposition process in sputter coating generally involves bombardment of the target surface with energetic positively charged ions to promote a high-density material flux toward the substrate to be coated. With high temperature and vacuum evaporation or plasma sputter bombardment, the physical process of coating occurs resulting in a strong attachment between the coating and the substrate, depending on properties of the film such as thermal coefficient of expansion and surface energy. Ring electrodes can be fabricated as an outer film layer on the insulated wire. For example, a pulled capillary or insulated wire is sputter coated or coated by vacuum evaporation from all sides by a metal film [10, 11]. The ring thickness is mainly controlled by the deposition period. Although ring electrode fabricated by PVD is time–consuming, a continuous and uniform ring which is concentric to the disc is achievable. This offers the benefit to complicated generation – collection measurement in particular, allowing the application of numerical or asymptotic methods to predict performance, most importantly the collection efficiency and the time-of-flight from generator to collector.

2.2 Types of sensor

2.2.1 Ring – disc electrode

Due to the limitations of lithography and CVD, fabrication of ring – disc devices in our work is based on PVD method. The major benefit of the PVD method is that it allows all conductive material to be sputtered. However, the uniformity and radial symmetry strongly depend on the position of the material placed on top of the target. Another concern is the cost of the process. Most of the sputtered target is wasted during the deposition step; this is particularly in the case when a precious metal is used. To optimise with respect to these parameters, a novel PVD method for metallic ring-disc fabrication was developed [12, 13]. Instead of a flat metal target, a hollow cylindrical target was employed with a controlled spooling mechanism to drive the substrate through the radially arranged target is to enhance the deposition rate and improve the uniformity [14, 15]. The cost of target is decreased and the lifetime of the target is increased by using a small cylindrical target and not filling the vacuum chamber with precious metal. The gap between the metal target and the coated wire is also reduced, which result in increased deposition rate. The design and development work were in association with Torr Scientific Ltd. UK. The diagram of this PVD machinery is illustrated in Figure 2.1. This offers a compromising method to deposit metal layer in all directions as the wire is gradually inserted through the hollow target.

(A) (B)

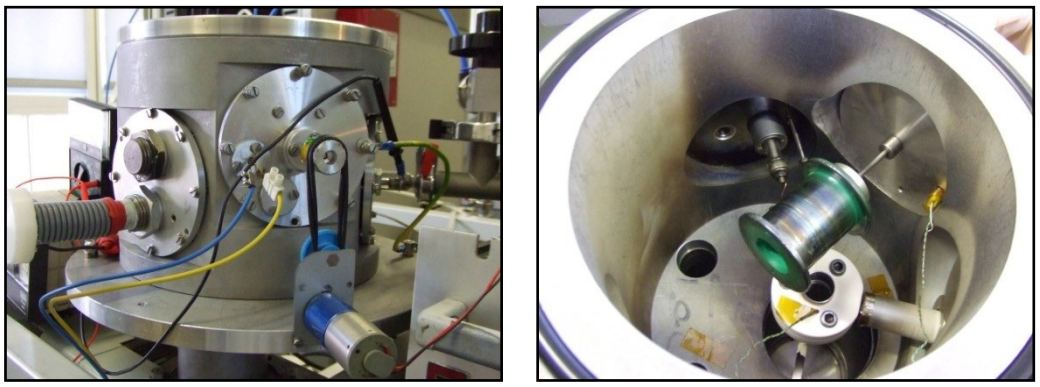

(C)

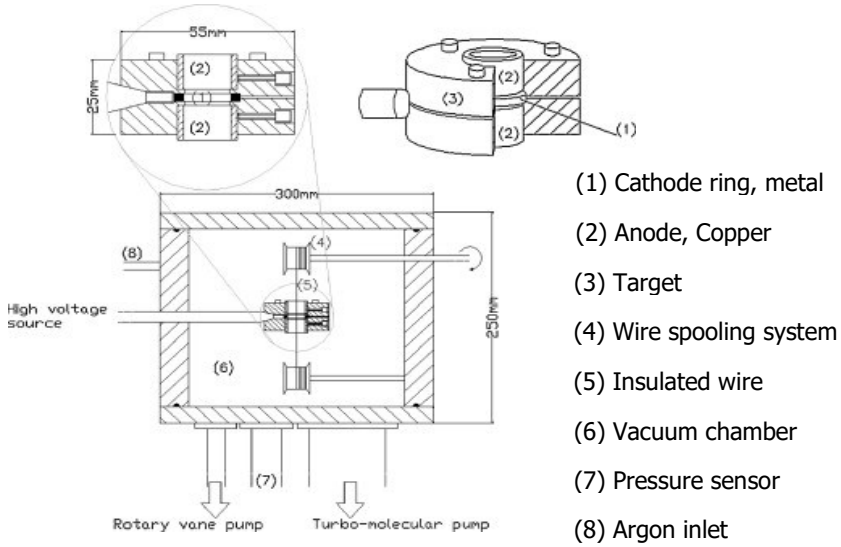

Figure 2.1 Set up of PVD showing pictures from outside (A) and inside (B) of the chamber with schematic diagram of inverted hollow cylindrical sputter coater (C) used for deposition of Pt layer on insulated Pt wire, adapted from Harvey *et al.* 2008 [16].

Pt/Pt ring-disc electrode fabrication

Insulated Pt wires (99.99% Goodfellow) with different diameters were sputter coated with Pt using the process developed by Harvey *et al* [16]. Prior to coating, each wire was cleaned with ethanol and water. The wires were dried with filtered nitrogen and then placed in the PVD system. The wire diameter is typically 50 μm with insulation layer thickness of 7.5 μm. Separated connections to the inner core Pt and the outer sputtered Pt layer were made using conductive epoxy (Circuit Works). After the connections were made, the whole assembly was encapsulated with epoxy resin (CY1301 + HY1300, Robnor Resin, Swindon) which was cured overnight at room temperature. The epoxy assembly was then cut perpendicularly the wire with a diamond saw (Buehler) to expose the Pt/Pt ring–disc surface. Before first use, the electrodes were polished using successive aqueous alumina slurries of 1.0, 0.3 and 0.05 μm on polishing pads (Buehler) with sonication in water between grades and at the end to remove embedded abrasive. Figure 2.2 shows a schematic of the electrode fabrication process and a photograph of three completed Pt/Pt ring – disc microelectrodes.

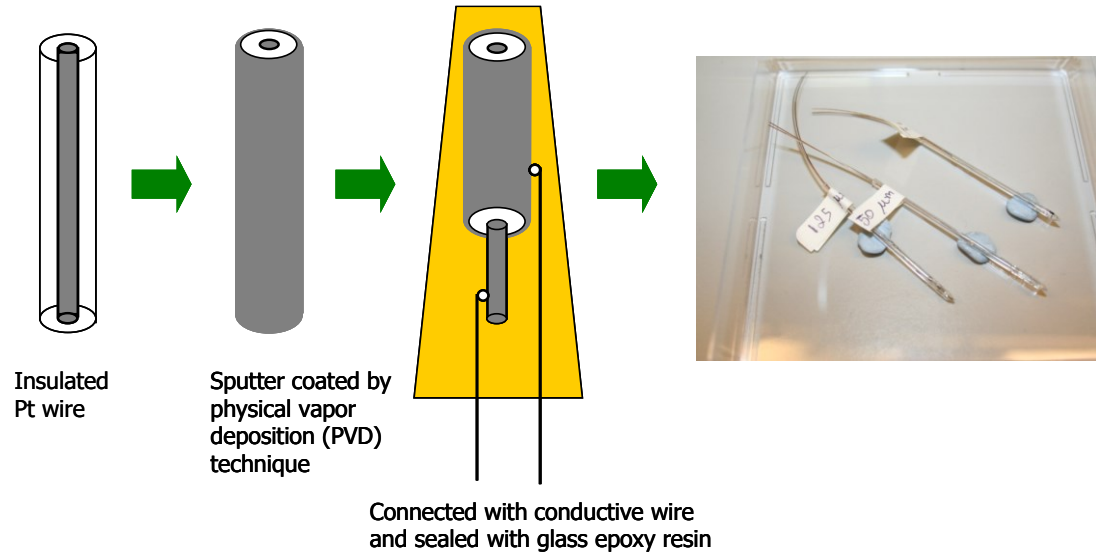

Figure 2.2 A schematic picture illustrated the fabrication of Pt/Pt ring – disc sensor.

Carbon ring-disc electrode fabrication

Carbon fibre in micron size (99.99% Goodfellow) was used as C disc, whereas C ring was made of carbon paint (Electrodag, Agar). For C disc electrode, a 30 □m carbon fibre was first sealed in a pulled borosilicate glass capillary (Clark Electromedical). Then C ring was deposited by rotational coating or dipping with the carbon paint. C ring was left at room temperature to evaporate the solvent. Silver wires were connected to each disc and ring with conductive silver epoxy (Circuit Works). The whole assembly was insulated in epoxy potting resin (CY1301+HY1300 Robnor Resins, Swindon) and cured according to the manufacturer's instructions: 24 hours set at room temperature followed by one hour cure at 70 °C. Finally, C/C ring – disc was exposed by cross sectional slice using a diamond wafering saw at the tip. A schematic of the process of electrode fabrication and a photograph of the C/C ring – disc electrode is shown in Figure 2.3.

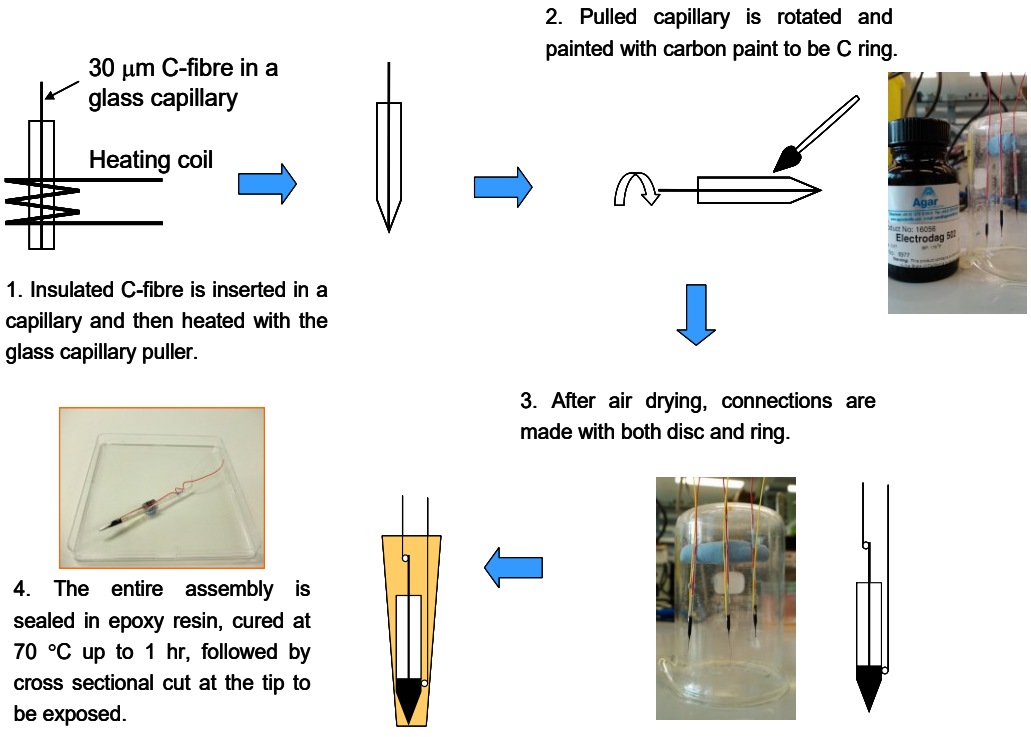

Figure 2.3 A schematic picture illustrated the fabrication of C/C ring – disc sensor.

2.2.2 Dual disc electrode

Dual disc electrode is an alternative generator – collector sensor geometry which can be fabricated using either commercial metal wires or carbon fibres. In this work, metallic dual disc electrodes are of interested and simply made of two Pt or Au wires. Ideally, both discs are coplanar with a fixed known distance. Pt and Au wires with known diameter (99.99% Goodfellow) were selected. These two wires were placed close together (less than half millimetre from each other) after connection wires were separately attached. In order to bring two wires into closed distance, small diameter capillary, sealed capillaries and theta glass capillaries were used for electrode assembly. The insulated wires were inserted into the capillary to ensure close proximity without risk of short circuit. After each connection was made, the assembly was sealed in epoxy resin and sawn perpendicularly to uncover disc electrodes. Schematic diagram of dual disc fabrication is shown in Figure 2.4. Each type of capillary is feasible to use for electrode fabrication. The pulled and sealed capillary gives a benefit of small distance between two metal wires at the capillary tip. With theta glass, each wire was inserted into each open tubular channel which is separated by the septum. The theta glass can be pulled and sealed to decrease the distance while complete insulation is expected. Although dual disc fabrication is less difficult compared to ring-disc fabrication, precise control of the distance between two discs is difficult to achieve. The fabricated sensor was cut and cleaned as above for characterisation and measurement studies.

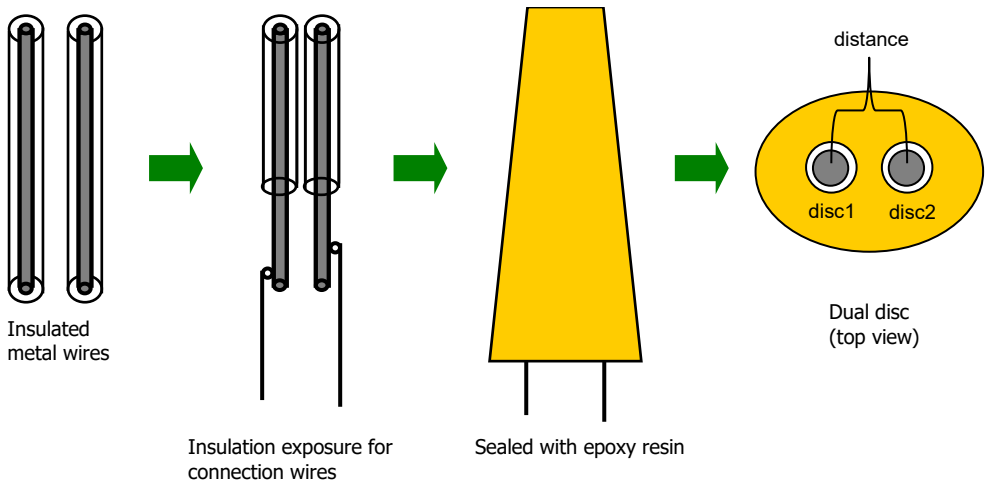

Figure 2.4 A schematic of the fabrication process for the dual disc sensor.

2.3 Sensor Characterisation

To most home-built devices, methods of characterisation are essential and useful to define our sensor dimension and surface properties which affect sensor behaviour. Generally, image analysis and electrochemical method are performed. For micrometre sized electrodes, scanning electron microscope (SEM) is commonly used as an imaging tool which gives information of sensor surface condition and distance. In SEM, the sample surface is imaged by scanning with a high-energy beam of electrons, producing signals that contain information of surface morphology, composition and crystalline structure [17]. The signal results from the interaction between electrons and atoms surrounding sample surface. SEM can provide a high resolution image (resolved to less than 1 nm). Sample preparation such as coating with conductive material is required for insulating materials. However, SEM would not be ideal for sensor characterisation in everyday work. Bulky objects of irregular shape are required to mount with a conductive adhesive on the sample holder in practical. Electrochemical techniques are an alternative method for sensor characterisation. Steady state current and dynamic profiles are influenced by electrode size and geometry. Each sensor will be characterised and current-voltage relationship is recorded for a well-characterised reversible redox reaction. Theoretically, a known property of chemical reaction, concentration and sensor surface are related to the steady state current as previously mention in Section 1.6.1. In practice, the voltammetric method is widely performed and often reported for successive test or a comparison of pre- and post-measurement. Electrode diameter and surface area can be monitored from the diffusion limited current and the charging current from the double-layer region and any variation surface property can be routinely checked under this approach, such as changes in the solvent limits. Moreover, the electrochemical method can offer an understanding of surface property for chemically modified sensor where electron transfer is applicable.

However, it is important to note that the length scale, or resolution, of different surface measurement techniques vary and that it is important to establish the relevant length scale. Diffusion-limited currents will not be affected by asperities or imperfections smaller than the diffusional length scale, typically $(2Dt)^{1/2}$. Methods based on capacitance resolve to around the Debye length, which obviously depends on ionic strength but is around 0.5 nm at physiological ionic strength. Absolute area

determination from capacitance is rarely possible, but the method is useful for identifying adsorption or failures of the conductor-insulator seal. The most reliable quantitative methods for are determination use oxide peak areas from cyclic voltammetry (Pt, Au) or hydride adsorption peaks (Pt) which have spatial resolution around the size of the unit cell. Methods for determining electrode surface areas for different purposes are presented in the IUPAC review of Trasatti [18].

For most of the work on sensor characterisation, the sensors were cleaned, polished and characterised to ensure they are satisfied the expected values according to both dimensional and electrochemical properties prior to the measurement or any surface modification. Roughness factors, the microscopic area from oxide peaks or hydride peaks divided by the projected geometric macroscopic area allows assessment of surface preparation.

2.3.1 Pt/Pt ring-disc electrode characterisation

Imaging tool

Sensor tip (several millimetres) were sawn off using the diamond wafering saw (Buehler) and were prepared for SEM to enable measurement of sensor dimensions without having to sacrifice the sensor. The removed thin section was polished with water-wetted emery paper from coarse 600 grit to finer 2500 and 4000 grit and then cleaned in water under sonication. Prior to imaging, the sensor tip was metallised using chromium film to prevent charge clouds. The image analysis was carried out using an SEM model JSM-6400 (JEOL Ltd., Japan). SEM micrographs of Pt ring-disc sensor were shown in Figure 2.5. From SEM images, Pt disc electrode which is made from commercial 50 μm wire showed an actual disc diameter of 50.9 μm. The thickness of Pt ring was found to be approximately 0.8 to 1.0 μm.

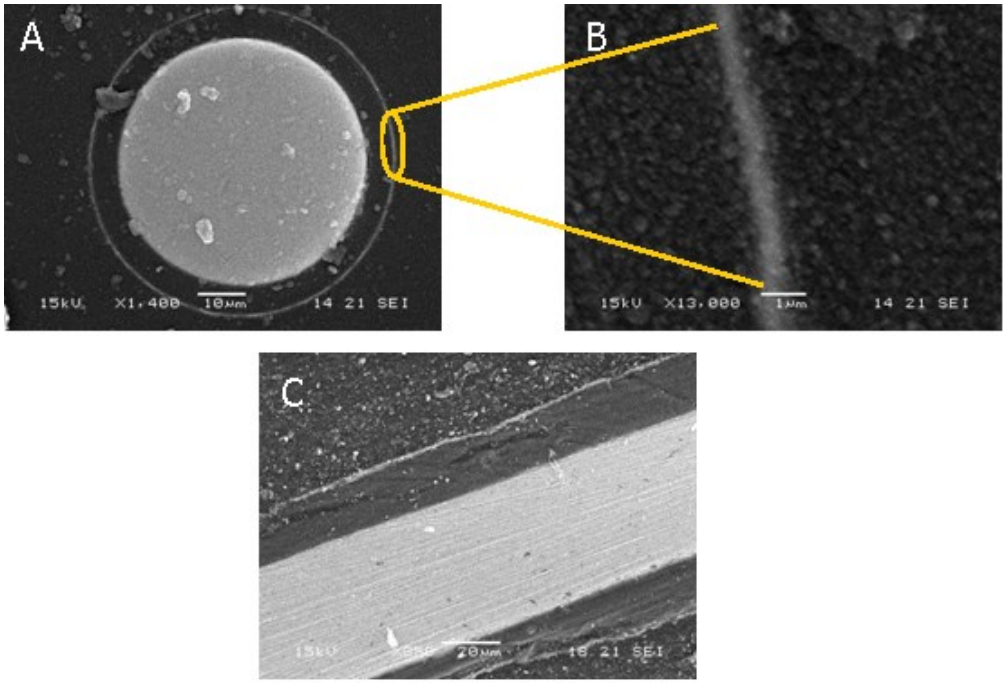

Figure 2.5 SEM images of Pt/Pt ring-disc sensor obtained from 50 µm Pt disc with a cross sectional view (A), magnified ring thickness (B) and perpendicular view (C).

Electrochemical method

To characterise the sensor, steady state voltammetry of ruthenium (III) and (II) redox couple was carried out. Ruthenium hexaammine (III) chloride (99%, Sigma-Aldrich), $Ru(NH_3)_6Cl_3$, at a concentration of 10 mM was dissolved in aqueous 1 M potassium chloride (analytical grade, Fluka), KCl, as background electrolyte. Experiments were performed in stationary solution in an electrochemical cell equipped with ring-disc working electrode, silver/silver chloride (Ag/AgCl) reference electrode and a large Pt mesh counter electrode. A multichannel potentiostat CHI model 1030 (CH Instruments Inc., Texas) was used to control the voltage at the disc and the ring in the electrochemical cell. The counter electrodes were Pt gauze or wire coils and the reference electrode was Ag|AgCl|KCl (aq) (3 M). Before the experiment, the ring-disc sensor was cleaned in 50% methanol (Analar grade, Sigma-Aldrich), aqueous detergent (Decon), methanol (Analar grade, Sigma-Aldrich) and hot water (Milli Q water) with sonication. The electrode surface was then electrochemically cleaned with 0.5 M sulfuric acid (98.5%, Sigma-Aldrich) by applying up to 50 cycles of a potential scan from -1.5 V to 1.5 V (versus Ag/AgCl) at 100 mV/s scan rate. Steady state currents of disc and ring electrodes follow to a different relationship as reported in the literature

[19, 20].Both theoretical equations are shown in figure 2.6, where n is 1, F is 96485 C mol^{-1}, r is disc radius, a and b are inner and outer ring radius, respectively.

Current-voltage (i-V) curves are shown in Figure 2.7. From the i-V curves, limiting currents of the disc and ring were obtained. Good agreement between recorded i-V profiles and those reported in literature are achieved. In comparison with calculated current ($i_{calculated}$) from the theory, both observed limiting currents ($i_{observed}$) from disc and ring are acceptable. Slightly larger current was found in the ring possibly due to uneven surface or protruding effect due to differential erosion during the polishing step. We can look in more detail of surface property from the characterization of the cyclic voltammogram. More details of platinum surface can be further investigated using electrochemical measurement with sulfuric acid. The information of Pt surface can be obtained from both the capacitance value and coulometric evaluation of platinum-hydride (Pt-H) peak from the voltammogram. Pt-H peak area occurs from proton (H^+) reduction at the surface while negative potential is applied. This is a characteristic property of Pt electrodes. And the area of Pt-H peak is related to the real Pt surface [21]. Capacitance is based on the electrical double layer influenced from charged species attracted and formed at surface proximity. At the region where no chemical changes, the capacitance is solely affected by the surface cleanliness.

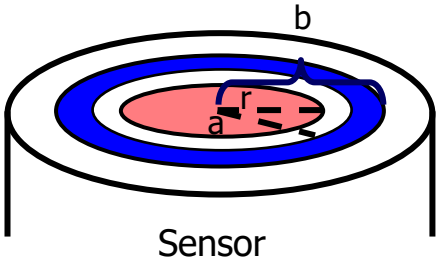

$$i_{disc} = 4nFD_A C_A r$$

$$i_{ring} = nFD_A C_A \frac{\pi^2 (a+b)}{\ln[16(b+a)/(b-a)]}$$

Figure 2.6 Schematic picture and limiting current equations for disc (i_{disc}) and ring (i_{ring}) electrode summarised from [19, 20, 22].

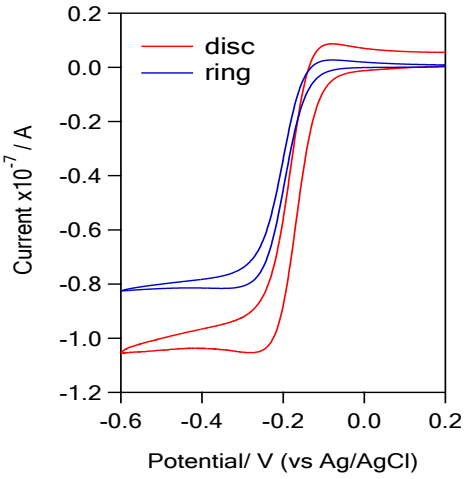

Electrode	$i_{observed}$ / A ($\times 10^{-8}$)	$i_{calculated}$ / A ($\times 10^{-8}$)
disc	9.04 ±0.60	7.45
ring	8.09 ±0.23	6.63

Figure 2.7 i-V curves separately measured on 50 µm Pt disc (red) and Pt ring (blue) using 10 mM $Ru(NH_3)_6Cl_3$ in 1 M KCl from 0.2 to -0.6 V versus Ag/AgCl reference electrode at a scan rate 50 mV/s. Solid lines in blue and red represent ring and disc current, respectively. Inset table shows observed and calculated currents based on theoretical prediction (n=5).

Cyclic voltammetry in 0.5 M sulfuric acid (H_2SO_4) is commonly performed for electrode cleaning and can conveniently also be used for characterisation. The voltammogram of H_2SO_4 reported in the literature is shown in Figure 2.8. H_w and H_s peaks represent Pt-H peak of each reduction step. For our sensor, cyclic voltammetry of 0.5 M H_2SO_4 was separately performed on the Pt disc and ring working electrodes after the normal cleaning process described above. And the Pt-H peaks are expected to appear at -0.24 to -0.30 V (versus Ag/AgCl).

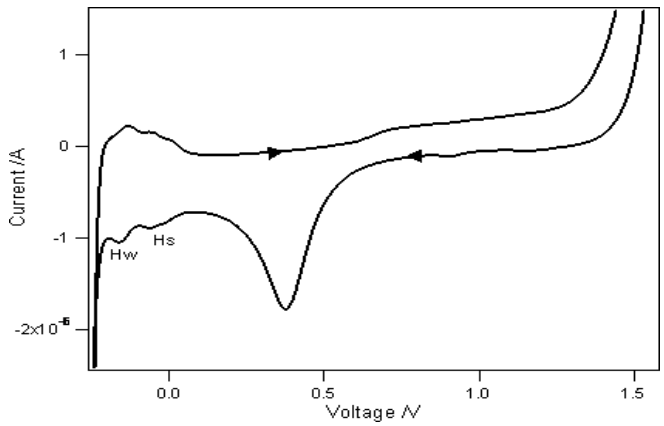

Figure 2.8 Cyclic voltammogram from 125 µm Pt electrode in 0.5 M H_2SO_4 at scan rate of 100 mVs^{-1} (versus Ag/AgCl reference electrode), adapted from [23, 24].

Votammograms of disc and ring are shown in Figure 2.9. The qualitative pattern of the Pt disc voltammogram was similar to that reported in the literature, whereas the magnitude of the Pt-O reduction peak was relatively smaller for the ring. The reason of peak distortion in the ring is still unknown though it is possible that the very thin films of Pt, the grain size of the Pt oxide may be a constraining factor. Similar results for the reduction of gold oxide nanoparticles have been observed by Compton *et al.* [25]. Observed Pt-H peaks of both disc and ring are not well defined. Proton reduction on Pt surface is based on the interaction in atomic level. Unresolved Pt-H peaks are possibly due to other interferences adsorbed on the electrode surface. Thus, Pt-H peaks can be implied of surface cleanliness or purity. For example; chloride ions can strongly adsorb on the Pt surface and partially block the Pt surface. Therefore, the freshness and purity of the sulfuric acid solution can also effect to the CV pattern. One source of the undefined peak could be an uneven electrode from fabrication step. Careful polishing is needed along with electrode cleaning.

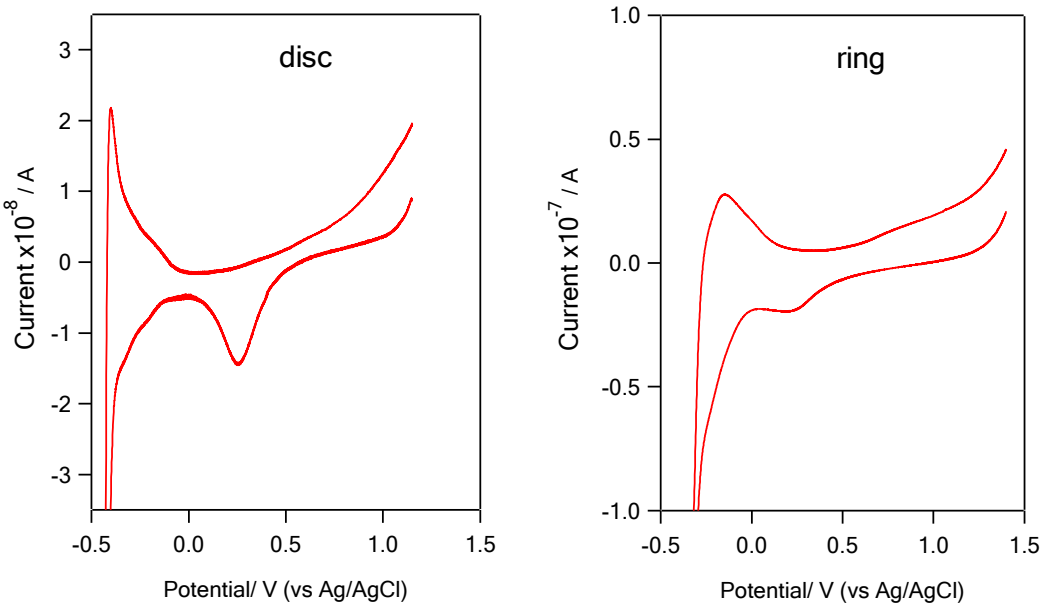

Figure 2.9 Cyclic voltammograms of different size of Pt/Pt ring-disc microelectrodes in 0.5 M H_2SO_4 at 100 mVs^{-1} scan rate from 1.2 V to -0.4 V (versus Ag/AgCl reference electrode).

Apart from Pt-H peaks, current monitoring in the double layer region can indicate the cleanliness of electrode surface as well. To look in more detail of our sensor surface, the capacitance value at the region where no chemical change occurs was calculated and compared to those reported in the literature.

The reported capacitance in the literature for polycrystalline Pt is approximately 0.2 F m^{-2} [23, 26]. Observed capacitance of each electrode was calculated from the charge per area at a fixed potential (0.75 V) from the cyclic voltammogram of Pt/Pt ring-disc microelectrodes in 0.5 M sulfuric acid (H_2SO_4) in the experiment as described in Figure 2.9. The Pt disc capacitance is up to 40 times higher while the capacitance of Pt ring electrode was found to be greatly higher (5 orders of magnitude) from the literature, reported in table 2.1. The precise cause of these discrepancies remains obscure, but for the ring may be due to coupled capacitances between ring and disc and through the dielectric. Large differences between the capacitance calculated from the fabricated disc and ring electrodes than that of the commercial Pt electrode were found. This can support the idea that determination of capacitance is sensitive to Pt surface area, in comparison with steady state current.

Table 2.1 Capacitance values obtained from 0.5 M H_2SO_4 cyclic voltammograms of disc and ring electrode taken at 0.75 V (see figure 2.9).

Electrode	Expected capacitance (F m^{-2})	Observed capacitance (F m^{-2})
disc	0.2	7.8
ring	0.2	3.4×10^4

The length scale of capacitance is determined by the screening length (Debye length) in the electrolyte solution. Since the ionic strength will be a little over 0.5 M (the bisulfate ions will be partly dissociated) we would predict a Debye length of 0.42 nm [27].This is of a similar size to a hydrated ion and only twice the size of a Pt atom. It will therefore be exceptionally sensitive to even the smallest imperfection on an unsmoothed surface. Surface characteristics of Pt disc and Pt ring could be different

from the formation method- the Pt ring would be only a few thousand atoms thick. Larger capacitance per unit area of Pt ring implies of the structure of Pt surface that allows higher number of charge interactions than in the Pt disc or coupling between the insulator and the electrolyte solution. The ring will also be highly sensitive to protrusion effects if the insulator is abraded back faster than the Pt. Nevertheless, commercial microelectrodes insulated with resin or glass seldom show capacitance that range within two orders of magnitude of the predicted values. The process of renewing or refreshing the electrode surface should be controlled to maintain the surface property.

The Pt-H peaks were not clearly resolved probably due to the large capacitance current. Cleaning process has been carried out prior to perform the sulfuric acid CV, however; the effect of the large capacitance remains existing. Although lacking details on the real surface area of real Pt surface, the measurement of the steady state current is mainly concerned as this is related to the electrochemical reaction of interest. Overall, the Pt ring-disc electrodes fabricated by our PVD method exhibit reasonable electrochemical characteristics. They are stable and fit for purpose for our experiments.

2.3.2 C/C ring – disc electrode characterisation

Imaging tool

Similar sample preparation was done for C/C ring-disc sensor. SEM images of C/C ring–disc sensor were captured using the same method and are shown in Figure 2.10. From SEM image, the carbon fibre disc revealed a diameter of 33.3 μm, which is close to its reported size. However, C ring fabricated using carbon paint was found to be unsmooth and uneven. SEM picture shows large area of groove and crack in the ring layer. The ring shape is not uniform while ring thickness ranges from 4 to 20 μm approximately. This can indicate that the deposition and curing of carbon paint during fabrication are inadequately controlled. Under the manner of painting, uniformity and smoothness along one plane is hard to achieve. Nevertheless, electrochemical properties can be tested to establish if the C ring is able to operate for the generation-collection purpose.

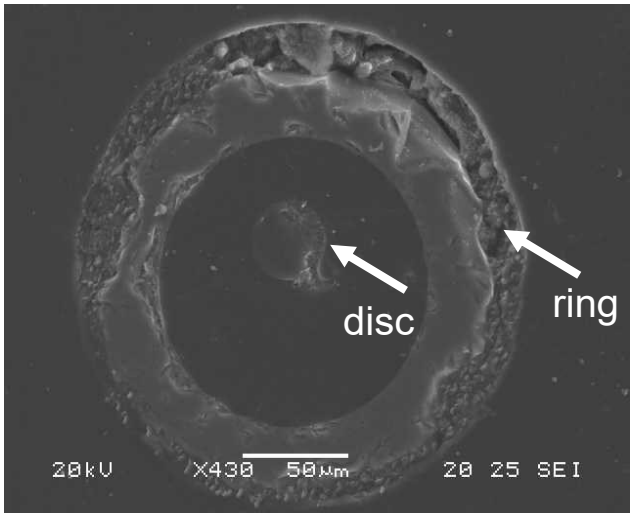

Figure 2.10 SEM images of C/C ring – disc sensor obtained from 30 µm carbon fibre and ring layer of carbon paint.

Electrochemical method

Prior to characterisation, similar cleaning protocol under ultrasonic bath was conducted. Steady state voltammetry in standard 10 mM $Ru(NH_3)_6Cl_3$, 1 M KCl was performed. All experiment conditions are followed as previously mentioned in Pt/Pt ring–disc characterisation, otherwise stated. i-V curves of C/C ring-disc electrode and steady currents are shown in Figure 2.11. Steady state current under the tested conditions can be achieved from both disc and ring electrodes. Slightly higher disc current was observed as expected from the larger than expected diameter measured from SEM. The observed ring current was found to be much larger than the calculated value. This is mainly due to the large area of the actual ring surface. Actual thickness is defined by the inner and outer diameter of the ring; however, cracks can also increase the surface area of the electrode. It is not clear that these were present in the finished devices, or at least accessible to the electrolyte solution since the i-V hysteresis is reasonable. We would not expect the diffusion limited current to be greatly increased however, as it is not sensitive to defects smaller than the average diffusional length scale, $(2Dt)^{1/2}$ which here would be of the order of 10 µm Although the real surface area of the ring electrode is difficult to determine since unlike Pt or Au there are no well-defined oxide or hydride peaks representing unit cells of known size), informative electrochemical experiments were nonetheless able to be performed and were encouraging for further generation-collection measurement.

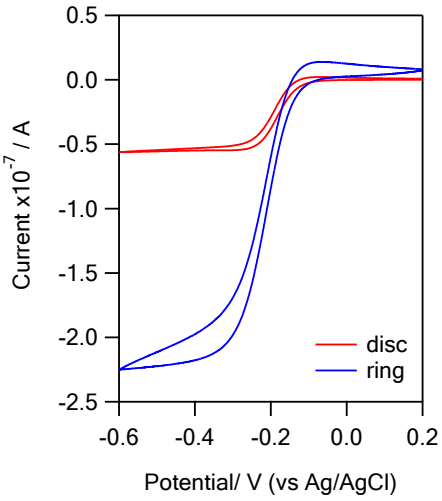

Electrode	$i_{observed}$ / A ($\times 10^{-8}$)	$i_{calculated}$ / A ($\times 10^{-8}$)
disc	5.28±0.17	4.95
ring	22.2±1.8	7.90

Figure 2.11 i-V curves separately measured from 30 μm C disc (red) and C-paint ring (blue) using 10 mM $Ru(NH_3)_6Cl_3$ in 1 M KCl from 0.2 to -0.6 V versus Ag/AgCl reference electrode at scan rate 50 mV/s. Solid line in blue and red represent ring and disc current, respectively. Inset table shows observed and calculated currents based on theoretical prediction (n=5).

2.3.3 Dual disc electrode characterisation

Imaging tool

SEM images of dual disc sensors with geometries were imaged are shown in Figure 2.12 and 2.13. For a dual sensor made from commercial 75 μm gold insulated wires, measured diameters of electrode 1 and 2 (DG1 and DG2) are 81.9 and 80.7 μm, respectively, with less than 10% difference of the reported diameter. The uniformity of each disc is an advantage arising from choice of well characterised wire. Distance between two discs is hard to be systemically varied, but fixed distance is obtained at a time of sensor tip exposure. From the SEM of the tip from this DG sensor, distance (d) between centre to centre of each disc was established to be 355 μm.

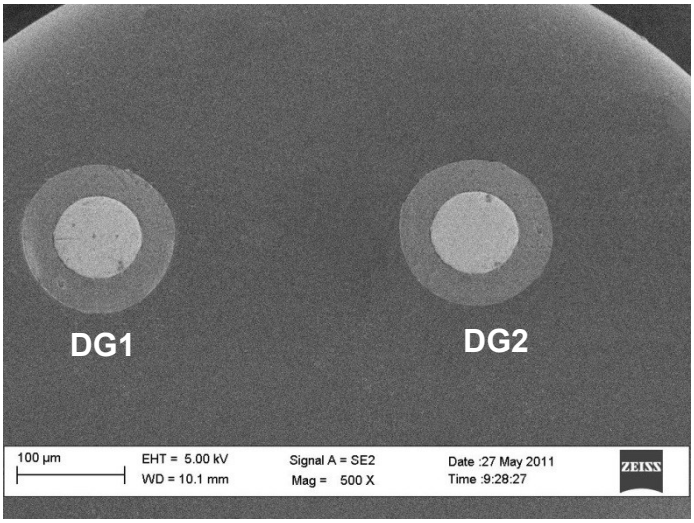

Figure 2.12 SEM image of dual disc sensor obtained from 75 µm insulated gold wires.

Another dual disc sensor with smaller area was made from commercial 25 µm Pt. The SEM micrograph of dual Pt disc respectively demonstrates electrode diameter of DPt1 and DPt2 for 32.3 and 30.8 µm, illustrated in Figure 2.13. These are slightly larger than the nominal specified size. Less than 30% difference in reported diameter of the Pt wire compared with the diameter from measurement of the SEM micrograph were obtained. Centre to centre distance was found to be 195.4 µm.

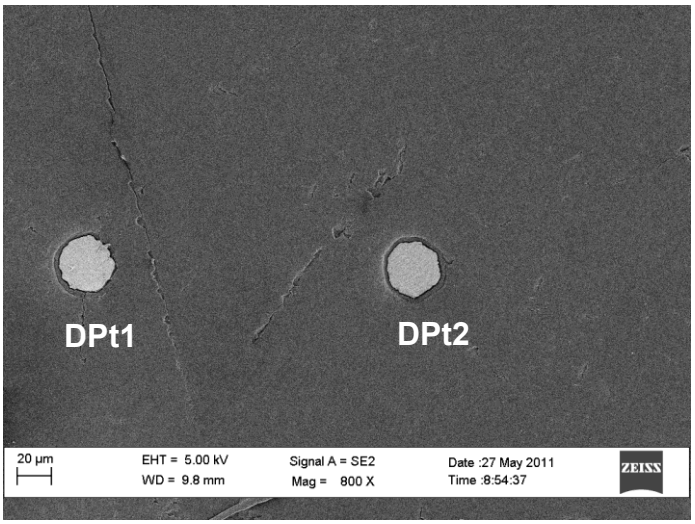

Figure 2.13 SEM image of dual disc sensor obtained from 25 µm insulated platinum wires.

Electrochemical method

Steady state voltammetry of standard 10 mM $Ru(NH_3)_6Cl_3$ 1 M KCl was separately run under previously indicated conditions. Plots of i versus V and limiting currents obtained from DG1 and DG2 are shown in figure 2.14. Observed diffusion-limited currents from each disc agree well with theoretical estimation with less than 5% of difference.

Steady state current of dual Pt sensor fabricated from 25 μm insulated wires was determined and reported in figure 2.15. Observed currents from DPt1 and DPt2 are found to be closed to theoretical prediction. Additional cleaning was undertaken when the steady current deviated from characterised value.

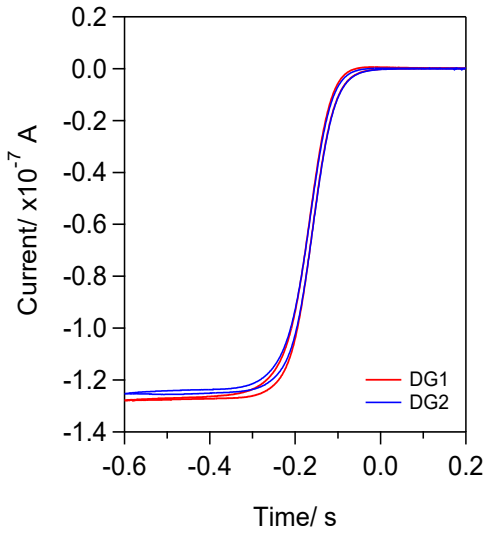

Electrode	$i_{observed}$ / A ($\times 10^{-7}$)	$i_{calculated}$ / A ($\times 10^{-7}$)
DG1	1.26 ±0.06	1.21
DG2	1.25 ±0.02	1.20

Figure 2.14 i-V curves separately measured from dual disc sensor where DG1 (red) and DG2 (blue) using 10 mM $Ru(NH_3)_6Cl_3$ in 1 M KCl at 5 mV/s scan rate (quasi-steady). Inset table shows observed and calculated currents based on theoretical prediction (n=6).

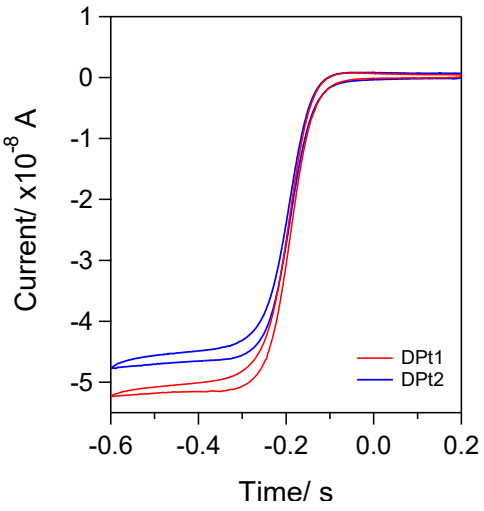

Electrode	$i_{observed}$ / A ($\times 10^{-8}$)	$i_{calculated}$ / A ($\times 10^{-8}$)
DPt1	5.09 ±0.17	4.80
DPt2	4.60 ±0.18	4.58

Figure 2.15 i-V curves separately measured from dual disc sensor where DPt1 (red) and DPt2 (blue) using 10 mM $Ru(NH_3)_6Cl_3$ in 1 M KCl under 5 mV/s scan rate. Inset table shows observed and calculated currents based on theoretical prediction (n=6).

2.4 Generation – Collection Characterisation

In this section, the relationship between two electrodes were attempted and investigated. Consider a chemically reversible process; the species which is electrochemically generated at one electrode will be collected and detected at the other electrode in this approach. The electrochemical response will be a function of distance, electrode geometry and analyte concentration. The standard 10 mM $Ru(NH_3)_6Cl_3$ in 1 M KCl was mainly used for the experiments. Only the Pt ring–disc electrode device, which is currently the most promising for in channel detection, was tested under a flow system.

2.4.1 Pt/Pt ring-disc electrode under generation–collection

With this type of dual electrode, methods of operation include employing disc generator with ring collection (and vice versa). In this work, we are interested in the disc generation – ring collection mode initially in a stationary solution, and subsequently under flow system. For our tested system, a negative voltage scan was performed at Pt disc while a fixed voltage was applied for the reverse reaction at Pt ring, typically at the potential for the diffusion limited reaction. The disc generation–ring collection

process is illustrated schematically in Figure 2.16. Using the $Ru(NH_3)_6^{2+/3+}$ redox couple, the process started with the reduction of $Ru(NH_3)_6^{3+}$ at the disc, and oxidation of the electrogenerated $Ru(NH_3)_6^{3+}$ species at the ring follows. These processes are simultaneously operated.

The collection efficiency (CE) of the process can be calculated using the ratio of current from collector (i_{col}) to the current from generator (i_{gen}), and %CE can be described as

$$\%CE = \left| \frac{i_{col}}{i_{gen}} \right| \times 100 \qquad (2.1)$$

i-V curve of both disc and ring were shown in figure 2.17. CE was calculated using the observed currents with the collector electrode poised at 0.4 V, where oxidation is diffusion limited.

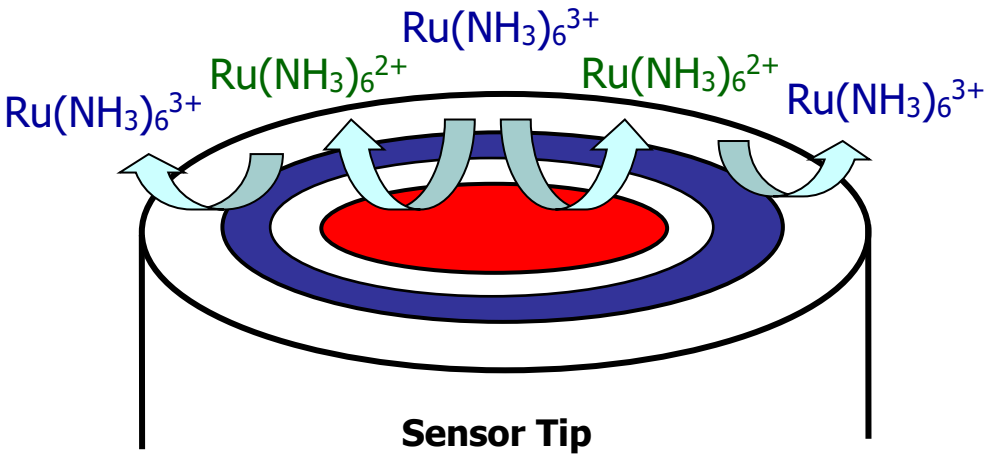

Figure 2.16 Diagram illustrating disc generation – ring collection process using $Ru(NH_3)_6^{2+/3+}$ redox couples.

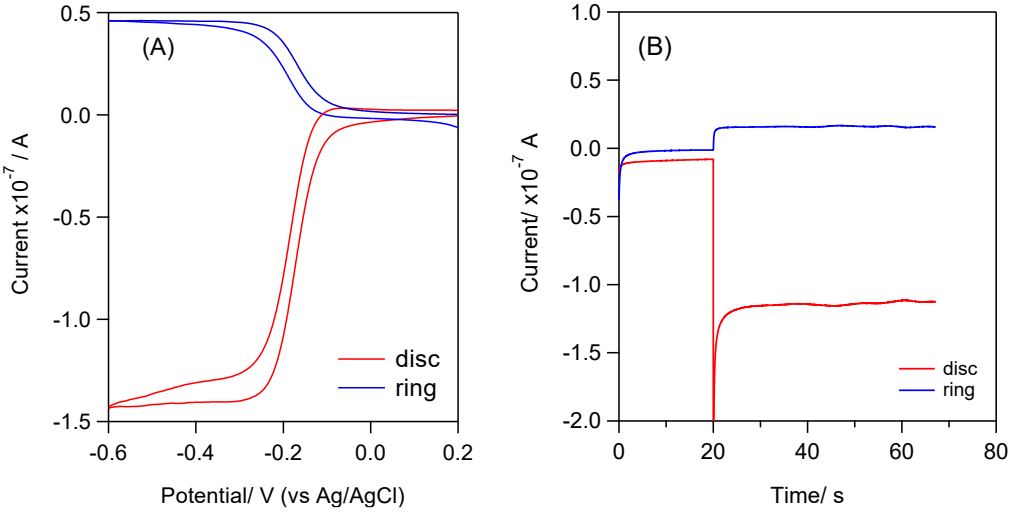

Figure 2.17 i-V curves of generation – collection process using 10 mM $Ru(NH_3)_6Cl_3$ in 1 M KCl from Pt/Pt ring – disc sensor. Potential was scanned (A) from 0.2 to -0.6 V at disc (red) under 50 mV/s scan rate where 0.2 V was fixed for ring (blue). In (B), disc and ring potentials were fixed at -0.6 and 0.2 V, respectively (B).

As seen from Figure 2.17A, as the reduction current negatively increases, positive current from the ring is higher due to oxidation of the generated species within a second. This confirms that generation and collection processes during the applied voltage has occurred. Once disc current reaches diffusion limited, the ring current becomes steady as well. From the i-V curves, %CE was found in a range of 32.5 %. The expected value of CE has been predicted and reported with 49.5%, based on theoretical model from previous work by O'Hare's group [6]. The %CE was less than the model. This is likely to be caused by imperfections of electrode geometry. Harvey *et al*. [6] numerically modelled the effects of small deviations from the inlaid plane and showed that large losses in collection efficiency can result from tiny micron scale asperities. One possible factor is if the ring surface is recessed and shielded by the insulation. The shielding effect is expected when both electrodes are under a competitive reaction. Consider the amperometric mode in Figure 2.17B, the results give different limiting currents. This is possibly due to a change in feedback mechanisms. Feedback happens in a recurrence of redox reaction to generator and collector. In our work, feedback current is expected as the product of the ring, $Ru(NH_3)_6^{2+}$, is the reactant of disc reaction. Thus, both currents should be enhanced.

With symmetrical geometry and promising generation – collection characteristics, Pt/Pt ring – disc sensor was further studied under a flow environment, as described in previous work [7]. The aim is to understand the flow effect on CE, which can provide the idea of sensor performances while working with flow injection analysis or separation techniques. The experimental set up is shown in Figure 2.18. The flow rate is varied by the HPLC pump and the detection occurs at the flow cell equipped with three electrodes. The ring-disc sensor was placed at the end of the channel and its position controlled using a micromanipulator. The electrodes were connected to potentiostat and amperometric measurement was performed using 10 mM $Ru(NH_3)_6^{2+/3+}$ redox couples in 1 M aqueous KCl. Fixed electrode potentials were applied to both disc and ring at -0.4 V and 0 V (versus Ag|AgCl| 3M KCl), respectively, where each current is limiting. To start with end channel detection under the flow, ring-disc sensor was finely adjusted to be in the middle of channel using the micromanipulator observed with a simple magnifying glass.

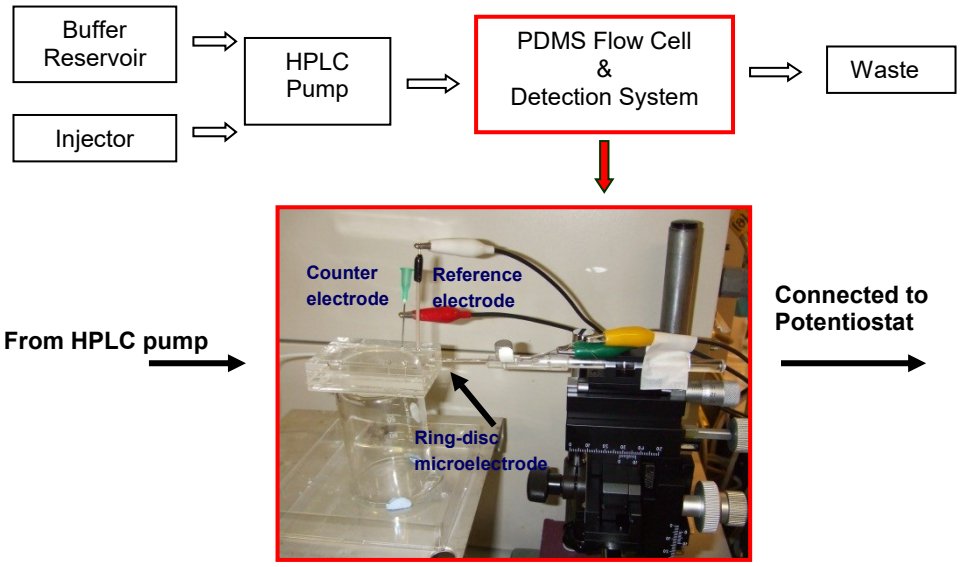

Figure 2.18 Schematic diagram of flow analysis and the setup using PDMS flow cell probed with three-electrode system; Ag/AgCl reference electrode, stainless steel counter electrode and Pt/Pt ring – disc electrode, connected to a controlled potential source.

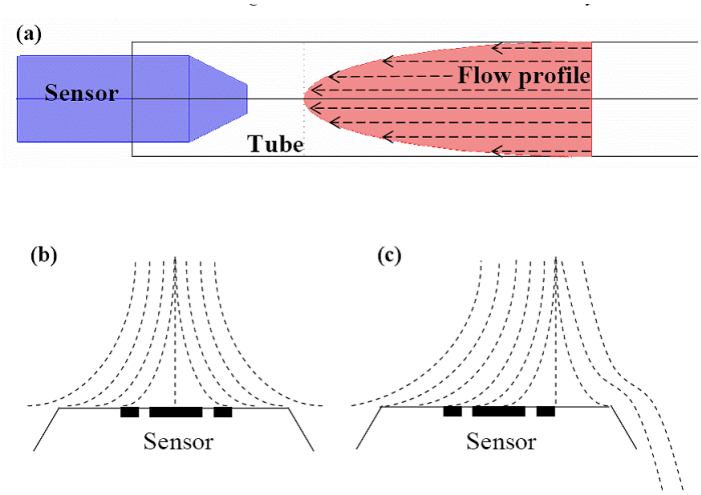

Figure 2.19 Schematic diagram of flow profile in the tube (a) and the effect of impinging flow onto surface which is centred (b) and eccentric to sensor, adapted from [24].

The collection efficiency (%CE, expressed as a percentage) is expected to be lowest when sensor is placed in the centre because of the symmetrical flow profile, which has been studied in previous work of our group [7]. Laminar flow profile exhibits highest velocity in the centre of the flow which will result in changes to the collection efficiency in different position after reaching electrode surface. Relative positions of the sensor and flow profile in the tube are illustrated in Figure 2.19. After ring-disc sensor was centred to the flow, change in flow rate was applied. Lower flow rate was started (0.1 ml/min) with the approximate increment of 1.0 ml/min. Steady state generation and collection currents were monitored at each flow rate. When both currents reached steady values, the flow rate was increased. %CE was calculated from the ratio of average currents and then plotted against applied flow rate. Plots of observed currents and %CE under the flow are shown in Figure 2.20. For disc generation–ring collection process, the generating currents increased whereas the collecting currents decreased with higher flow rate. The CE was found to decrease with the increased flow rate, as expected. As seen in Figure 2.20A, higher flow rate allows more species to migrate and reach to the disc, causing more generation. However, the generated species will then be washed away rapidly resulting in less collection at the ring. The ring current was then dropped (Figure 2.20B) and hence the overall CE was reduced (Figure 2.20C). With flow rate higher than 4.0 ml/min, no significant change in CE was observed. The periodic fluctuations occurring in the recorded data are caused by the reciprocating pump.

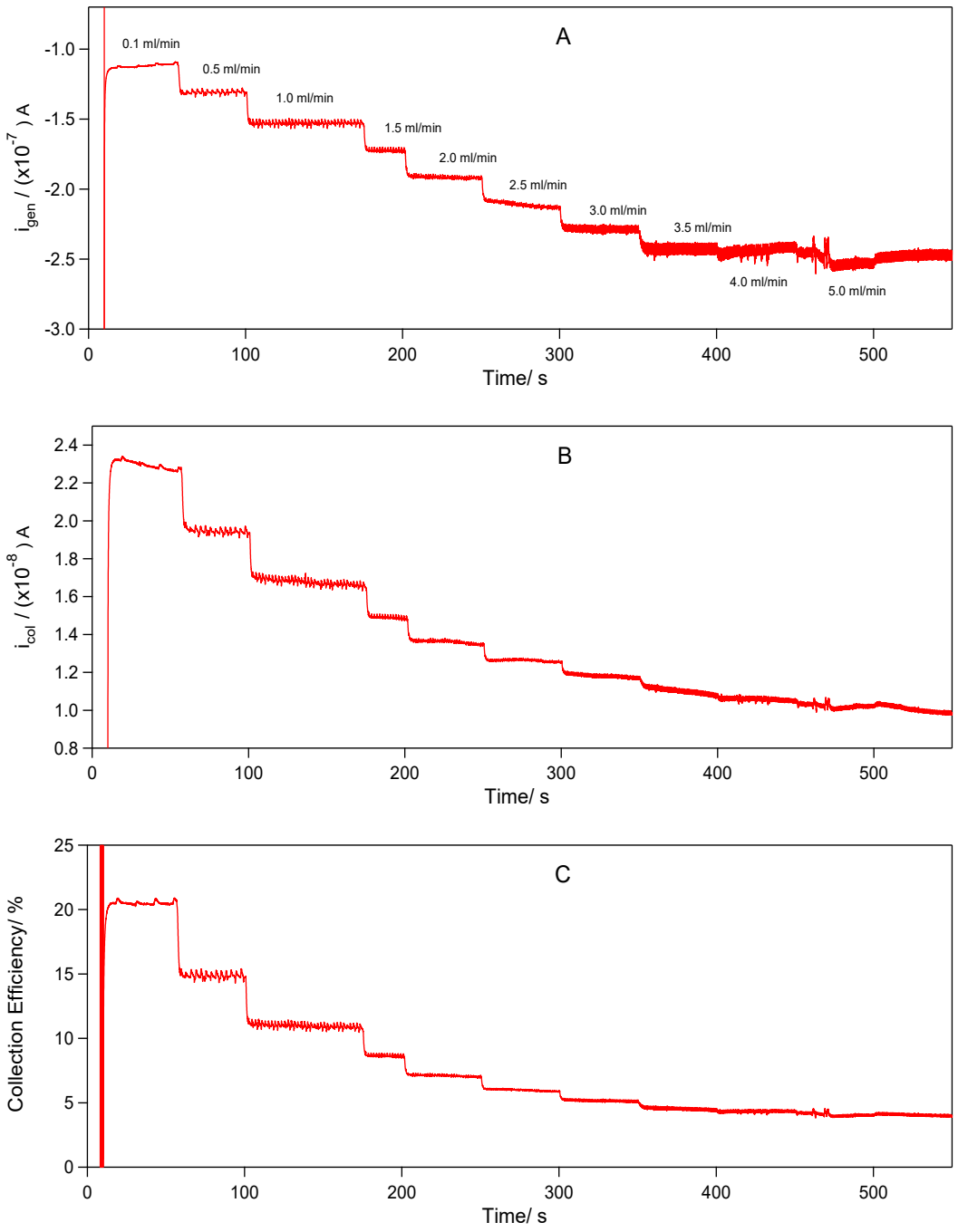

Figure 2.20 Effect of flow on generation current (A), collection currents (B) and collection efficiency (C) tested with 10 mM $Ru(NH_3)_6Cl_3$ in 1 M KCl using disc generation–ring collection mode. The potentials were set at -0.4 V for disc and 0.2 V for ring electrode. Experiments were obtained from 50 µm Pt/Pt ring – disc sensor.

Experimental data were compared to a numerical model from the impinging jet flow model developed as similar in end-column detection for HPLC [6, 7]. This has been described in previous work where our experiment data has been compared. Only disc generation - ring collection is presented because the ring generation case did not agree well with the prediction. One possible reason could be uneven electrode surface which directly contributes to a shielding of redox reaction occurred between disc and ring [24]. Polishing or surface renewal is a possible solution to reduce the effect of the uneven surface. In our comparison for the disc generation case, similar trends were observed with larger drop of experimental CE along with flow rate increment, as seen in Figure 2.21. This is emphasized that CE strongly depends on the flow and higher flow rate are limited by the sensor performance. Residence times in the convective boundary layer are shorter than the time of flight for high flow rates. Simulation is useful for an estimation and verification of the tested condition. However, there are various reasons which can disrupt the generation-collection process and can lead to poor agreement with the model. At this state, we are able to apply the model as a guideline for a flow measurement where particular dynamic range is concerned. In our case, the sensor offers adequate detection and is capable to work with flow rate less than 2.0 ml/min.

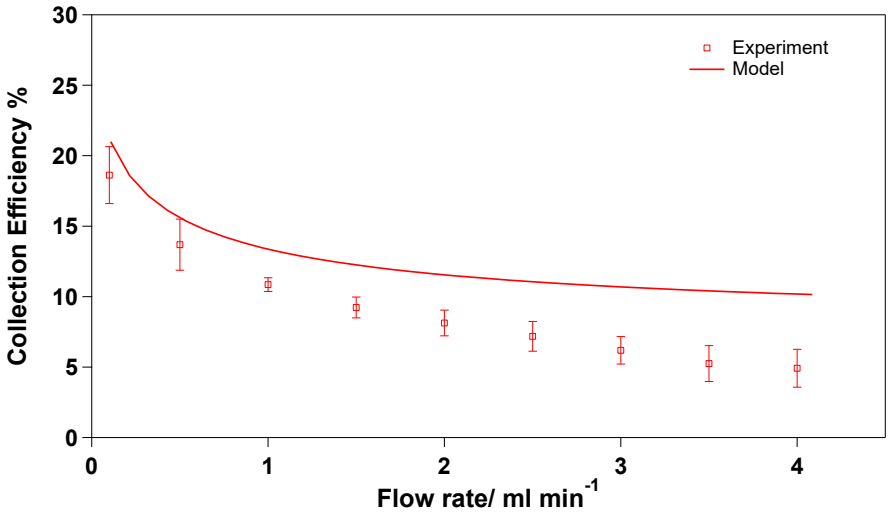

Figure 2.21 Comparison between numerical and experimental data of %CE with applied flow rate, measured by 50 μm Pt/Pt ring–disc electrode with 10 mM $Ru(NH_3)_6Cl_3$ in 1.0 M KCl under disc generation-ring collection mode (n = 4). Solid line refers to numerical data [6, 7].

2.4.2 C/C ring – disc electrode under generation – collection process

The sensor was investigated with similar generation–collection process as the Pt/Pt ring–disc electrode experiment. Generation–collection behaviour was observed and is shown in Figure 2.22. Similar i-V profile of disc current was achieved though ring current exhibits larger capacitance than observed for the Pt-Pt device, presumably due to the particulate nature of the carbon ink. Both currents were also monitored in the steady state when generation and collection potential were both fixed. The calculated CE from C/C ring – disc sensor is 22.6%, which is relatively low compared to previous study [6]. This infers that a lower fraction of generated species is collected. The CE mainly depends on the distance between two electrodes. Our sensor image shows that the distance between carbon ring and disc is fairly large therefore, the complementary reaction occurs to a lesser extent, resulting in small CE. There is no estimation of CE from the theoretical prediction because of the uncertainty in estimation of ring surface. However, as long as stable and reproducible responses from both C electrodes are obtained, as it is here, it is possible to use the sensor for evaluation as an analytical device.

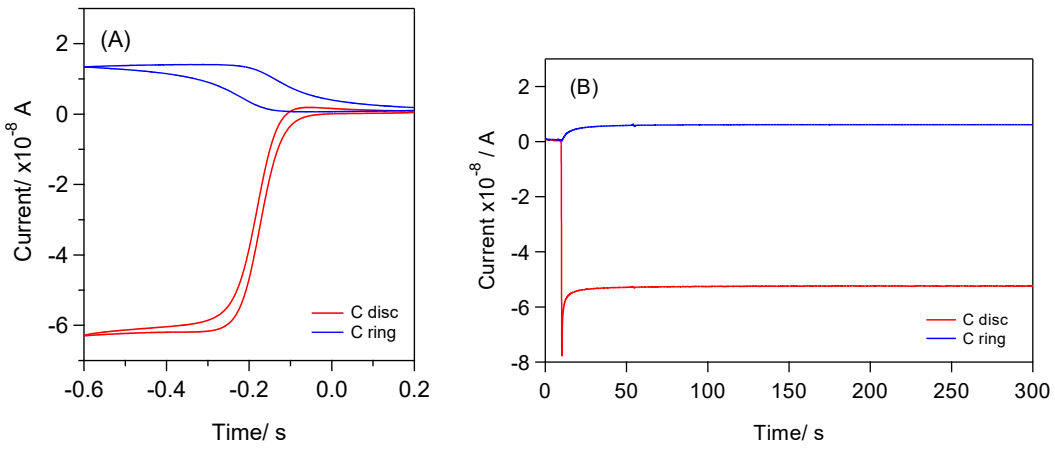

Figure 2.22 i-V curves of generation–collection process using 10 mM $Ru(NH_3)_6Cl_3$ in 1 M KCl from C/C ring–disc sensor under 50 mV/s scan rate. A), Potential was scanned from 0.2 to -0.6 V at C disc (red) where 0.2 V was fixed for C ring (blue). In B), both disc and ring potentials were fixed at -0.6 and 0.2 V, respectively.

2.4.3 Dual disc electrode generation–collection experiments

Generation–collection experiments for dual disc electrode were performed by generating at the first disc and collecting at the second disc. Both disc electrodes were made from commercial wires which are precisely manufactured. They are less difficult to handle and characterise, compared with self-fabricated ring-disc electrodes. The generation and collection processes can be switched between each disc and expected for insignificant difference. The 75 μm dual gold sensor was initially tested under the same generation–collection method. Once both discs are well polished and characterised, CE mainly depends on the distance between two discs for the same analyte. However, the distance between centre to centre is equal to 355 micron which is relatively large compared to our ring – disc electrodes. With larger distance, it causes longer time of generated species to reach the collector, resulting in higher chance of ions to diffuse away in solution. Thus, lower CE within the same period is expected. Observed currents were recorded and are shown in Figure 2.23. The current from generation shows a steady value while collection current is extremely low, giving the observed CE with the value of 6.5%. From Figure 2.23C, fixed potentials were applied at potentials corresponding to the diffusion-limited currents of the redox reaction, and the increase in collection current can be observed. As seen from the collection curve, time to reach the steady value is of the order of a minute, consistent with the diffusional length scale. This is also observed for 25 μm dual disc sensor. To improve generation–collection process, different assembly and approaches that reduce the gap between two discs are required. Alternative ways could be a prediction of the steady value from the electrode geometry and working condition using an analytical model. More details about dual disc system with generation – collection mode will be investigated in Chapter 5.

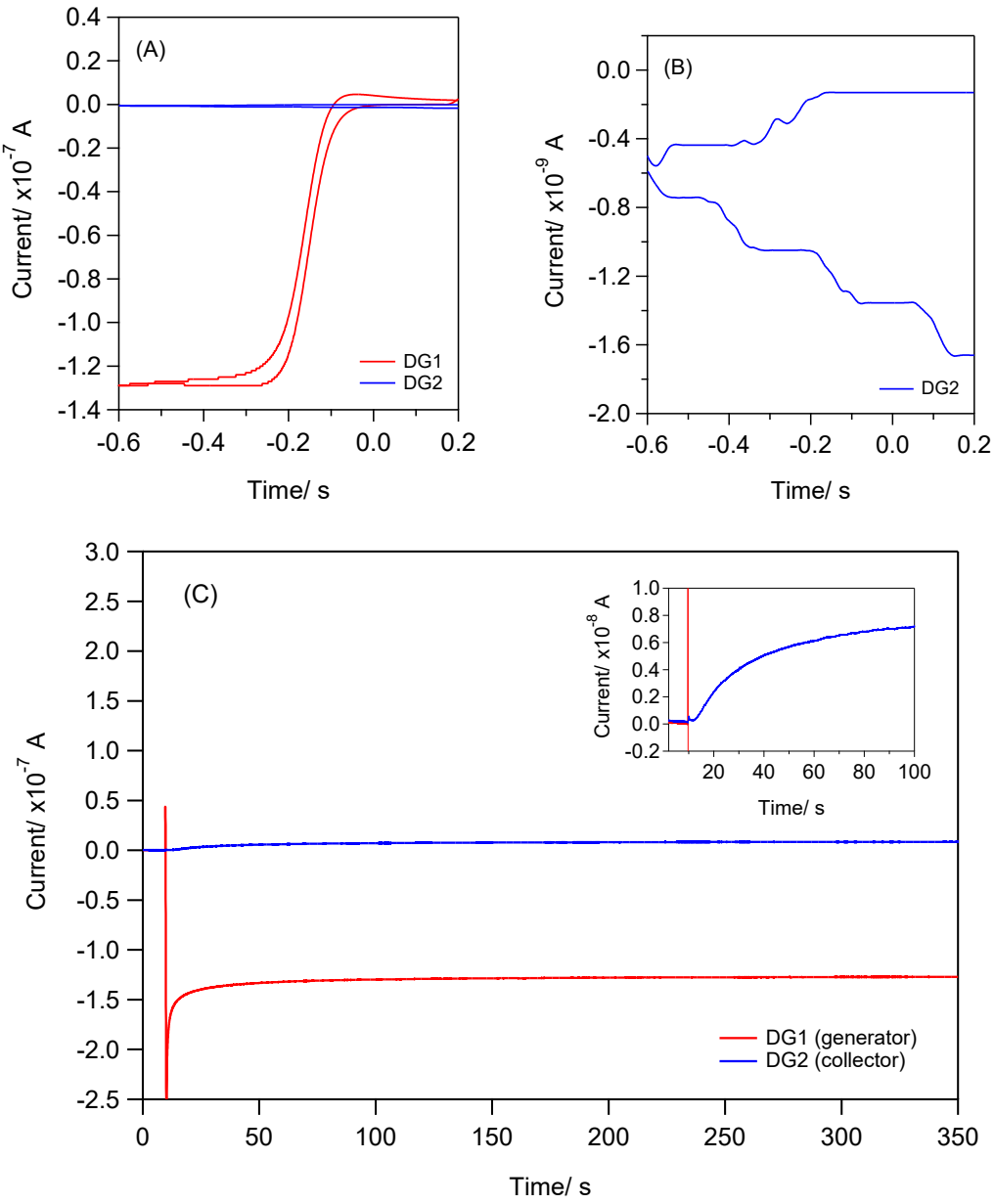

Figure 2.23 i-V curves of generation–collection process using 10 mM $Ru(NH_3)_6Cl_3$ in 1M KCl from dual gold sensor under 10 mV/s scan rate of both electrodes (A) and collector DG2 alone (B). Potential was scanned from 0.2 to -0.6 V at DG1 (red) where 0.2 V was fixed for ring DG2 (blue). Picture (C) obtained from fixed potential at -0.6 and 0.2 V at DG1 and DG2, respectively, with the inset of first 100s of recorded collection current.

2.5 Conclusion

The generator – collector systems were successfully developed and investigated through the fabricated ring-disc and disc-disc electrodes. Ring-disc electrode was fabricated using C-fibre and metal wire. Platinum (Pt) ring-disc microelectrode was practically fabricated by using the PVD method as previously reported by our research group [16]. Carbon ring-disc electrode was customised by using C-fibre disc and conductive carbon paint as the ring electrode. Dual disc electrode was effectively produced using known diameter of insulated metal wire (gold or platinum) or C-fibre. The fabricated electrodes were characterised and applied as a sensor for generator – collector system and the standard redox species were selected to test as a model.

The fabricated sensors were characterised and investigated using imaging technique (SEM) and electrochemical method to define both electrode geometry and electrode behaviour. SEM images revealed electrode size, geometry and imperfection which is mainly resulted from the fabricated process. Electrochemical characterisation was used for investigation on individual electrode and generator – collector process on the reversible redox couple which are ferrocene derivatives, ruthenium hexaammine (III/II) and ferro/ferricyanide. Experimental data showed that the effects of geometry, size and generator current density the uniformity of the flux. The sensor performance in both the steady state and transient mode were compared with numerical and analytical models as previously described by our research group [28]. Good agreements were achieved for metal ring-disc and disc-disc electrode compared to C-ring and C-fibre electrode where the imperfection is extensively presence.

Results from the tests undertaken in specially built flow cells equipped with the Pt ring-disc sensor for end column detection demonstrated the viability for the application in flow injection analysis (FIA) and LC detection. Reasonable agreement was found between experimental data and numerical model, convincing that the generation – collection process can be implemented from our fabricated generation – collection devices as ring-disc and disc-disc electrode [6, 7].

References

1. Albery WJ, Hitchman ML: **Ring-disc electrodes**. Oxford: Clarendon Press; 1971.
2. Chen Y, Pepin A: **Nanofabrication: Conventional and nonconventional methods**. *Electrophoresis* 2001, **22**(2):187-207.
3. Niwa O, Morita M: **Carbon film-based interdigitated ring array electrodes as detectors in radial flow cells**. *Analytical Chemistry* 1996, **68**(2):355-359.
4. Niwa O, Morita M, Solomon BP, Kissinger PT: **Carbon film based ring-disk and split-disk dual electrodes as detectors for microbore liquid chromatography**. *Electroanalysis* 1996, **8**(5):427-433.
5. Liu ZM, Niwa O, Kurita R, Horiuchi T: **Carbon film-based interdigitated array microelectrode used in capillary electrophoresis with electrochemical detection**. *Analytical Chemistry* 2000, **72**(6):1315-1321.
6. Harvey SLR, Parker KH, O'Hare D: **Theoretical evaluation of the collection efficiency at ring-disc microelectrodes**. *Journal of Electroanalytical Chemistry* 2007, **610**(2):122-130.
7. Harvey SLR: **Developing an electrochemical tissue perfusion sensor**. Imperial College London; 2008.
8. Zhao G, Giolando DM, Kirchhoff JR: **Chemical vapor deposition fabrication and characterization of silica-coated carbon fiber ultramicroelectrodes**. *Analytical Chemistry* 1995, **67**(15):2592-2598.
9. Kovalcik KD, Kirchhoff JR, Giolando DA, Bozon JP: **Copper ring-disk microelectrodes: fabrication, characterization, and application as an amperometric detector for capillary columns**. *Analytica Chimica Acta* 2004, **507**(2):237-245.
10. Liljeroth P, Johans C, Slevin CJ, Quinn BM, Kontturi K: **Disk-generation/ring-collection scanning electrochemical microscopy: Theory and application**. *Analytical Chemistry* 2002, **74**(9):1972-1978.
11. Liljeroth P, Johans C, Slevin CJ, Quinn BM, Kontturi K: **Micro ring-disk electrode probes for scanning electrochemical microscopy**. *Electrochemistry Communications* 2002, **4**(1):67-71.
12. Wang ZH, Cohen SA: **Hollow cathode magnetron**. *Journal of Vacuum Science & Technology A* 1999, **17**(1):77-82.
13. Thornton JA: **Magnetron sputtering - Basic physics and application to cylindrical magnetrons**. *Journal of Vacuum Science & Technology* 1978, **15**(2):171-177.
14. Kaneko T, Nittono O: **Improved design of inverted magnetrons used for deposition of thin films on wires**. *Surface & Coatings Technology* 1997, **90**(3):268-274.
15. Amberg M, Geerk J, Keller M, Fischer A: **Design, characterisation and operation of an inverted cylindrical magnetron for metal deposition**. *Plasma Devices and Operations* 2004, **12**(3):175-186.

16. Harvey SLR, Coxon P, Bates D, Parker KH, O'Hare D: **Metallic ring-disc microelectrode fabrication using inverted hollow cylindrical sputter coater**. *Sensors and Actuators B: Chemical* 2008, **129**(2):659-665.
17. Wells OC: **Scanning electron microscopy** New York: London : McGraw-Hill; 1974.
18. Trasatti S, Petrii OA: **Real surface area measurements in electrochemistry**. In: *Pure Appl Chem.* vol. 63; 1991: 711.
19. Lindsay AE, Greenbaum AR, O'Hare D: **Analytical techniques for cyanide in blood and published blood cyanide concentrations from healthy subjects and fire victims**. *Analytica Chimica Acta* 2004, **511**(2):185-195.
20. Bitziou E, Rudd NC, Unwin PR: **Microjet ring electrode (MJRE): Development, modelling and experimental characterisation**. *Journal of Electroanalytical Chemistry* 2007, **602**(2):263-274.
21. Trasatti S, Petrii OA: **Real surface area measurements in electrochemistry**. *Pure Appl Chem* 1991, **63**(5):711 - 734.
22. Macpherson JV, Unwin PR: **Radial flow microring electrode: Development and characterization**. *Analytical Chemistry* 1998, **70**(14):2914-2921.
23. Fried I: **The chemistry of electrode processes**. London: Academic Press; 1973.
24. Gandhi SI: **Lab-on-a-chip device to quantify buffer capacity of blood**. In: *Bioengineering.* vol. PhD thesis: Imperial College London; 2015.
25. Wang Y, Laborda E, Crossley A, Compton RG: **Surface oxidation of gold nanoparticles supported on a glassy carbon electrode in sulphuric acid medium: contrasts with the behaviour of 'macro' gold**. *Physical Chemistry Chemical Physics* 2013, **15**(9):3133-3136.
26. Rodriguez JMD, Melian JAH, Pena JP: **Determination of the real surface area of Pt electrodes by hydrogen adsorption using cyclic voltammetry**. *J Chem Educ* 2000, **77**(9):1195-1197.
27. Bard AJ, Faulkner LR: **Electrochemical Methods: Fundamentals and Applications**, 2nd edn. New York; Chichester Wiley; 2000.
28. Bell CG, Seelanan P, O'Hare D: **Microelectrode generator-collector systems for electrolytic titration: theoretical and practical considerations**. *Analyst* 2017, **142**(21):4048-4057.

Chapter 3:

Electrochemical Methods for Biomolecule Detection

3. Biomolecule detection

Biomolecule refers to a molecule produced from a living organism. Typical examples include small molecules such as vitamin, hormone, neurotransmitter and metabolite as well as a group of large polymeric molecules, for examples lipids, polysaccharides, peptides and proteins. Numerous works of biomolecule determination have been reported for a particular group of species related to their interested application. In our work, the focus is on amino acids, peptides and proteins.

3.1 General approaches for amino acid, peptide and protein

In order to analyse a mixture of amino acids and proteins, a separation method is required. Several separation techniques have been developed and are available for qualitative and quantitative analysis. In protein analysis, gel electrophoresis coupled with mass spectrometry is normally used [1]. However, the problems of this method include low reproducibility, cost and laborious time-consuming preparation. An alternative technique with good sensitivity is the use of protein microarrays. Protein microarrays involve detection of the target protein with highly selective ligand attached on the surface as an array [2]. The protein microarray method has drawbacks due to the difficulties involved in selection of suitable selective ligand and the requirement of typically fluorescent labelling. Typically, detection of proteins are done by UV-visible detection or fluorescence detection of their derivatives in a flowing system such as flow injection analysis (FIA), capillary electrophoresis [3, 4] and high-performance liquid chromatography (HPLC) [5, 6]. Since UV-visible detection has poor sensitivity for low concentration of analyte and fluorescence detection is applicable for only molecules containing a fluorophore, derivatisation is required to enhance the sensitivity prior to protein detection. Either pre-column or post-column derivatisation with a labelling chemical agent can be applied. Although lower detection limits can be obtained, the process for derivatisation can be laborious and make the experiment more complicated. Besides, the determined amount of amino acids and peptides depend on the reactivity and stability of the derivatising agent; there is no guarantee that different amino acids, for example, will show the same reaction yield. An alternative method with a simple set up, good sensitivity and fast analysis time is electrochemical detection.

Electrochemical detection has been reviewed and shown to be a suitable analytical measurement of amino acid in mobile electrolytes for FIA and after HPLC separation [7]. In most work, microelectrodes were used as an electrochemical sensor providing an electrical signal that scales with the quantity of analytes. The response is straightforward and the technique is also suitable for a miniaturised system. In the beginning, we will focus on particular amino acid and peptide detection. Since amino acids and peptides are the basic units of proteins, protein determination can be developed based on measurement of its monomers.

3.2 Amino acid detection with electrochemical methods

In this section, electrochemical methods applied for amino acid and peptide detection are reviewed. Since, amino acid is a small unit of peptide and protein, study of non-complex molecule of amino acid could lead to different applications for biomolecule measurement. Detection of amino acids will be principally addressed. Twenty standard amino acids can be classified into groups based on chemical properties. The chemical structures of standard amino acids are listed in Figure 3.1, where the chemical property of each amino acid effectively governed by their substituted (R) group. Most amino acids contain an aliphatic or aromatic group, where their chemical structures exhibit a low ability of electron transfer. With lack of electrochemically active groups in the molecule, electrochemical detection of amino acid detection is hard to achieve [8, 9]. To overcome this limitation, different approaches have been developed. Applicable methods include pre-column or post-column derivatisation of amino acid with reductive, oxidative, photochemical or chemical conversion reagents. Although application of derivatising agent can provide adequate sensitivity and selectivity of amino acid detection, the process requires extra instrumentation for sample handling systems [10-12]. Moreover, adding the derivatising agents can lead to peak broadening and dilution of the analytes concentration while separation is continuing [13]. Modified electrodes such as nickel oxides, copper, glassy carbon and composited electrode have been used for *in situ* chemical reaction at the electrode surface. The modified electrodes simplify the instrumentation and remove the need for additional reagents.

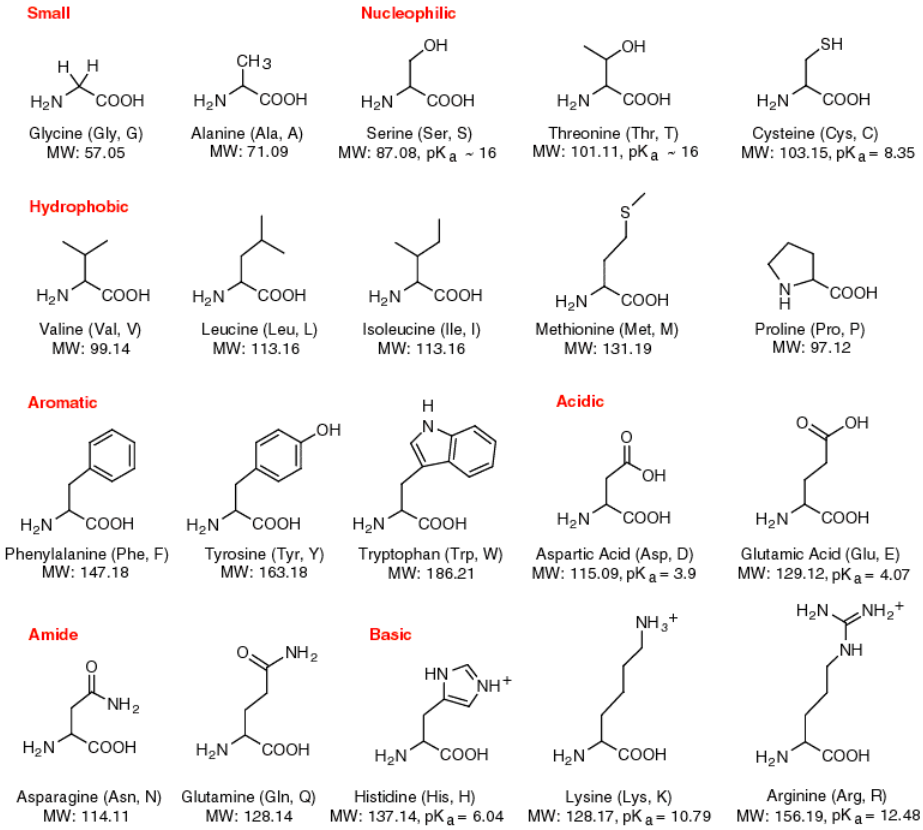

Figure 3.1 A schematic picture of standard amino acid structures, adapted from [14].

However, the modified electrodes may be more selective and sensitive for specific amino acids giving a differential response to different amino acids. This is not an ideal approach. Dual electrodes system has been introduced as an alternative way for detection of amino acid. This system contains two working electrodes either with the similar geometry (disc-disc or band-band electrodes) or different geometry. To operate the dual electrode, the first electrode generates a species to be detected at the second electrode. The non-electroactive analytes, such as amino acids, can react with the generated species. Change in current is observed and related to the analyses' concentration. Indirect detection of amino acid is then achieved. Previous work on dual electrodes with amino acid titration claim the advantages of versatility and sensitivity. Generally, titration of amino acids has been done using bromine in both acidic and basic solution [9, 15-17]. In our work, indirect detection of amino acid by titration using bromine species will be investigated using our dual electrode sensor. More details and experimental approaches are discussed in the next section.

3.3 Generation –collection detection

Titration using dual electrodes is a simple technique and capable of detecting non-electroactive species under a suitable chemical reaction. The general approach is illustrated in Figure 3.2. A species is generated at one electrode called titrant (T). This electrode has functioned as the generator. While the generation rate of titrant is controlled by the generator, the analyte (A) in solution is transported to the electrode surface by convection and diffusion. A is then titrated rapidly by T in a diffusion layer of the electrode surface. Titration which is quantitatively proceeding in the vicinity of electrode can be called diffusion layer titration [18]. Consequently, excess T is then reversed back to reactant species (R) by the downstream electrode called collector. This process is classified as an indirect detection and the signal change from the depletion of titrant by analyte of interest will be related to analyte concentration. Diffusion layer titration using dual electrodes has been reported for amino acid and protein detection in flow injection analysis [19], chromatographic separation [16, 17, 20, 21] and electrophoretic separation [22].

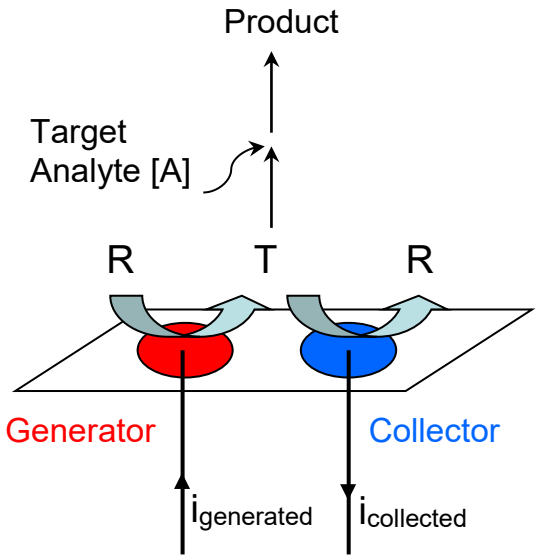

Figure 3.2 A schematic picture of the titration process where target analyte (A) is titrated with the generated titrant (T). The excess amount of T will be collected and turn to initial reactant (R) after titration is completed.

3.4 Indirect detection of amino acid

3.4.1 Ring – disc titration

The ring-disc electrode is one of the dual electrodes used for indirect detection of amino acids in a system with controlled hydrodynamic or electrophoretic flow. Generally, electrogenerated bromine in either acidic or basic condition is carried out for titration of amino acids. Considering a controlled flow system, bromine is generated at the upstream electrode by oxidation of bromide and collected at the downstream electrode in a dual electrode system. The amino acid (A) is titrated with electrogenerated bromine ($T_{generated}$) on the upstream electrode. The remaining amount of electrogenerated bromine (T_{excess}) is detected at the downstream electrode and the signal change is proportional to the amount of the titrated amino acid. Albery *et al*. have reported on this system for identification of proteins in HPLC using ring-disc titration [9, 15]. Their work introduced the idea of employing the ratio of bromine number to identify the type of protein and to measure protein concentration. Schematic reactions for amino acid titration in both acidic and basic conditions are shown in Figure 1.3. The success of this method depends on a fast reaction of amino acid and electrogenerated bromine species [9, 23]. If the reaction is very slow, the generated bromine will reach the downstream electrode without reacting with target amino acid.

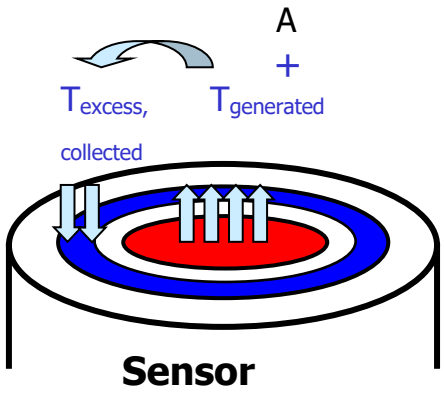

Figure 3.3 A schematic picture of the titration process on the ring-disc electrode.

3.4.2 Mode of titration

The titration of amino acid with electrogenerated bromine in a controlled flow system has been performed under the flow analysis described in Section 2.4. In theory, the titration can undergo both acidic and basic solution. Titration conditions and reactions are presented in figure 3.3. Titrations depend on a fast reaction between target amino acid and electrogenerated bromine, where k is greater than 10^6 $M^{-1}s^{-1}$ [9, 23]. If the N atom of an amine group ($-NH_2$) is protonated, the reaction rate will be very slow for this technique. The amount of generated bromine consumed by amino acid will also depend on pH. From the titration of protein with electrogenerated bromine, it was found that bromination of $-NH_2$ group is slow compared to the time taken by bromine to travel from the generator to the collector at pH 5. On the other hand, most amine groups are not protonated in pH 9.2 which result in a fast reaction of N-H with OBr^- to form N-Br bond [9]. When the titration is done at pH 9.2, higher number of electrogenerated bromine species are consumed which make the technique more sensitive.

Figure 3.4 Reactions of amino acid titration with electrogenerated bromine in acidic and basic condition, adapted from Albery *et al.* [9].

Method and Materials

In our work, amino acid titration was performed under basic condition which predicts better sensitivity. Selected amino acids; glycine (Gly), alanine (Ala) and methionine (Met) were obtained from Sigma-Aldrich. Stock solutions of 2.5 M potassium bromide, KBr, (Fluka) and 10 mM amino acids were prepared using the MilliQ water. Diluted concentrations of each amino acid were dissolved in 25 mM sodium tetraborate decahydrate, $Na_2B_4O_7.10H_2O$ pH 9.2 (Sigma-Aldrich) and 0.5 M KBr. pH adjustment was achieved using diluted hydrochloric acid, HCl (Sigma-Aldrich). All solutions were

dissolved in MilliQ water, otherwise stated. A multichannel potentiostat CHI model 1030 (CH Instruments inc., Texas) was operated to control the voltage at the disc and the ring in an electrochemical cell containing a large Pt mesh as a counter electrode and Ag|AgCl reference electrode. Commercial Pt electrodes with diameter of 2 mm and 25 μm were used for standard measurements. Prior to each experiment, the ring-disc microelectrode was sonicated in dilute aqueous Decon solution, warm water, methanol, and then warm water under ultrasonic bath, respectively. If the electrode surface was found contaminated, it was then electrochemically cleaned by an applying up to 50 cycles of potential from -1.5 V to 1.5 V (vs SCE) at 100 mV/s scan rate in 0.5 M H_2SO_4 solution. Electrode polishing with aqueous alumina slurry is required for a permanent electrode fouling or where visible damage is detected. In flow experiments, background electrolytes were pumped into flow cell by the HPLC pump (model 1050, Hewlett-Packard). Injection volumes were varied from 5 to 20 μl using the equipped auto-injector (Hewlett-Packard). PDMS flow cell placed with Ag|AgCl reference electrode, Pt counter electrode and ring-disc microelectrode were connected to the HPLC pump and used as electrochemical detection system. The ring-disc microelectrode was adjusted to the centre position in the flow channel using a micromanipulator. After the collection efficiency reached to the lowest value at fixed flow rate, ring-disc electrode is assumed to be at the centre of the channel and the detection process is prompt.

Results and discussion

Electrochemical indirect detection of amino acid was initially tested with KBr system using 50 μm Pt/Pt ring-disc electrode. Cyclic voltammograms were illustrated in figure 3.4. It can be seen that no well-behaved reduction or oxidation potential was observed between 0.5 to 0.8 V (vs SCE). Positive current was built up and clearly noticed after 0.8 V which is resulting from oxidation reaction of Br^- ion. Both Pt disc and Pt ring are able to generate OBr- species. Reduction of electrogenerated OBr^- is expected from negative current while large capacitance (or pseudocapacitance) is observed on the reverse scan. Flow injection analysis of amino acid was then investigated.

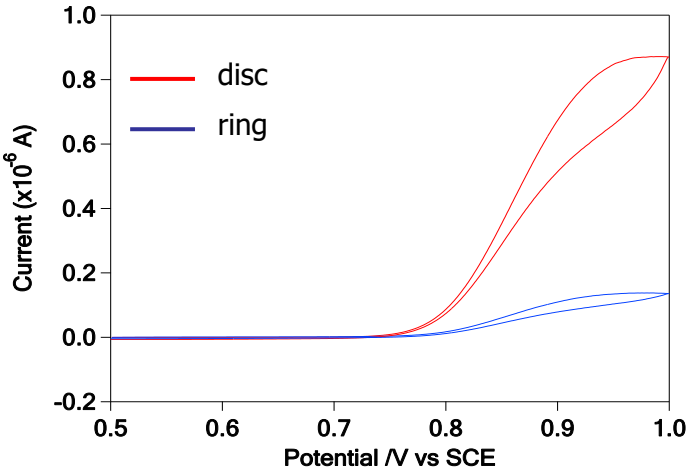

Figure 3.5 Cyclic voltamograms of 0.5 M KBr in 25 mM borate buffer pH 9.2.

With our ring-disc microelectrode, indirect detection of amino acids was performed by titration with hypobromite (OBr^-) from the upstream electrode in basic condition (borate buffer pH 9.2). Gly, Ala and Met were primarily tested. During titration process, the current signal obtained from the downstream electrode was degreased as the amount of OBr^- decreased at the vicinity of electrode. After the amino acid was completely titrated by the electrogenerated OBr^-, the CE fraction of unreacted OBr^- was collected at the downstream electrode resulting in an increase in the reductive current. Because the detection is applied under a flow system, a band of injected amino acid will move along the tube under parabolic flow profile. The injected band of amino acid will then react with the electrogenerated OBr^- once it hits to a surface of the sensor. Peak current is expected from the reaction the injected amino acid with electrogenerated OBr^-. Peak area will be related to the concentration of injected amino acid. Among the tested amino acids, only Met was successfully titrated providing a noticeable peak current. Consecutive injections of 10 mM Met with electrochemical detection using 50 μm Pt/Pt ring-disc microelectrode were carried out. The results are promising and recorded data are shown in Figure 3.5.

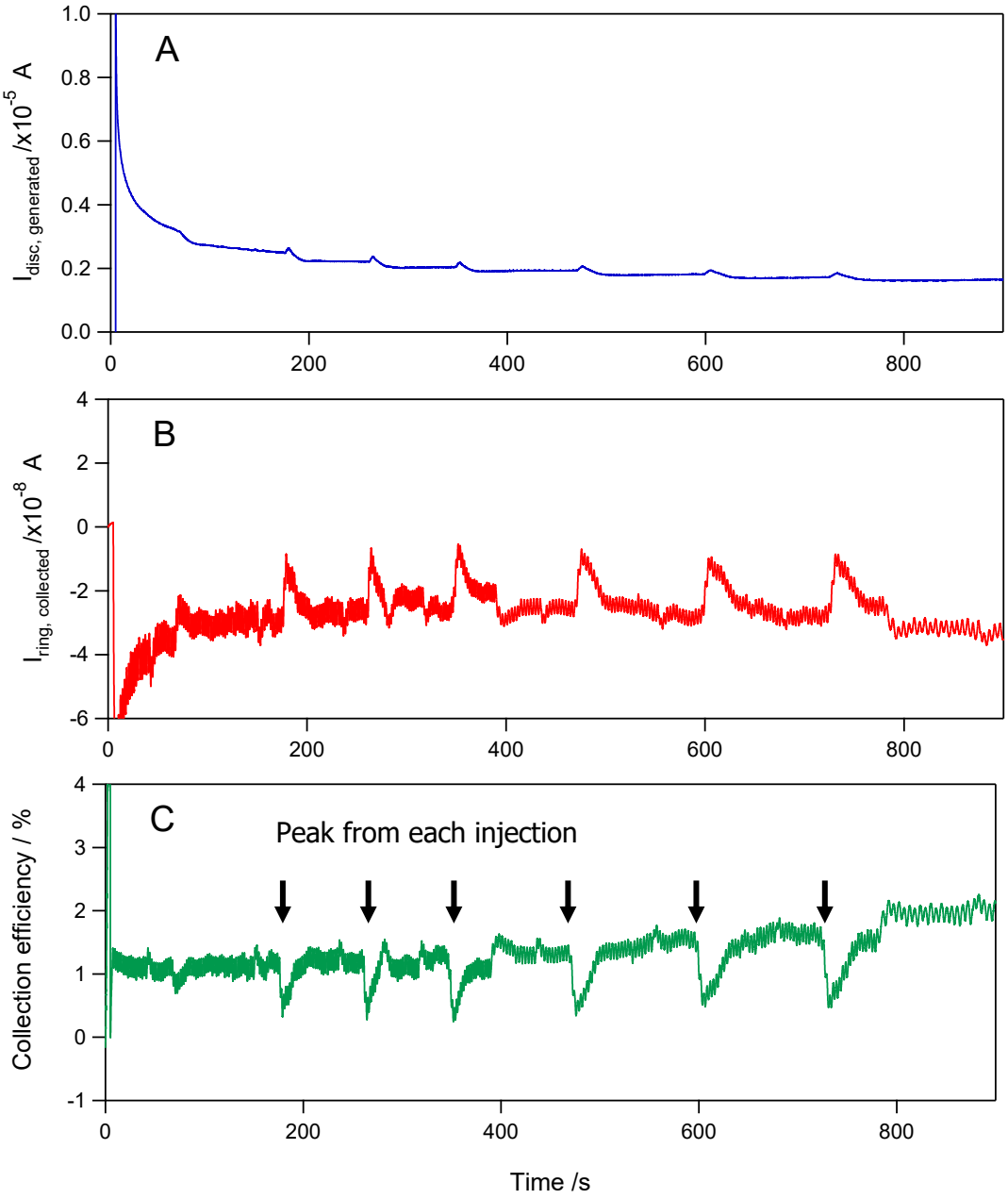

Figure 3.6 Detection of 1.0 mM methionine in 0.5 M KBr and 25 mM borate buffer; flow rate 1 ml/min. Disc generator-ring collector mode, E_{disc} 0.85 V and E_{ring} 0.50 V.

Although electrochemical detection of amino acid with ring-disc microelectrode is demonstrated, the signal to noise ratio was relatively low. As shown in Figure 3.5, the measured S/N ratios of the collection efficiency are approximately 3. There is comparably large of noise and fluctuations from HPLC pump plus limitation arising from a thin ring thickness of Pt and the resulting small current. The electrical noise and fluctuation from the pump could be addressed by the use of faraday cage and mathematical noise filtration [24, 25]. A large drop of generating current was observed

in the first 100 s with a continuous decrease of current after each peak of amino acid titration. The cause of this is obscure.

3.4.3 Sensor fouling

One of the most common and challenging problems in electrochemical sensing is fouling of the electrode surface. In general, working on biomolecules can lead to biofouling. Biofouling is caused by the adsorption of biomolecules onto electrode surface, reducing the sensor response. Once the electrode surface has been contaminated and blocked, the diffusion of analyte and the conductivity of the electrode can be interrupted. Electrocatalytic sites are up to adsorption, reducing activity. In addition, partitioning of the analyte or Donnan exclusion could also occur. Whatever the dominant phenomenon, empirically a decrease in signal is observed. Factors that could influence sensor fouling include electrode material, electrode geometry, applied voltage and sample matrix. Sensor fouling also occurred in our work and showed significant effect to our detection. After a number of tests of amino acid detection, sensor performance on generation-collection process is dropped and a poor inter run repeatability was obtained. The main causes which results in sensor fouling could arise from the adsorptions of Br^-, amino acid and/or product of amino acid titration onto Pt surface. Bromide ions have been found to adversely affect limit of detection and dynamic linear range of amino acid detection using carbon film ring-disc electrode [26]. In addition, bromide adsorption on a Pt crystal disc electrode is simultaneously presenting and blocking the Pt surface sites [27, 28]. In our experiment, the fouling was characterised by measuring the current response using standard redox ruthenium (III)/(II) solution. Electrochemical characterisation of 10 mM $Ru(NH_3)_6Cl_3$ with different flow rates was performed after the titration of amino acid. Figure 3.6 shows the current change with applied flow rates measured by amperometric detection of 10 mM $Ru(NH_3)_6^{3+}$ in 1 M KCl after the experiment of amino acid detection. A drop of collection efficiency and sluggish change in current are noticeable after a number of consecutive runs on amino acid titration. Up to approximately 20% drop of the detection sensitivity was observed.

As seen in Figure 3.6B, the fouling shows greatly effect on the ring electrode. This is probably due to the size of the ring which is very small compared to the disc. When the Br^- ion is oxidised to OBr^- ion at the disc, it will then be reduced to Br^- at the ring, which can lead to the bromide adsorption on the Pt surface. If the electrode surface is blocked by the bromide, the sensitivity will drop. Rate of titration reaction is decreased because less species can continue electron transfer at the electrode surface. The electrode fouling effect of our sensor was further investigated by studying on CV experiment. CV conditions of our working buffer was prepared and applied to measure for the effect of KBr.

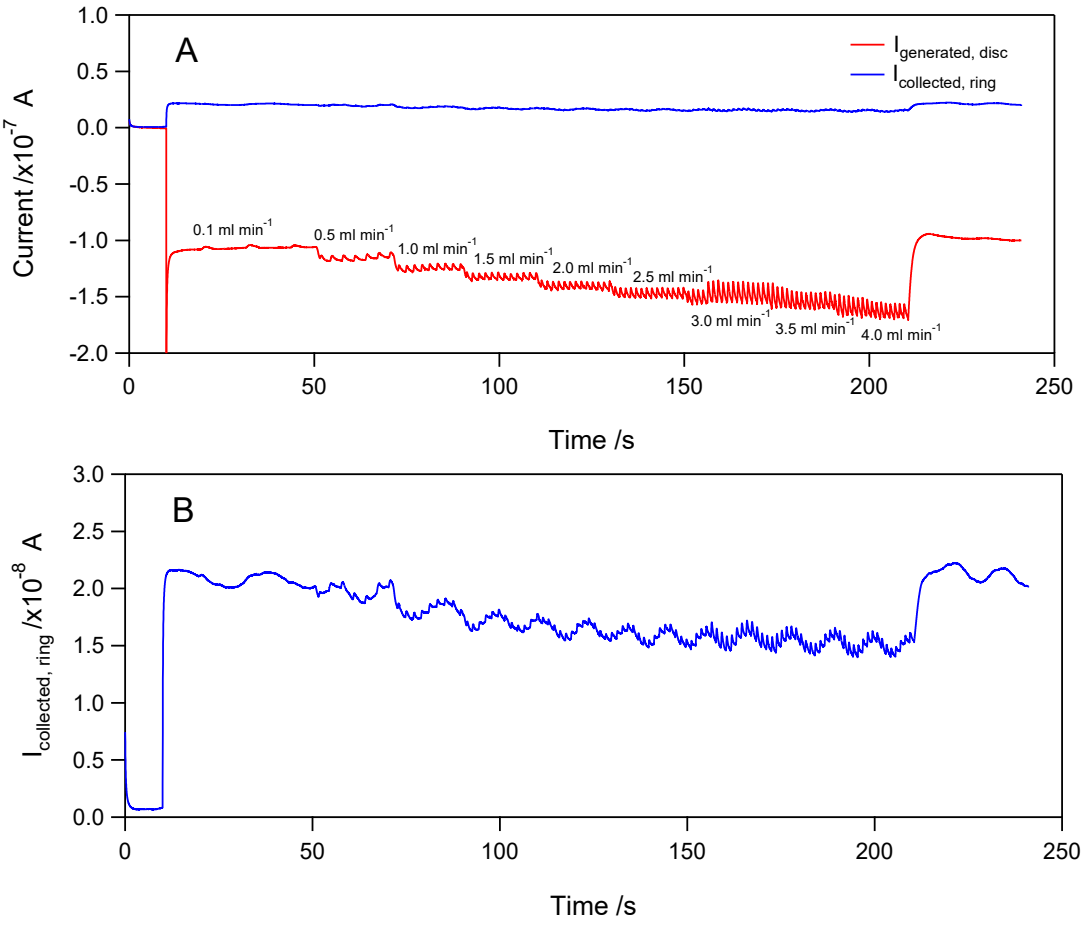

Figure 3.7 Amperometric detection of 10 mM $Ru(NH_3)_6Cl_3$ in 1 M KCl with different flow rates (after amino acid titration). The potentials of disc generator mode were set at -0.4 V for disc and 0.1 V for ring electrode versus Ag/AgCl. Experiments were obtained from 50 μm Pt disc/Pt ring sensor.

Successive 100 cycles of CV were performed in a non-flow system. Drop of currents in both generator and collector were clearly noticed after a few scans. In figure 3.7, the currents from generator (disc) and collector (ring) were extracted from specific CVs of 0.5 M KBr. Approximately 20 % drop of the limiting currents from disc and ring electrodes were observed. It can be concluded that the major cause of sensor fouling is from the bromine adsorption. Since an outer sphere redox couple was affected by this phenomenon, the significant effect must be a diffusional blocking or an insulation of large areas of the electrode, rather than losses of catalytic activity. The problem of fouling may be acceptable as long as enough sensitivity of sensor and adequate CE remain achievable. If sensors are not well behaved or functioned any longer, electrochemical cleaning and electrode polishing will be introduced.

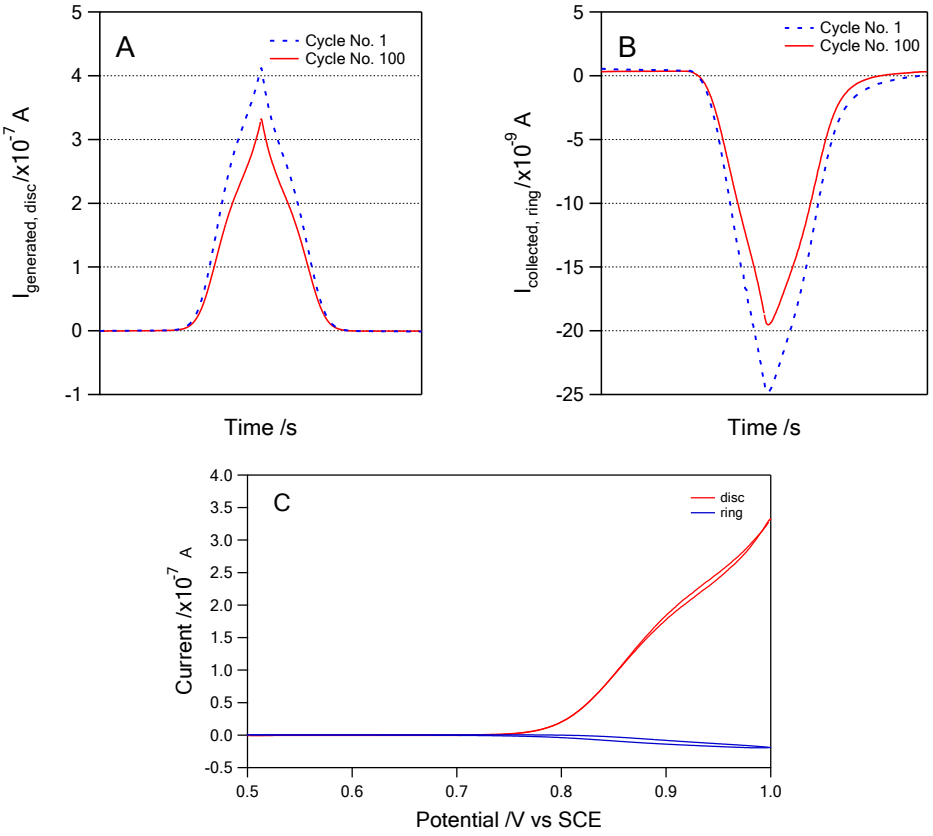

Figure 3.8 Successive runs of 100 cycles CV with 0.5 M KBr in 25 mM borate buffer, pH 9.2 using 50 µm Pt/Pt ring-disc sensor. The potential of disc was scanned from 0.5 to 1.0 V and fixed at 0.5 V for ring electrode. Data shown were selected and exported from the first and last cycles, represented the generating current (A) and collecting current (B) with time. CVs of generator and collector were shown (C).

3.5 Permanganate titration with generation-collection process

From previous section, titration of amino acid under the flow manifests a sensitivity decrease due to sensor fouling. Another titration based on generation-collection process has been tried out for a less complicated system. Classic titration of permanganate ion (MnO_4^-) with a standard redox species is a suitable application for titration sensing using the ring-disc sensor.

Method and materials

In this system, generation and collection processes are applied to standard $Fe^{3+/2+}$ redox couples. 50 mM $NH_4Fe(SO_4)_2$ and 10 mM $KMnO_4$ were prepared in acidic solution of 0.5 M H_2SO_4. The $KMnO_4$ solution was kept at low pH to prevent formation of MnO_2 [29]. Electrogenerated Fe^{2+} from the generator will be titrated with existing MnO_4^- in the solution. Less Fe^{2+} is then detected at collector, which results in a decrease in the collection current and collection efficiency. A schematic diagram of titration and involving reactions are shown in figure 3.8.

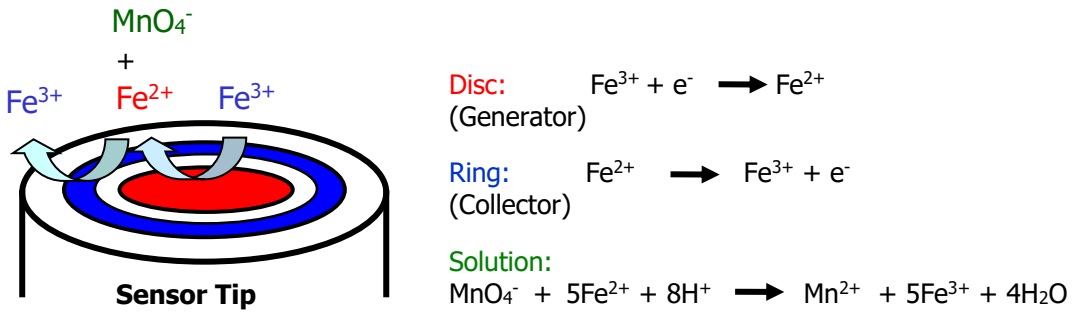

Figure 3.9 Schematic picture and reactions of MnO_4^- titration with electrogenerated Fe^{2+} on ring-disc electrode, adapted from [29].

Results and discussion

Prior to the titration, the collection efficiency of the tested system was measured in a non-flow solution. The collection efficiency (CE) was 17.6% in the absence of MnO_4^-. Although approximately 40% drop of CE was obtained from this system compared to a system of standard ruthenium (III), this is not entirely unexpected since the ferrous/ ferric reaction is an inner sphere reaction and sensitive to surface chemistry [30]; however, the electrochemical generation-collection process was well performed, as shown in figure 3.9. The decrease in CE could be influenced by the imperfections in the electrode (such as a recess). Cleaning and polishing methods were attempted but the theoretical CE value was not achieved. The sensor has been continued to perform on the analysis of MnO_4^- under the flow system.

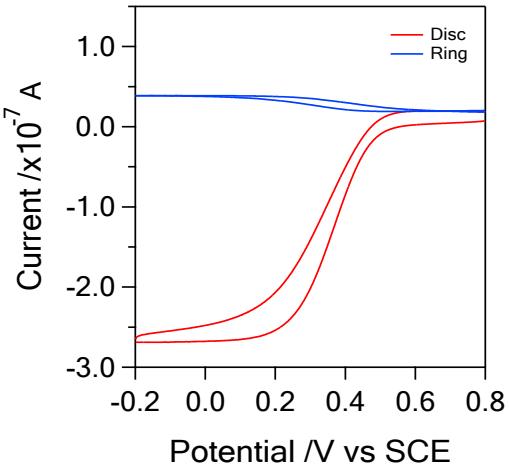

Figure 3.10 i-V curves of 50 mM $NH_4Fe(SO_4)_2$ in 0.5 M H_2SO_4 obtained from scanning of disc potential from 0.8 to -0.2 V and a fixed ring potential at 0.8 V using 50 mm Pt/Pt ring-disc electrode.

Flow injection analysis

A 10 mM aliquot of $KMnO_4$ was transferred to a vial. 10 µl of analyte from the vial was injected by auto-sampler injector (Hewlett-Packard) and then pumped to the electrochemical flow cell, as previously described in section 3.4.2 and the currents at Pt disc and Pt ring electrodes from the 50 µm Pt disc/Pt ring electrode were recorded. Amperometric detection of permanganate ion (10 mM $KMnO_4$) were carried out under the flow system. Plots of %CE versus time were determined using the current ratio from

generator and collector. Peaks from consecutive injections of 10 mM $KMnO_4$ under the flow rate of 0.5 ml/min are shown in Figure 3.10A. Further peak detection of the injected 10 mM $KMnO_4$ with different flow rates of 0.5 and 1.0 ml/min were shown in Figure 3.10B. The results show a better sensitive detection with higher collection efficiency, compared with amino acid titration. Good repeatability was observed with fewer drops in the monitored currents. Change in CE from MnO_4^- titration under varied flow rate was also found to be consistent. %CE obtained from 1.0 ml/min was lower than those obtained from 0.5 ml/min, which is in qualitative agreement with the theoretical prediction. Generation-collection process worked well with less concern arising from electrode fouling. Although amino acid detection with ring-disc electrode were not successfully progressed, proof of principle has been demonstrated for biomolecule detection with generation-collection type of sensor.

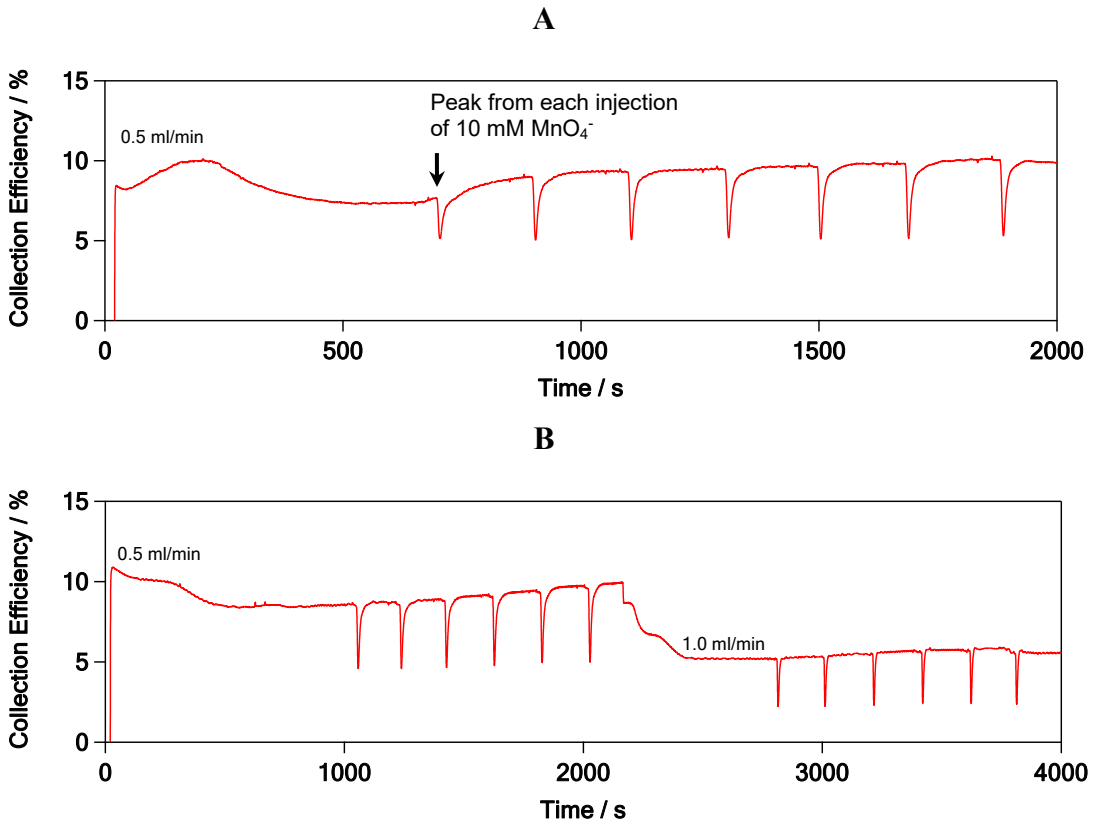

Figure 3.11 Plots of Collection Efficiency (%) versus time obtained from 10 µl injections of 10 mM $KMnO_4$ with the system of 50 mM $NH_4Fe(SO_4)_2$ in 0.5 M H_2SO_4 under flow rate 0.5 ml/min (A) and with 1.0 ml/min (B). Disc and ring potentials were fixed at -0.2 V and 0.8 V, respectively. Detection sensor is 50 µm Pt disc/Pt ring electrode.

3.6 Electrochemical detection of peptides

3.6.1 Peptide-biuret complex detection

The simple detection of peptides by electrochemical methods can be carried out using biuret reagent. Biuret reagent is a basic solution of copper (II) containing tartrate as a stabiliser. Peptides can form Cu(II)-peptide complexes using amine groups nitrogen backbone as electron donors to Cu(II) (see Figure 3.11). Many articles on the electrochemical detection of peptide-biuret complex have been reported by Weber's group [31-36]. The detection of peptides was achieved by monitoring the electrochemical signal from the oxidation of Cu(II)-peptide complex. Because this complex can undergo reversible redox reactions, dual electrode electrochemical detection can be used. The Cu(II)-peptide complex is oxidised at the first electrode, the generator, to the Cu(III)-peptide complex. The second electrode performs as a collector, reducing the product from the generator. The ratio of the current at the collector to the current of the generator is defined as collection efficiency. The selectivity of each peptide-biuret complex can be determined from the value of the collection efficiency.

Many publications on electrochemical detection of peptide with biuret reagent has been reported [31-33]. Separation methods such as HPLC and CE were carried out. In HPLC and CE, peptides must be derivatised to Cu(II)-peptide complex prior to detection. Either precolumn or postcolumn derivatisations with biuret reagent were performed. In the process of postcolumn derivatisation, the biuret reagent is pumped to the effluent after separation. This method yields good sensitivity among tested standard peptides. The first report of electrochemical detection using postcolumn derivatisation of small peptides with biuret reagent was reported by Warner and Weber [31].

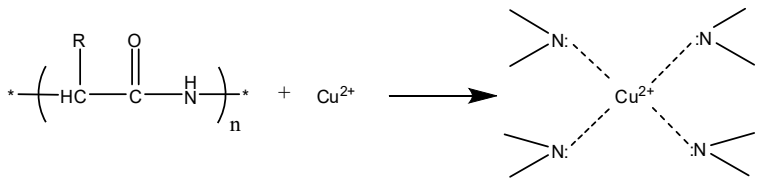

Figure 3.12 A schematic picture of Cu(II)-peptide complex, where n is the number of peptide bonds.

It was found that the biuret complex allows peptides that lack an electroactive group to be determined. Selectivity for the tested peptides can be up to 1,000 times higher compared to nonelectroactive amino acids. The collection efficiency increased with chain length for homologous peptides. Effects of medium on the complex of peptide with biuret reagent were also investigated. Since chromatography uses acidic or neutral conditions where organic solvents are present, an appropriate buffer system is required to maintain the pH in postcolumn addition [31]. The Cu(III)-peptide complex decomposed in the presence an organic solvent in the solution. Borate and phosphate buffer added in both aqueous and mixed organic and aqueous solutions led to the disappearance of the complex reduction peak. This demonstrates that the collection efficiency is sensitive to changes in solvent and buffer composition.

Tsai and Weber also studied the detection of small peptide complexes with biuret reagent and found the optimum conditions for peptide detection [32, 35]. However, shorter peptides have shorter lifetimes as a stable peptide-biuret complex. The detection at both generator and collector was poor for the dipeptides, resulting in low collection efficiency. The sensitivity strongly depends on the Cu(II) concentration and the applied potential [35]. A slight drop in sensitivity was observed at higher potential at the generator. At both high and low pH conditions, the selectivity of the detection for peptides is better with higher Cu(II) concentration.

Other effects such as temperature, biuret reaction time and column packing material were also investigated by Tsai and Weber [33]. For nonapeptide, the increasing postcolumn reaction time and temperature of the reactor led to higher detection sensitivity. They also suggested the precolumn incubation of peptides with biuret reagent can make its complex stable to both acidic and basic HPLC conditions [33]. HPLC separation using C_{18} column in acid condition and ZrO_2-polybutadiene (PBD) column were compared. The C_{18} column was used in acidic mobile phase while basic Cu(II) tartrate solution was carried out with the PBD, which is stable to base. It was found that sensitivities from electrochemical detection using these two chromatographic conditions did not differ. Their results are indicative of the stability of peptide biuret complex during the chromatographic process. The effect of operating parameters on selectivity and sensitivity was further studied. Chen and Weber worked on the major parameters such as electrode potential, ratio of the complex composition

and types of Cu(II)-peptide complex that control the detection selectivity in chromatographic separations of peptide mixtures [36, 37]. The effect of buffer types, pH, temperature, reaction time and generation potential were investigated. Selective chromatographic detection scheme for peptides was studied based on the reversible Cu(II)/Cu(III) couple. Weber *et al.* selected the model peptides triglycine (G_3), tetraglycine (G_4) and pentaglycine (G_5) to characterise the copper complex monitored by electrochemical detection using a rotating ring-disc electrode [38]. They found that the reaction of the G_3 complex was an ECE-like process while the G_4 and G_5 complexes are subjected to two consecutive CE processes. A kinetic study of complexation of N-blocked peptides with Cu(II) was also undertaken. The N-blocked peptides, which have slower reaction rate than free terminal amines, were investigated under influences of the rate law and the buffer composition [39].

Precolumn derivatisation for separation and detection of peptides was also developed [40]. Applications in protein assay [41] and peptide determination in biological environments were reported [42]. High selectivity and sensitivity were achieved. With biuret reagent, electrochemical detection offers a simple and specific method for analysing peptides.

3.6.2 Study of peptide-biuret complex with platinum and carbon electrodes

Most reports of electrochemical detection of peptide-biuret complexes have been performed using glassy carbon (GC) electrode. A system with dual GC electrode [31-33, 35] or rotating ring disc of GC disc and GC ring electrode was reported [36, 38, 43, 44]. Carbon fibre (C-fibre) electrode was introduced for detection of neuropeptides with HPLC-EC detection [40]. It was reported that the detection at C-fibre showed some differences in relative sensitivity for peptides compared to glassy carbon. This could be possibly because of the effect of modified electrode surface caused by the peptide or Cu^{2+} used in biuret reagent. The use of platinum (Pt) electrode for peptide-biuret complex is not popular. To the best of our knowledge, there is no reported of using Pt for electrochemical detection of peptide-biuret complexes.

Method and materials

The purpose of this work is to investigate and compare the detection of peptide-biuret complex with Pt, GC and C-fibre electrode. Experimental condition was repeated as previously reported in work of Weber *et al* [31]. The electrodes used were 3.0 mm GC, 2.5 mm Pt, 30 µm C-fibre and 25 µm Pt electrodes. Triglycine (G_3) was selected as a test peptide. Reaction of G_3 with biuret reagent is illustrated in figure 3.12. Interactions between Cu^{2+} ion and lone pair electron on N and O atoms in G_3 form a stable complex. The G_3 concentrations were varied from 1 to 10 mM, dissolved in biuret solution. The biuret reagent consisted of 11 mM Cu^{2+}, 33 mM tartrate and 0.52 M KOH. The ratio of Cu^{2+}:tartrate was set to be 1:3, as previously reported [36]. Stability of biuret complex was ensured with a high concentration of KOH. Cyclic voltammetry was operated by scanning the electrode potential from 0.1 to 1.0 V versus Ag|AgCl reference electrode. Between each run, electrodes were cleaned in an ultrasonic bath with surfactant, warm water, methanol and water, respectively. The electrode was then electrochemically characterized and routinely checked with standard 10 mM hexammineruthenium (III) solution until electrode characters were verified. Cyclic voltammograms of 2 mM G_3-biuret complex obtained from different electrodes are shown in figure 3.13.

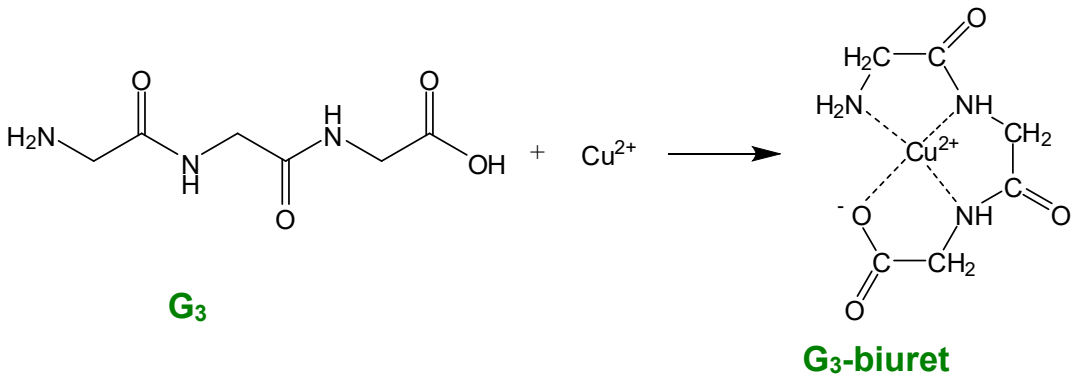

Figure 3.13 A schematic picture illustrating the reaction of G_3-biuret complex, adapted from [36].

Result and discussion

CVs from GC and C-fibre show an oxidation of Cu^{2+} to Cu^{3+} at a potential from 0.5 to 0.7 V versus Ag|AgCl. The observed shape of CV and the oxidative potential are similar to data reported in a previous study [31]. Higher potentials for Cu^{2+} oxidation state in a complex were found when Pt electrodes were used. Changes in current with different concentrations of peptide-biuret complex were then examined (Figure 3.14).

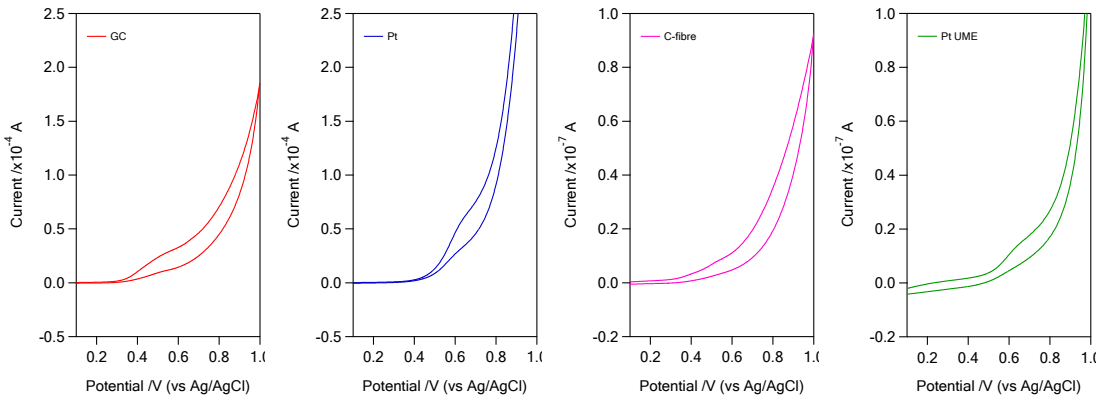

Figure 3.14 Cyclic voltamograms of G_3 – biuret complex with concentration of 2 mM G_3 using 2.5 mm glassy carbon (GC), 2 mm Pt, 30 µm C-fibre and 25 µm Pt microelectrode. Ratio of G_3:Cu^{2+}:tartrate concentration is 1:5:15.

Oxidative currents obtained from the complex increased with increasing complex concentration when using GC and C-fibre electrodes. However, currents from 1 mM and 2 mM G_3-biuret complex are not clearly different (top left). This behavior was also found in the currents obtained from C-fibre electrode with 2 mM and 5 mM G_3-biuret complex (bottom left). Experiments were repeated, no improvement was achieved. The reason behind this effect is still unclear. For Pt electrodes, changes in current were not related to Cu^{2+} or complex concentration. With more comprehensive response of carbon-type electrode for G_3-biuret complex, C/C ring-disc electrode will be focused on generation-collection detection.

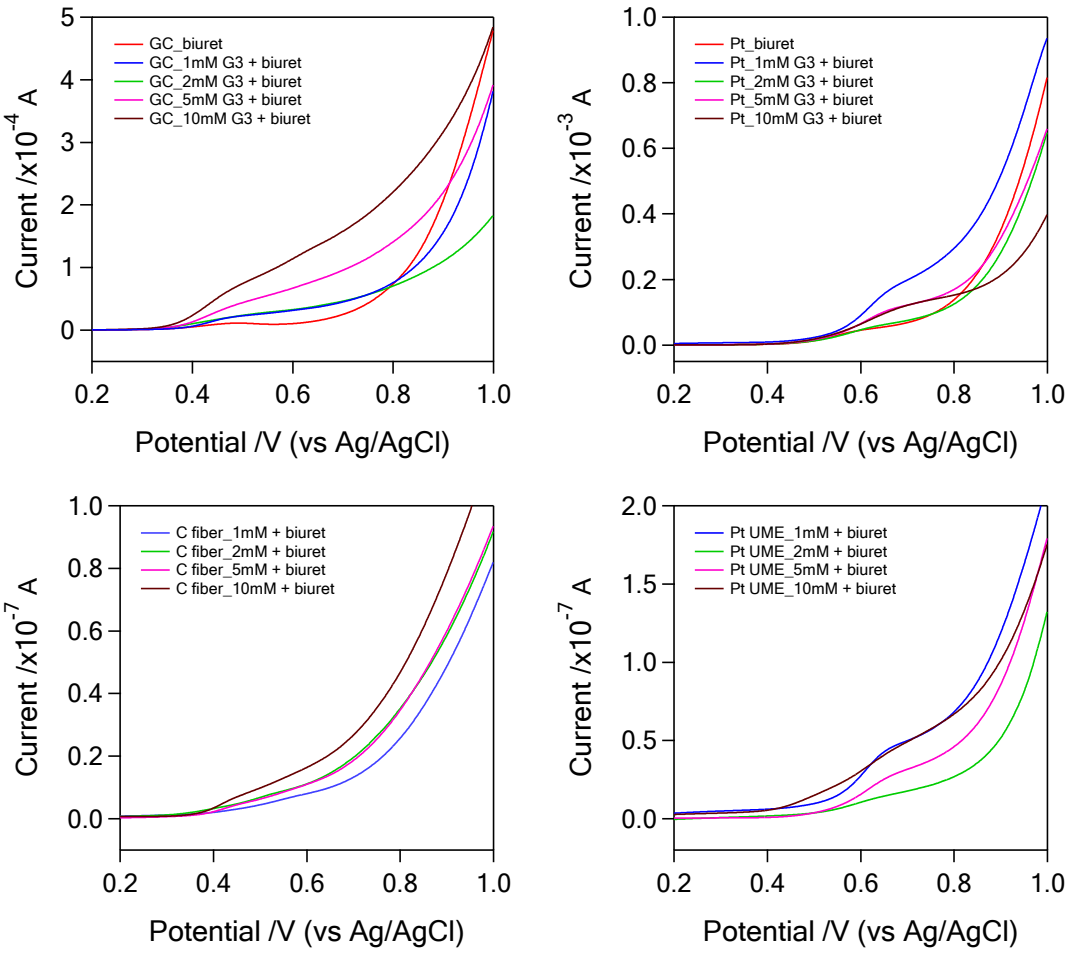

Figure 3.15 Cyclic voltamograms of G_3 – biuret complex from G_3 concentration of 0, 1, 2, 5 and 10 mM using 2.5 mm glassy carbon (GC), 2 mm Pt, 30 µm C-fibre and 25 µm Pt microelectrode. Selected currents from the forward scans were shown.

3.6.3 Generation-collection detection of peptide

Triglycine (G_3) was furthered investigated using our fabricated C/C ring-disc electrode. Cyclic voltammetry was performed on both disc and ring, and the relationship between currents and concentrations of G_3-biuret complex was examined.

Method and materials

The G_3 concentrations of 0, 1, 2, 5 and 10 mM were prepared in biuret reagent solution. Biuret reagent was consisted of 11 mM Cu^{2+}, 33 mM tartrate and 0.52 M KOH. Cyclic voltammetry was operated by scanning the electrode potential from 0.1 to 1.0 V versus Ag/AgCl reference electrode. Fabricated C/C ring-disc electrode was used as a standalone device in a stationary solution. Both disc and ring potentials were separately scanned for different concentrations of G_3-biuret complex. For generation-collection detection, disc electrode was operated as the generator, where the complex was collected at the ring electrode. Fixed potentials of 0.65 V and 0.2 V were applied to disc and ring, respectively. Disc and ring currents were simultaneously recorded and the collection efficiencies were then determined. Between each experiment, the electrode was regularly characterised using 10 mM hexammineruthenium (III) standard solution and cleaned under ultrasonic bath with surfactant, warm water, methanol and water, in sequence.

Results and discussion

Current-voltage curves from different concentrations of G_3-biuret complex showed a larger oxidative current at higher concentration, whereas the reverse reaction was not recognised. With higher surface area, C-ring provided bigger currents. Limiting currents were observed at 0.65 V (versus Ag/AgCl) and plotted against complex concentration (Figure 3.15). Both ring and disc currents exhibited linear responses to complex concentration. C/C ring-disc offers a direct relationship between measured signals to the concentration of analyte. However, in real sample or complicated matrix where interferences can be oxidised, generation-collection detection was employed to enhance the sensitivity over other common amine compounds.

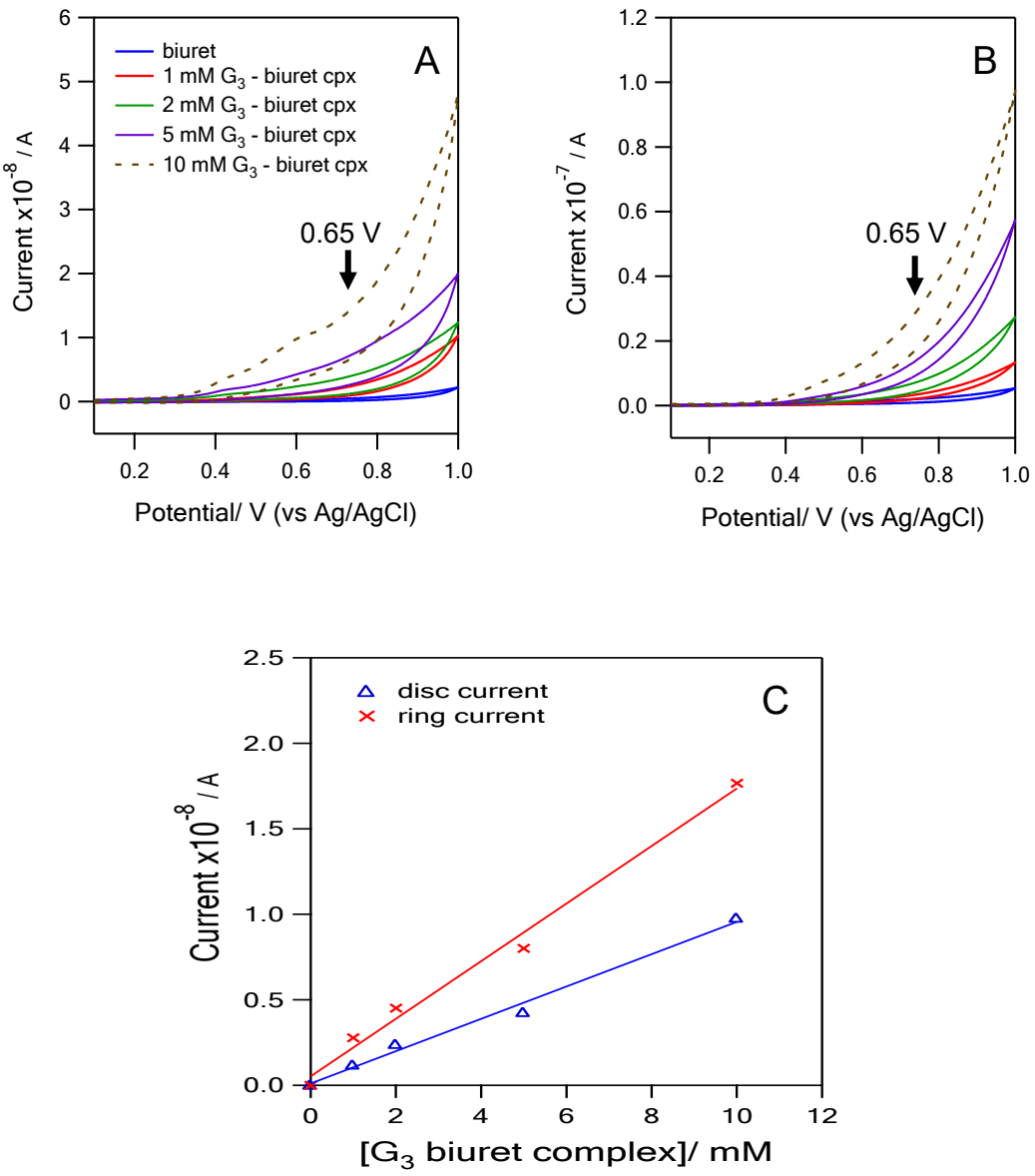

Figure 3.16 Cyclic voltammograms of 0, 1, 2, 5 and 10 mM G_3-biuret complex obtained from 30 µm C-disc (A) and C-ring (B) electrodes. Plots between G_3-biuret complex concentrations and oxidative current, monitored at 0.65 V (C).

Collection efficiency (CE) was measured and plotted versus time for a system with no complex, low (1 mM) and high concentration (10 mM) of G_3-biuret complexes (Figure 3.16). The %CE obtained from biuret solution was small (less than 0.1 %). This can imply that low amount of interference complex present in the system. %CE of 1 mM and 10 mM G_3-biuret complexes were extremely small and not significantly different from the measured value in the biuret solution. Sensor characterisation with standard rutheniumhexaammine(III) was repeated to check the electrode performance, no

significant evidence of electrode fouling was found. This is very unclear. Possible reasons are the slow rate of reversed reaction of G_3-biuret complex or lack of stability for collection. As seen from i-V curves of G_3-biuret complexes in figure 3.15A and 3.15B, the electrochemical reaction was not reversible. Longer chain peptides with stronger biuret complex formation should be compared. Our C/C ring-disc electrode for peptide detection is not well achieved. The ring made from C paint was not durable and lacked repeatability. The metal ring-disc electrode appear to show more promising characteristics and will be applied to a further biomedical application.

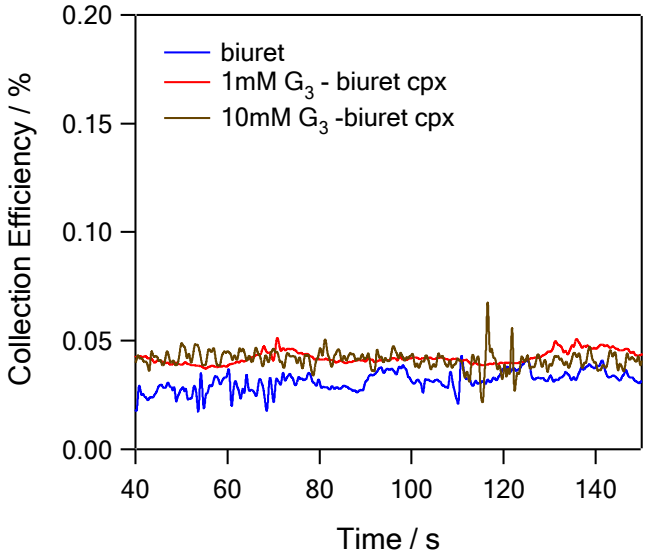

Figure 3.17 i-t curves showing the collection efficiency obtained from disc generator-ring collector mode with biuret solution, 1 mM and 10 mM G_3-biuret complexes. Disc potential was set at 0.65 V, ring potential was fixed at 0.2 V (vs Ag/ÁgCl).

3.7 Conclusion

Ring-disc microelectrode showed a versatile application as both a standalone device and as part of flow analysis and separation system. Sensor characterisations showed good agreements between theory and experiment results. Cleaning and polishing are recommended for replenishing and renew the surface efficiently prior to and after use.

The Pt/Pt ring-disc showed a promising result for amino acid detection. Detection of amino acid with bromide can be achieved. However, more complex behavior of Pt/Pt ring-disc sensor with an evidence of sensor fouling was observed than has been reported for macro electrode systems under similar conditions. A system of end-column detection under the flow cell using permanganate was studied and showed a promising response of the sensor under different flow rate. This is possibly due to less fouling effect of the permanganate system.

For peptide detection, the electrochemical biuret system showed less improvement in sensitivity with the generation-collection mode to small peptide molecule. Sensor fouling is dominant in blocking the electrode surface and hence less electroactive species will then be collected at the collector.

In conclusion, the self-fabricated ring-disc electrode can be miniaturised and has the advantage of uniform flux in generation-collection process; however, improvements in sensitivity, repeatability and robustness are needed for practical use in real samples.

References

1. Lilley KS, Razzaq A, Dupree P: **Two-dimensional gel electrophoresis: recent advances in sample preparation, detection and quantitation**. *Current Opinion in Chemical Biology* 2002, **6**(1):46-50.
2. Kodadek T: **Protein microarrays: prospects and problems**. *Chemistry & Biology* 2001, **8**(2):105-115.
3. Kasicka V: **Capillary electrophoresis of peptides**. *Electrophoresis* 1999, **20**(15-16):3084-3105.
4. Zhu R, Kok WT: **Postcolumn derivatization of peptide with fluorescamine in capillary electrophoresis**. *Journal of Chromatography A* 1998, **814**(1-2):213-221.
5. Meek JL, Rossetti ZL: **Factors affecting retention and resolution of peptides in high-performance liquid-chromatography**. *Journal of Chromatography* 1981, **211**(1):15-28.
6. Boppana VK, MillerStein C: **High-performance liquid chromatographic determination of peptide drugs in biological fluids by means of pre- and post-column fluorescence derivatization techniques**. *Analytica Chimica Acta* 1997, **352**(1-3):61-69.
7. Herzog G, Arrigan DWM: **Electrochemical strategies for the label-free detection of amino acids, peptides and proteins**. *Analyst* 2007, **132**(7):615-632.
8. A. SD, James. HF, R. CS: **Principles of instrumental analysis**, 6th edn. Pacific Grove, Calif. : Brooks/Cole ; London: Thomson Learning; 2007.
9. Albery WJ, Svanberg LR, Wood P: **The Estimation and Identification of Proteins by Ring-Disc Titration .1. Titration and Identification**. *Journal of Electroanalytical Chemistry* 1984, **162**(1-2):29-43.
10. Lindroth P, Mopper K: **High-performance liquid chromatographic determination of subpicomole amounts of amino acids by precolumn fluorescence derivatization with ortho-phthaldialdehyde**. *Analytical Chemistry* 1979, **51**(11):1667-1674.
11. Krull IS, Strong R, Sosic Z, Cho BY, Beale SC, Wang CC, Cohen S: **Labeling reactions applicable to chromatography and electrophoresis of minute amounts of proteins**. *J Chromatogr B* 1997, **699**(1-2):173-208.
12. Banks PR: **Fluorescent derivatization for low concentration protein analysis by capillary electrophoresis**. *Trac-Trends in Analytical Chemistry* 1998, **17**(10):612-622.
13. Jing P, Kaneta T, Imasaka T: **Band broadening caused by the multiple labeling of proteins in micellar electrokinetic chromatography with diode laser-induced fluorescence detection**. *Journal of Chromatography A* 2002, **959**(1-2):281-287.
14. Hughes AB: **Amino acids, peptides and proteins in organic chemistry**. Weinheim: Wiley-VCH; 2009.
15. Albery WJ, Svanberg LR, Wood P: **The Estimation and Identification of Proteins by Ring-Disc Titration .2. Application to Liquid-Chromatography**. *Journal of Electroanalytical Chemistry* 1984, **162**(1-2):45-53.
16. Sato K, Jin JY, Takeuchi T, Miwa T, Takekoshi Y, Kanno S, Kawase S: **Indirect amperometric detection of underivatized amino acids in microcolumn liquid chromatography with carbon film based ring-disk electrodes**. *Analyst* 2000, **125**(6):1041-1043.

17. Sato K, Takekoshi Y, Kanno S, Kawase S, Jin JY, Takeuchi T, Miwa T: **Plastic film ring-disk carbon electrodes for the indirect amperometric detection of underivatized amino acids in liquid chromatography**. *Analytical Sciences* 1999, **15**(10):957-961.
18. Bruckenstein S, Johnson DC: **Coulometric diffusion layer titrations using the ring-disk electrode with amperometric end point detection**. *Analytical Chemistry* 1964, **36**(11):2186-2187.
19. Zhao C, Zhang JC, Song JF: **Determination of L-cysteine in amino acid mixture and human urine by flow-injection analysis with a biamperometric detector**. *Analytical Biochemistry* 2001, **297**(2):170-176.
20. Fung YS, Mo SY: **Determination of Amino-Acids and Proteins by Dual-Electrode Detection in a Flow System**. *Analytical Chemistry* 1995, **67**(6):1121-1124.
21. Isaksson K, Lindquist J, Lundstrom K: **Reaction Detector for Liquid-Chromatography with Electrochemical Generation and Detection of Excess Bromine**. *Journal of Chromatography* 1985, **324**(2):333-342.
22. Holland LA, Lunte SM: **Postcolumn reaction detection with dual-electrode capillary electrophoresis-electrochemistry and electrogenerated bromine**. *Analytical Chemistry* 1999, **71**(2):407-412.
23. Albery WJ, Bartlett PN, Cass AEG, Craston DH, Haggett BGD: **Electrochemical sensors: theory and experiment**. *Journal of the Chemical Society, Faraday Transactions 1: Physical Chemistry in Condensed Phases* 1986, **82**(4):1033-1050.
24. Bell CG, Seelanan P, O'Hare D: **Microelectrode generator-collector systems for electrolytic titration: theoretical and practical considerations**. *Analyst* 2017, **142**(21):4048-4057.
25. Feuerstein D, Parker KH, Boutelle MG: **Practical Methods for Noise Removal: Applications to Spikes, Nonstationary Quasi-Periodic Noise, and Baseline Drift**. *Analytical Chemistry* 2009, **81**(12):4987-4994.
26. Mayeux R: **Biomarkers: Potential Uses and Limitations**. *NeuroRx* 2004, **1**(2):182-188.
27. Karley D, Gupta D, A T: **Biomarkers: The Future of Medical Science to Detect Cancer**. *Journal of Molecular Biomarkers Diagnosis*:118.
28. Strimbu K, Tavel JA: **What are Biomarkers?** *Current opinion in HIV and AIDS* 2010, **5**(6):463-466.
29. Rajantie H, Williams DE: **Electrochemical titrations of thiosulfate, sulfite, dichromate and permanganate using dual microband electrodes**. *Analyst* 2001, **126**(1):86-90.
30. McDermott CA, Kneten KR, McCreery RL: **Electron transfer kinetics of aquated $Fe^{+3/+2}$, $Eu^{+3/+2}$, AND $V^{+3/+2}$ at carbon electrodes - Inner sphere catalysis by surface oxides**. *Journal of the Electrochemical Society* 1993, **140**(9):2593-2599.
31. Warner AM, Weber SG: **Electrochemical detection of peptides**. *Analytical Chemistry* 1989, **61**(23):2664-2668.
32. Tsai HY, Weber SG: **Electrochemical detection of dipeptides and dipeptide amides**. *Journal of Chromatography* 1990, **515**:451-457.
33. Tsai HY, Weber SG: **Electrochemical detection of oligopeptides through the precolumn formation of biuret complexes**. *Journal of Chromatography* 1991, **542**(2):345-350.

34. Tsai H, Weber SG: **Influence of tyrosine on the dual electrode electrochemical detection of copper(II) peptide complexes**. *Analytical Chemistry* 1992, **64**(23):2897-2903.
35. Weber SG, Tsai HY, Sandberg M: **Electrochemical detection of dipeptides with selectivity against amino acids**. *Journal of Chromatography* 1993, **638**(1):1-8.
36. Chen JG, Woltman SJ, Weber SG: **Sensitivity and selectivity of the electrochemical detection of the copper(II) complexes of bioactive peptides, and comparison to model studies by rotating ring-disk electrode**. *Journal of Chromatography A* 1995, **691**(1-2):301-315.
37. Chen JG, Weber SG: **Detection of bioactive oligopeptides after microbore HPLC with electrochemical detection of their Cu(II) complexes: Effect of operating parameters on sensitivity and selectivity**. *Analytical Chemistry* 1995, **67**(19):3596-3604.
38. Woltman SJ, Alward MR, Weber SC: **Rotating ring-disk electrode study of copper(II) complexes of the model peptides triglycine, tetraglycine and pentaglycine**. *Analytical Chemistry* 1995, **67**(3):541-551.
39. Shi F, Woltman SJ, Weber SG: **Kinetics of the post-column complexation reaction of Cu(II) with N-formylmethionyl chemoattractant and chemotactic peptides**. *Analytica Chimica Acta* 2002, **474**(1-2):1-9.
40. Shen H, Witowski SR, Boyd BW, Kennedy RT: **Detection of peptides by precolumn derivatization with biuret reagent and preconcentration on capillary liquid chromatography columns with electrochemical detection**. *Analytical Chemistry* 1999, **71**(5):987-994.
41. Schwarz A, Bagel O, Girault HH: **A sensitive electrochemical protein quantification method**. *Electroanalysis* 2000, **12**(11):811-815.
42. Woltman SJ, Chen JG, Weber SG, Tolley JO: **Determination of the pharmaceutical peptide TP9201 by post-column reaction with copper(II) followed by electrochemical detection**. *Journal of Pharmaceutical and Biomedical Analysis* 1995, **14**(1-2):155-164.
43. Chen JG, Logman M, Weber SG: **Effect of peptide primary sequence on biuret complex formation and properties**. *Electroanalysis* 1999, **11**(5):331-336.
44. Meng R, Weber SG: **The rotating ring-disk electrochemistry of the copper(II) complex of thyrotropin-releasing hormone**. *Journal of Electroanalytical Chemistry* 2007, **600**(2):325-334.

Chapter 4:

Measurement of Buffer Capacity using Generation – Collection Sensor

4. Measurement of Buffer Capacity using Generation – Collection Sensor

4.1 Overview of buffer and buffer capacity

Buffers are used to control the pH of a system. In a solution containing buffer, change of pH in solution will be minimized on addition of acid or base, pH of solution to be virtually constant. Generally, buffer consists of weak acid or weak base and its conjugated species. The relationship between a weak acid and its conjugate base is simplified and shown in equation 4.1,

$$\mathrm{HA}(aq) + \mathrm{H_2O}(l) \leftrightarrow \mathrm{H_3O^+}(aq) + \mathrm{A^-}(aq) \qquad (4.1)$$

where HA is weak acid and A^- is its conjugate base. The equilibrium between acid and conjugate base in one buffer plays a major role to resist a pH change. The pH can be maintained by titrating off an acid or base species added to the solution under the equilibrium of the buffer system. The buffer works efficiently when the concentrations of the weak acid and its salt are relatively large compared to the addition or removal of protons (acid) or hydroxide (base) ions. Consider the buffer system of HA/A^-, pH of the solution is related to pK_a and the concentration of each species as described in equation 4.2,

$$pH = pK_a + \log\frac{[A^-]}{[HA]} \qquad (4.2)$$

where [HA] is molar concentration (mol dm^{-3}) of the acid, $[A^-]$ is molar concentration of the conjugate base and K_a is acid dissociation constant. This equation is well known as the Henderson–Hasselbalch equation, derived from the equation of K_a. Theoretically, the ability to resist a pH change of buffer is highest when the buffer stay at pK_a, and gradually drop when the pH of buffer is away from pK_a. Practically, optimal pH range where buffer works efficiently can be estimated by standard titration. The example of titration curve of acetic acid (CH_3COOH) with strong base is shown in Figure 4.1.

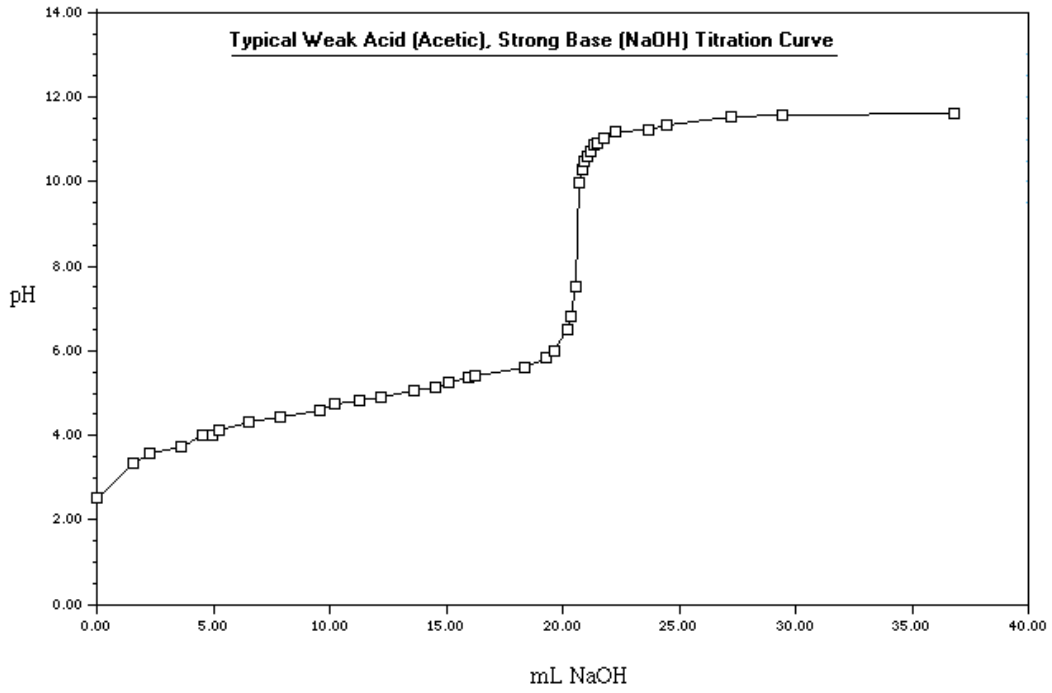

Figure 4.1 Titration curve of 0.5 M acetic acid (pK_a 4.75) with 0.5 M NaOH.

In titration curve, the pH of acetic acid solution is plotted after adding a strong base of sodium hydroxide (NaOH) into the solution. Initial pH of acetic acid where no NaOH added to the solution is approximately 2.5. The pH of acetic acid increases after NaOH is added. Slight change of pH is observed at the presence of acetic acid-acetate equilibrium. Small pH change can be found within a range of pK_a ±1 (pK_a of acetic acid equals to 4.75). Once the titration reaches to the end point of (after 20.0 mL adding of NaOH), pH sharply increases with a small amount of NaOH addition. The acetate buffer plays a part on pH resistance at the start of NaOH addition to the observed end point (after titration is completed). Changing of pH value at each step can refer to the capability of buffer to maintain its pH. This is widely known as buffer capacity.

Buffer Capacity

Buffer capacity, β, represents the ability of a buffer to resist changes in pH. Traditionally, buffer capacity has been determined by performing a titration of the buffer solution with an acid or base and then examining the change in pH (*dpH*) of the solution. Buffer capacity can be mathematically described as,

$$\beta = \frac{dn}{dpH} \tag{4.3}$$

where *dn* is change in moles of acid or base added to the solution. From equation 4.3, a large value of β represents a great capacity to resist change in pH of the solution. Higher buffer concentration gives a better buffer capacity, represented in figure 4.2.

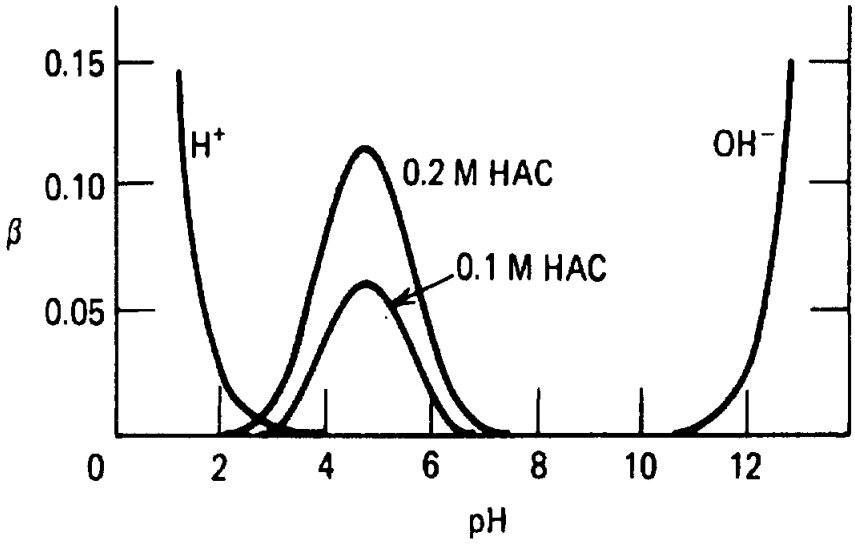

Figure 4.2 Plots of buffer capacity, β, versus solution pH of 0.1 and 0.2 M acetic acid (HAC), adapted from [1].

4.2 pH in physiological fluid

The pH of different cellular compartments, body fluids, and organs is tightly regulated via a process called acid-base homeostasis. Nutrients, ions and waste in our cells will be exchanged with the surrounding external fluid [2]. Blood is the main physiological fluid where pH is controlled by a buffer system. The pH of blood is usually maintained at a constant level of 7.35 to 7.45 [1]. This permits biochemical processes to perform properly. Many of the chemical reactions that occur in the body are pH-dependent. For example, if the pH of the body becomes too low, a condition known as acidosis results and if left untreated, irreversible cell damage can occur and death can ultimately follow.

4.2.1 Control of pH in human blood

The most important buffer for maintaining acid-base balance in the blood is the carbonic-acid-bicarbonate buffer. The simultaneous equilibrium reactions of this buffer are shown below.

$$H^+(aq) + HCO_3^-(aq) \leftrightarrow H_2CO_3(aq) \leftrightarrow H_2O(l) + CO_2(g) \qquad (4.4)$$

With bicarbonate buffer, the pH of blood is dependent on the **ratio** of the concentrations of **CO_2** concentration to **HCO_3^-** (bicarbonate ion) present in the blood. When H^+ is added to the blood as a result of normal activities and metabolic processes, the amount of HCO_3^- decreases to absorb of H^+. However, the change is relatively small compared to the amount of HCO_3^- present in the blood. The concentrations of the buffer components (HCO_3^- and CO_2) are insignificantly different after adding of H^+ to the blood. The ratio of buffer species remains relatively constant to after the perturbation is diminished and the buffer system reaches to equilibrium. The relationship between bicarbonate buffer and carbon dioxide concentration limits the range of our blood pH. The Henderson–Hasselbalch equation relates blood pH to the components of the bicarbonate buffer system and can be shown in equation 4.5,

$$pH = pK_a + \log \frac{[HCO_3^-]}{(0.03)P_{CO_2}} \qquad (4.5)$$

where K_a is acid dissociation constant of bicarbonate buffer, $[HCO_3^-]$ is molar concentration of bicarbonate ion and P_{CO_2} is partial pressure of carbon dioxide. Figure 4.3 represents a diagram of buffer composition in human blood. Buffer system in normal blood contains the CO_2 giving pH range 7.35 to 7.45. Metabolic activities of human affect to the pH of body fluid. Excess of acidity or alkalinity in the blood will cause an imbalance. Technical terms described the processes of an excess acid and base in blood are acidosis and alkalosis, respectively. The acid-base imbalance in the blood can be categorised into types based on their buffer compositions, as presented in Figure 4.3. Types of acid-base imbalance are clinically recognised as metabolic and respiratory effects. When the acid-base imbalance occurs in our body, the kidney, liver and brain

help to maintain regular homeostasis. An inability to maintain the regular homeostasis leads to a disease or death. To investigate and prevent our pH imbalances, patients are clinically monitored by measuring of the blood pH.

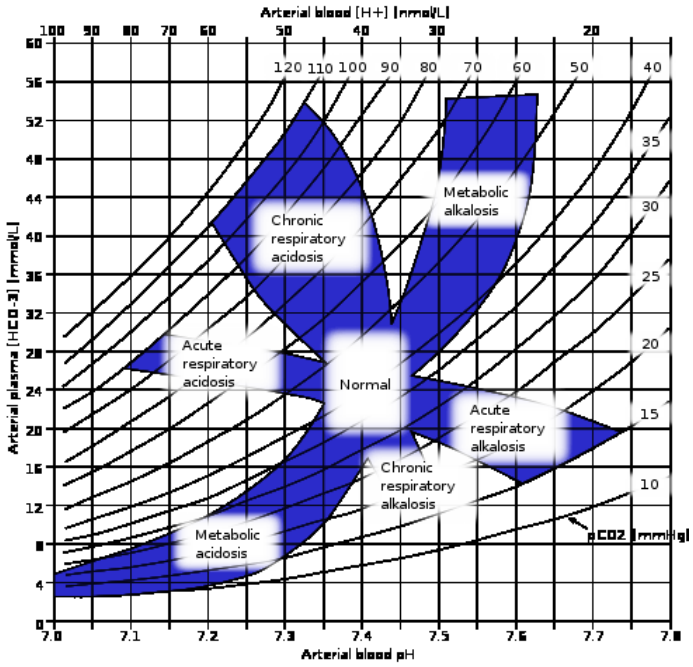

Figure 4.3 Diagram of relationship between buffer composition of the blood and acid-base homeostasis [1].

4.2.2 Acidosis

Acidosis is a disorder where an increase in hydrogen ion (H^+) concentration to the blood and other body tissue are involved. Consider of the blood, a blood pH refers to acidity of the blood plasma. Acidosis occurs when blood pH falls below 7.35 influenced by the disturbance of respiratory or metabolic activity. An increase in H+ concentration will result in an increase in the HCO_3^- concentration and a decrease in the pH. Thus, a patient under acidosis disorder is found to have a low blood pH [3].

Respiratory acidosis results from an increase in carbon dioxide to the blood due to hypoventilation. It is caused by most pulmonary problems as frequently found after long period exercise or in many athletes. On the other hand, it can also occur as a compensatory response to chronic metabolic alkalosis. In respiratory acidosis, the CO_2

level is increased while the bicarbonate concentration is either normal (uncompensated) or increased (compensated). The increased CO_2 will react with water and produce H^+ resulting in lower pH. Bicarbonate buffer will work to resist pH change by titrating off the increasing H^+. Extra bicarbonate infusion will be introduced to compensate acidosis, while partial buffering through renal bicarbonate retention is also found in chronic phase.

Metabolic acidosis results from the increase of metabolic acids or disturbances in the ability to excrete acid via the kidneys. Renal acidosis is associated with an accumulation of urea and creatinine as well as metabolic acid residues of protein catabolism. An increase in the production of other acids may also produce metabolic acidosis; for example, a severe fall in the rate of oxygen diffusion from arterial blood to tissues, lack of oxygen delivery to tissues from hypoperfusion or acid consumption from poisoning, elevated levels of iron in the blood. A decrease in the production of bicarbonate may also causes metabolic acidosis. Metabolic acidosis is balanced in the lung by exhalation of carbon dioxide, shifting the equilibrium to less acidic value. This is a result of stimulation to chemoreceptors which increase alveolar ventilation, hence leading to respiratory compensation. If this situation persists, the patient is at the risk of exhaustion leading to respiratory failure. When metabolic acidosis is severe and cannot be sufficiently compensated by the lung, neutralising with infusions of bicarbonate may be required.

4.2.3 Alkalosis

Alkalosis is a condition in which the body fluids have excess base (alkali). This condition occurs when pH of the blood exceeds 7.45 which is the opposite of acidosis. Types of alkalosis can be categorised into respiratory alkalosis and metabolic alkalosis.

The major cause of respiratory alkalosis is a loss of carbon dioxide from hyperventilation or a lung disease. Others reasons may involve a fever, lack of oxygen, liver disease and poisoning. Compensatory mechanisms include dissociation of the carbonic acid buffering intermediate into hydrogen ions and bicarbonate. This would raise the blood pH.

Metabolic alkalosis is caused by too much bicarbonate in the blood. This can be from prolonged vomiting, resulting in a loss of hydrochloric acid with the stomach content. It can also be caused by severe dehydration and the consumption of alkali. Compensated alkalosis occurs when the body restores the acid-base balance to normal in cases of alkalosis, but bicarbonate and carbon dioxide levels remain abnormal. Slow breathing by the lungs to increase serum carbon dioxide can be compensated for metabolic alkalosis. This is in a way toward respiratory acidosis. As respiratory acidosis often accompanies metabolic alkalosis and vice versa, a delicate balance occurs between these two conditions.

4.3 pH measurement using electrochemical based technique

In order to measure the pH in a solution, static mode of electrochemical technique can be applied. Potentiometry is commonly introduced and developed for pH sensing. Generally, the ion selective electrode will sense the H^+ species in the cell and report as the potential which is related to pH. Because no current flows through electrochemical cell, the cell composition remains unchanged. This has made potentiometry a very useful technique for quantitative pH analysis.

4.3.1 Relationship between pH and potential

Quantitative potentiometric applications developed from the Nernst equation, which relates the potential of an electrochemical cell to the concentration of electroactive species in the cell. The potential of a potentiometric electrochemical cell is described as

$$E = E_C - E_A \tag{4.6}$$

where E_C and E_A are reduction potentials for the redox reactions at the cathode and the anode, respectively. The reduction potential is given by the Nernst equation as followed,

$$E = E° - \frac{RT}{nF} \ln Q \qquad (4.7)$$

where $E°$ is the standard state reduction potential, R is the gas constant, T is the temperature (in Kelvins, K), n is the number of electrons in the reaction, F is Faraday's constant, and Q is the reaction quotient.

At a temperature of 298 K, the Nernst equation become

$$E = E° - \frac{0.05916}{n} \ln Q \qquad (4.8)$$

where E is given in volts.

Typical potentiometric electrochemical cell equipped with ion selective electrode can be illustrated in Figure 4.4. The electrochemical cell includes two reference electrodes. One reference electrode is immersed in the ion-selective electrode's internal solution and the other is in the sample and the basis for measurement is the membrane potential difference which, due to selective interaction between the membrane and the analyte, protons in this case, varies logarithmically with concentration.

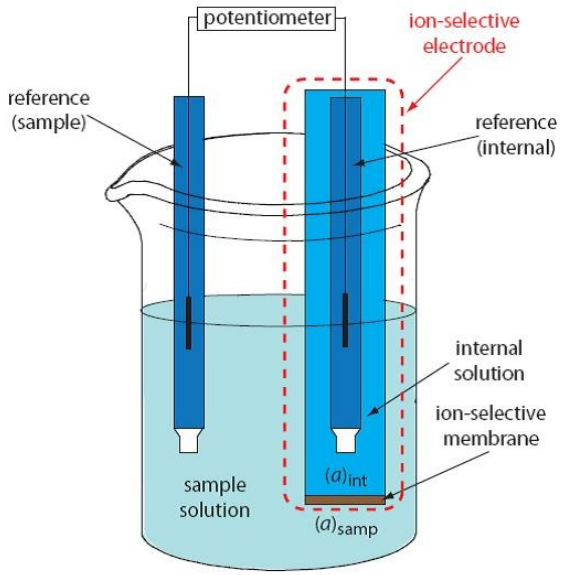

Figure 4.4 A schematic picture of potentiometric system including the ion-selective electrode (red line) [4].

The cell potential is equal to

$$E_{cell} = E_{ref(\text{int})} - E_{ref(sam)} + E_{mem} + E_j \qquad (4.9)$$

where E_{mem} is the potential across the membrane and E_j is junction potential. Since the potential of the two reference electrodes and the junction are constant, any change in E_{cell} depends on a change in the membrane's potential. The membrane potential is generated from the analyte's interaction on the membrane due to a difference in the activity between two sides. Current is carried through the membrane by the movement of the ions in the membrane's matrix. The membrane potential is given by the following Nernst-like equation

$$E_{mem} = E_{asym} - \frac{RT}{nF} \ln \frac{(a_A)_{\text{int}}}{(a_A)_{\text{sam}}} \qquad (4.10)$$

where $(a_A)_{sam}$ is the analyte's concentration in the sample, $(a_A)_{int}$ is the concentration of analyte in the internal solution of ion selective electrode, and z is the analyte's charge. Ideally, E_{mem} is zero when $(a_A)_{int} = (a_A)_{samp}$. The term E_{asym}, which is an asymmetry potential, accounts for the fact that E_{mem} is usually not zero under these conditions. Substituting equation 4.10 into equation 4.9, assuming a temperature of 25 ^{o}C and rearranging give

$$E_{cell} = K + \frac{0.05916}{z} \log(a_A)_{\text{sam}} \qquad (4.11)$$

where K is a constant that includes the potentials of the two reference electrodes, the junction potentials, the asymmetry potential, and the analyte's activity in the internal solution. Equation 4.11 is a general equation and applies to all types of ion-selective electrodes.

4.3.2 pH sensor

The key of sensor is to relate the electric potential of the electrode system in solution to the changes in the content of a certain type of ions, which is reflected in the dependence of the electromotive force (EMF) of galvanic element concentrations of these ions. A number of fabricated sensors relate change of H^+ concentration in galvanic cell to potential have been reported. Typically, the sensor surface exhibits or will be modified to respond to H^+ ion. The glass electrode is the conventional sensor used for pH measurement as it is naturally H^+ sensitive and relatively closely follows the Nernst equation. Alternative materials include semiconductor surfaces and metal oxide film. They are capable of performing ion-exchange enabling H^+ sensing.

4.3.2.1 Glass membrane pH electrode

The first commercial glass electrodes were manufactured with a composition of 22% Na_2O, 6% CaO and 72% SiO_2, approximately. After immersed in an aqueous solution, the outer layer of the membrane's surface becomes hydrated, resulting in the formation of negatively charged sites, —SiO^-, where sodium ions (Na^+) serve as counter ions. Because H^+ binds more strongly to —SiO^- than Na^+, they displace the sodium ions and then give rise to the membrane's selectivity for H+. Equation 4.12 illustrates the ion exchange process at the glass membrane.

$$H^+ + -SiO^-Na^+ \leftrightarrow -SiO^-H^+ + Na^+ \tag{4.12}$$

The potential of a glass electrode using Corning 015 obeys the equation

$$E_{cell} = K + 0.05916 \log a_{H^+} \tag{4.13}$$

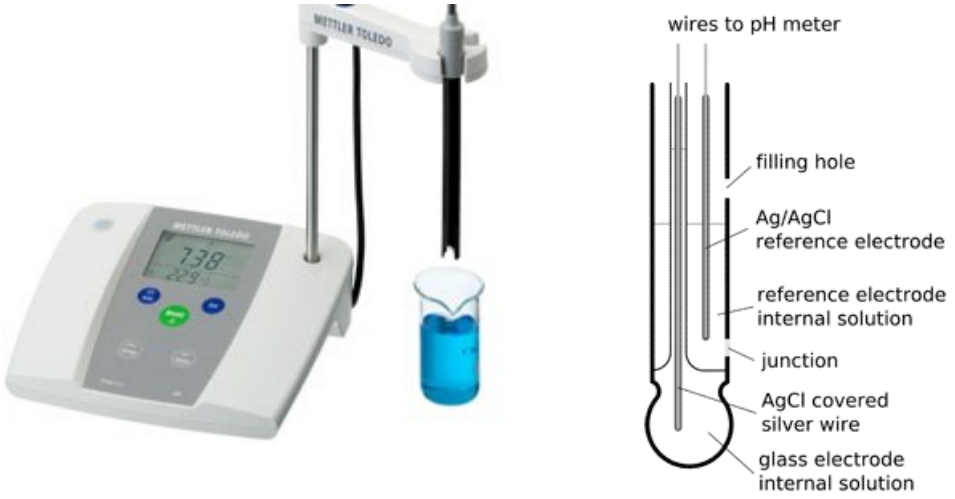

Figure 4.5 A commercial pH device of Mettler (A) and internal diagram of glass pH electrode (B), adapt from [5].

4.3.2.2 ISFET

The ion-sensitive field-effect transistor (ISFET) is a charge sensitive device and can be used for measuring ion concentrations in solution. The ISFET was first demonstrated by Bergveld in 1970 [6]. It is composed by oxide layers of semiconductor. Commercial pH sensor, inside chip device and cross-sectional view structure of ISFET are presented in Figure 4.6. Typical gate materials are SiO_2, Si_3N_4, Al_2O_3 and Ta_2O_5. The gate electrode is separated from the channel by a barrier which is sensitive to hydrogen ions (H^+). The contact to the electrolyte gate is provided by a reference electrode. The voltage between substrate and oxide surfaces of ISFET depends on the pH of the substance in contact with its ion-sensitive barrier. Detection is based on the charge adsorption at the ion-solid interface between the sensing layer containing hydroxyl groups and the electrolyte. In this process a double-layer capacitance is created with a potential drop, which influences the threshold voltage of the transistor depending on H^+ concentration. Once the ion concentration changes, the current through the transistor will change accordingly.

(A) (B)

(C)

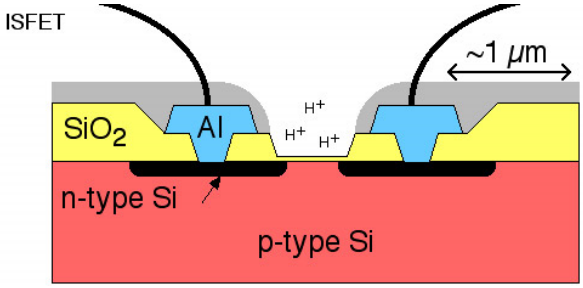

Figure 4.6 Pictures of develop product of ISFET (A), bare ISFET chip (B) and a cross-sectional view of ISFET (C).

The mechanism responsible for the oxide surface charge can be described by the site binding model, which describes the equilibrium between the Si–OH surface sites and the H^+ ions in the solution. The hydroxyl groups coating an oxide surface such as that of SiO_2 can donate or accept a proton and thus behave in an amphoteric way as illustrated by the following acid-base reactions occurring at the oxide-electrolyte interface:

4.3.2.3 Metal oxide electrode

Consider of pH measurement in field works or biological applications, non-glass based hydrogen selective electrode is preferred for a robust electrode. Metal oxide surface has been introduced and modified for pH measurement. Metal oxide electrode has a benefit over glass pH electrode in terms of mechanical stability, tolerance in high temperature and pressure, fast response time and ease of miniaturisation. The miniaturised sensor is needed for pH measurement of blood as well as extracellular fluid which make glass pH sensor less suitable to *in vivo* application. In biological and clinical investigation, durability, stability, sensitivity and compatibility to continuous monitoring are essential. As a consequence of the shortcomings of the most widely used glass membrane electrode, there has been substantial interest in metal oxide electrode.

Different oxides developed for pH sensors have been reported, such as PtO_2, IrO_2, RuO_2, molybdenum bronzes, OsO_2, Ta_2O_5, TiO_2, PdO, SnO_2, ZrO_2, Co_2O_3, WO_3, PbO_2, and Sb_2O_3. The most promising metal oxide pH sensors are RuO_2 and IrO_2 due to their chemical stability and high conductivity. In our work, pH sensors based on hydrated iridium oxide (IrOx) have been investigated. Several methods for preparing IrOx pH devices have been reviewed by Glab *et al*. [7]. Two types of IrOx fabrication are classified: electrochemically generated iridium oxide films (widely known as anodic iridium oxide film, AIROF) and thermally generated iridium oxide.

4.4 Iridium oxide (IrOx) pH sensor

Iridium oxide is recognised as an electrochromic oxide material which inhibits strong absorbance by the visible spectral region. It shows a bright colour change which is blue in the oxidised state and colourless in the reduced state. The redox reaction of IrOx can be described as in equation 4.14.

$$\mathrm{Ir(OH)}_n\,(\text{colorless}) \rightarrow \mathrm{IrO}_x\mathrm{(OH)}_{n-x}\,(\text{blue}) + x\mathrm{H}^+ + x\mathrm{e}^- \qquad (4.14)$$

The advantages of IrOx over other metal oxide electrodes include a potential stability over a wide range of temperature and pressure in aqueous solution, a wide pH response change, fast response time, high sensitivity, low potential drift and low sensitivity to redox interference [8]. Different techniques have been applied to produce iridium oxide pH electrode. Iridium oxide layer can be formed onto a conducting metal using thermally oxidised iridium oxide film (TOIROF), sputtered iridium oxide film (SIROF) or electrochemical deposition. SIROF is a less practical method due to the need for large quantities of expensive iridium, while TOIROF requires complex procedure of high-temperature treatment. Electrochemical deposition has found a wide range of practical applications because of their simplicity of fabrication, versatility of electrodeposition on surfaces of different geometries and low cost. An iridium oxide film could be obtained by either cathodic or anodic electrodeposition. It has been reported that the anodically electrodeposited iridium oxide film (AEIROF) exhibited faster electrochomic colour change than the cathodically electrodeposited iridium oxide film (CEIROF). In this work, AEIROF was applied to fabricate iridium oxide pH

sensor. Characterised dual electrode will be modified using iridium electrodepositing solution and then examined under known pH values of standard buffer. Application of titratable acidity was performed over the fabricated IrOx pH sensor.

4.4.1 Electrodeposition of IrOx

AEIROF was achieved using the protocol described by previous works of our group [9, 10]. Metal electrodes which are Pt disc and Au disc were chosen to be coated with iridium oxide film. The solution for electrochemical deposition of iridium oxide film was prepared base on original work reported by Yamanaka [11, 12]. Electrodeposition was carried out in a stationary solution at a constant potential. More details of IrOx electrodeposition are presented below.

Material and method

Iridium tetrachloride hydrate, $IrCl_4$ (99.9%), hydrogen peroxide (H_2O_2) solution (30% w/w), oxalic acid dihydrate, and anhydrous potassium carbonate used to make the IrO_2 deposition solution, were all purchased from Sigma-Aldrich and prepared using ultra purified water (MilliQ system).

Iridium oxide solution

The deposition solution containing iridium oxalate was made according to the method reported by Yamanaka [9, 11, 13]. To start with, 0.15 g of iridium tetrachloride was dissolved in 100 ml of water by magnetic stirring for 30 min. Next, 1 mL of 30% w/w H_2O_2, and 0.5 g of oxalic acid dihydrate were gradually added in the solution at each 10 min intervals and left to dissolve in a stirred solution. Anhydrous potassium carbonate was then gradually added to the solution until the pH reached 10.5, forming a pale yellow solution. The solution was then covered and left at room temperature for 48 hours to stabilise until a colour change to pale blue was achieved. The blue solution was stored in the refrigerator and used for a few months to successfully produce IrO_2 films.

Results and discussion

Prior to iridium oxide deposition, the bare electrode was cleaned with diluted DECON solution, warm water, methanol and water, successively with sonication. Electrode characterisation was carried out as previously described in Section 2.3. Cyclic voltammograms in 0.5 M sulfuric acid were recorded before and after certain period of deposition. Electrochemical deposition was performed under constant potential mode. Anodic potential of 0.6 V versus a non-leak Ag|AgCl reference electrode and the Pt mesh auxiliary electrode was applied to the Pt disc for two minutes. Chemical reaction of the oxidation process is shown in Equation 4.14.

As seen in oxidation reaction, the oxalate ligand was oxidized to carbon dioxide during deposition leaving a thin and uniform layer of iridium oxide over the Pt disc electrodes. After the deposition process was completed, cyclic voltammograms obtained in sulfuric acid were compared to confirm the presence of iridium oxide layer. Figure 4.7 shows CV in sulfuric acid, pre- and post-deposition. Higher current was observed from post anodic current. The iridium oxide coated microelectrodes were stored in deionised water prior to use to hydrate the film and stabilise the potential reading.

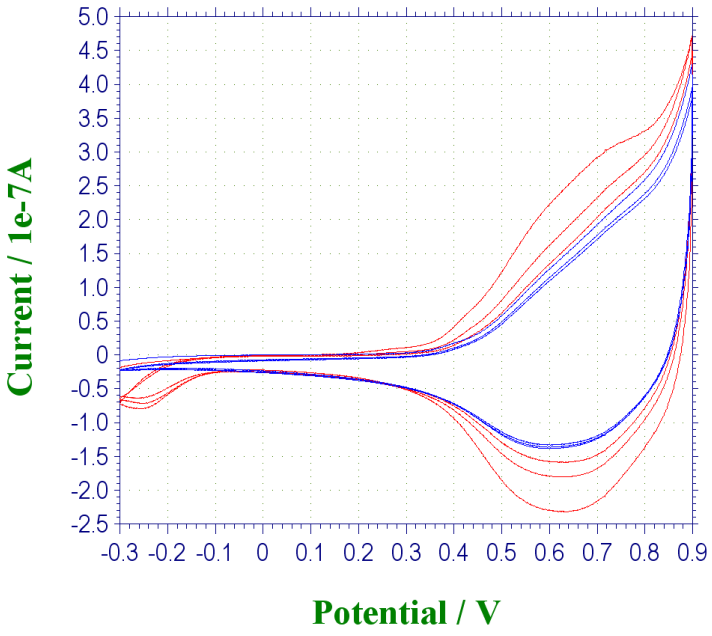

Figure 4.7 CV of 0.5 M sulphuric acid, pre- (blue line) and post-deposition (red line) with iridium oxide film.

4.4.2 pH sensor calibration

After leaving the iridium oxide film hydrated for 2 days, pH electrodes were calibrated in Britton-Robinson and HEPES buffer where the open-circuit potential (OCP) between the pH electrode and a standard reference electrode was recorded. Sensitivity and stability of self-fabricated sensor to pH were reviewed using calibration.

Material and method

Britton-Robinson buffer pH 2 to 12 was prepared by a mixture of 0.04 M phosphoric acid (H_3PO_4), 0.04 M acetic acid (CH_3COOH) and 0.04 M boric acid (H_3BO_3) and titrated with diluted NaOH. HEPES buffer pH 4-8 was prepared by dilution of 100 mM HEPES stock solution followed with pH adjustment using diluted NaOH or HCl. All chemicals were purchased from Sigma-Aldrich and prepared with ultra-purified water (MilliQ stytem). Calibrations were performed under open circuit potential mode versus a non-leak Ag/AgCl reference electrode and the Pt mesh auxiliary using CHI1030 (CH Instrument, USA). Potentials were continuously monitored and recorded. Plots of average steady potential versus pH were made and used to calibrate each sensor.

Results and discussion

Calibration data obtained from pH sensor fabricated on Pt disc by a stepwise increase in pH using the series of Britton-Robinson buffers in the pH range of 2 to10 are shown in Figure 4.8. IrOx film deposited from our prepared solution showed maximum sensitivity of -71 mV/pH, exhibiting super Nernstian response as reported by others for hydrated iridium oxide [13, 14]. It has been reported that mechanism of one transferred electron under the hydrated iridium oxide exhibits a slope approximately 70-90 mV/pH [14]. Our calibration shows a near super Nernstian response which indicates the prevalence of a hydrated form of iridium oxide. Similar sensitivity was observed in a series of HEPES buffer pH 4-8 and also showed the near super Nernstian response with slope -72 mV/pH, illustrated in figure 4.8. The sensitivity of our IrOx pH electrode remained practically constant more than a week storage time in deionised water. However, it has been found that dry storage led to a noticeable drop of the sensitivity.

Soaking the pH sensor in deionised water or tested buffer for an hour can restore the electrode sensitivity to the original value.

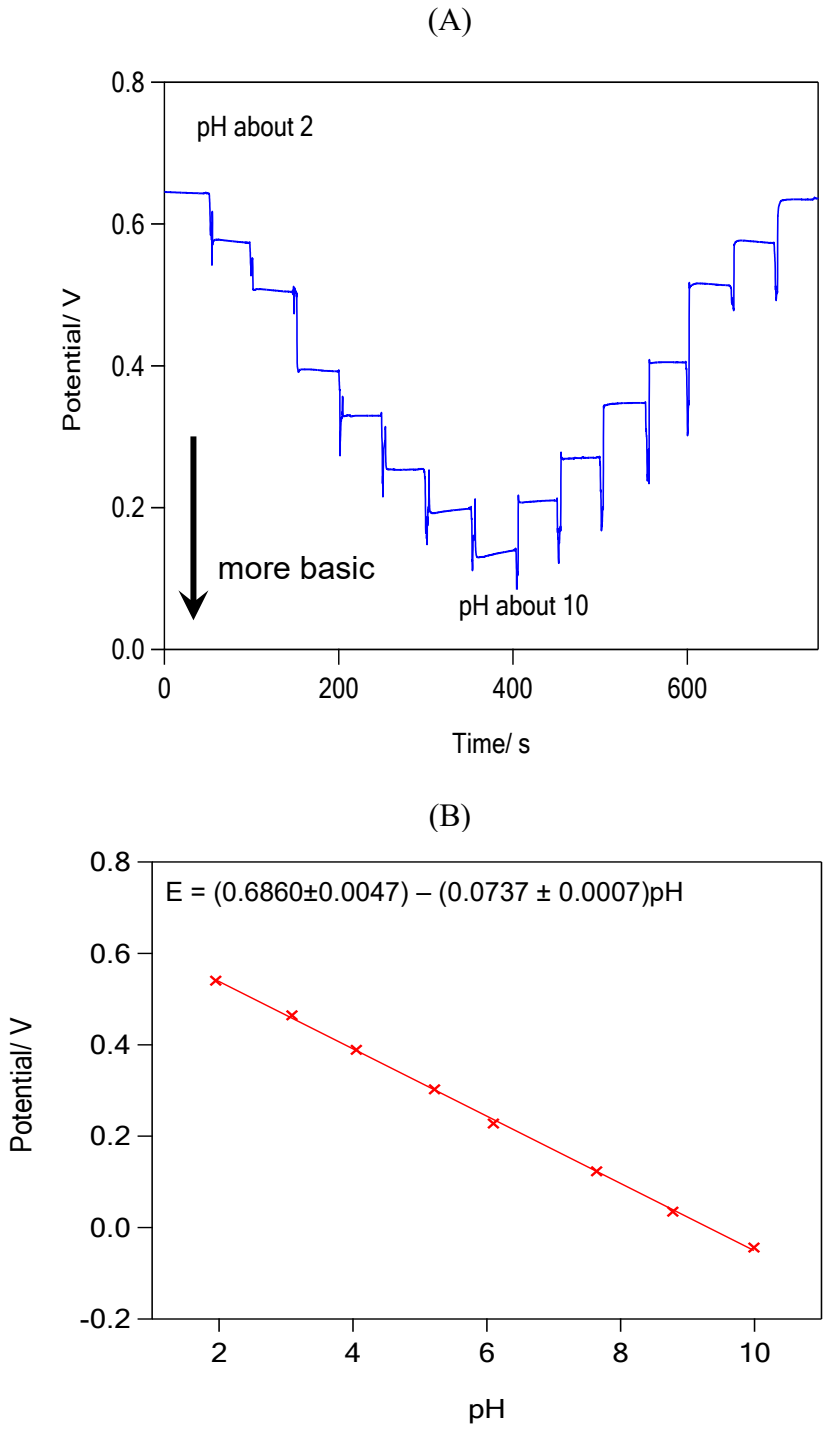

Figure 4.8 Calibration data obtained from pH sensor fabricated on Pt disc by a stepwise increase in pH using the series of Britton-Robinson buffers in the pH range of 2 to10 (A) and calibration plot (B).

4.5 Generation-collection sensor for buffer capacity measurement

In practice, buffer capacity, β, of buffer is calculated by titration with known concentration of acid or base. Change in pH of buffer by the amount of titrant added into buffer solution is monitored, β is calculated using equation 4.3. We applied our dual electrode to a titration system. One electrode acts as H^+ generation and another is for pH detection. Results and estimation the β were discussed and summarised in next parts.

4.5.1 Titratable acidity sensor

Metal/metal ring-disc microelectrodes were fabricated and used as the titratable acidity sensor. A platinum (Pt) ring was used to generate H^+ from the oxidation of water (Figure 4.9). Disc electrode was modified to be pH sensor. Anodic electrodeposition of an iridium oxide film on disc electrode using alkaline solution of iridium oxalate was performed and successfully achieved. Iridium oxide film is H^+ selective and exhibits a higher sensitivity of about 80 mV per pH unit which refer to super-Nernstian response (It should be note that the sensitivity of typical glass pH electrode is 59 mV/pH). Local pH change can be monitored simultaneously when H^+ is generated and then titrated with base species in the system.

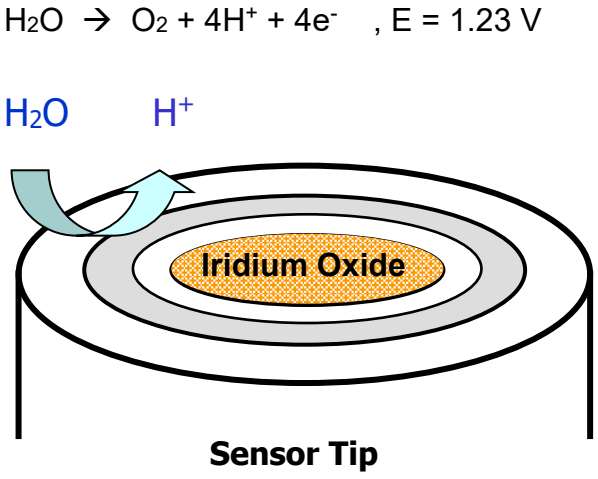

Figure 4.9 A schematic picture representing the iridium oxide/disc and Pt/ring electrode and water oxidation process at the ring.

4.5.2 Titratable acidity under HEPES buffer

Titratable acidity using our ring-disc sensor was initially tested with HEPES system, a well-known physiological buffer. pK_a of HEPES is about 7.55. Experiments were carried out using a stationary solution of HEPES buffer. Ring-disc sensor was placed in the solution and connected to both constant current and potential sources. When positive current is applied, H^+ is generated. Local pH monitored by the iridium oxide/Pt disc is recorded as potential. Change in potential is due to the change in amount of H^+ generated and titrated in a particular condition.

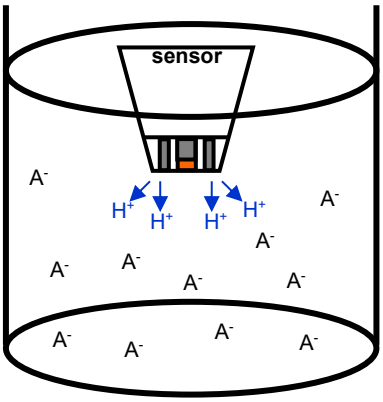

Figure 4.10 Schematic of experimental set up (Pt-ring generates H^+, IrO_2/Pt-disc is pH detector).

Experimental section

All solutions were dissolved in deionised water, otherwise stated. 10 mM HEPES buffers were prepared by diluting from a stock solution of 100 mM HEPES and adjusted to a desired pH with an appropriate amount of diluted sulfuric acid. Ring-disc sensor was placed in the electrochemical cell containing a large Pt mesh as a counter electrode and Ag/AgCl reference electrode. The modified 50 µm Pt disc was used as pH sensor and Pt ring was operated as the generator electrode. Multichannel potentiostat CHI model 1030 (CH Instruments inc., Texas) was operated to control and measure the voltage at the disc and operated as open circuit potential. Precision current source KEITHLEY model 6220 (Keithley Instruments, Inc., Ohio) was operated on the Pt ring in the constant current generation (I_{gen}) mode. Prior to each experiment, the disc pH sensor was calibrate using the prepared Britton-Robinson buffers under pH 2 to 10.

Result and discussion

The ring generator-disc pH sensor was tested on the titratable acidity by H^+ generation at the Pt ring in 10 mM HEPES at pH 6.0. A constant current of 10 nA was primarily applied as I_{gen} mode while the potential of the disc pH sensor was simultaneously monitored. A consecutive run of 10 nA generation for 50 seconds was performed on the Pt ring. While H^+ was generated, change in disc potential was observed to be higher. This was qualitatively consistent with the expected change in pH (higher potential, lower pH). In the stagnant solution, local pH change is observed. The local potential is gradually increased while H^+ is generated. After H^+ generation stops, the potential is dramatically dropped to the initial potential representing the pH of the buffer. This shows that our sensor can monitor H^+ changes influenced by the production at the Pt ring. Consistent responses and changes are obtained under the repeated H^+ generations at the applied generation time.

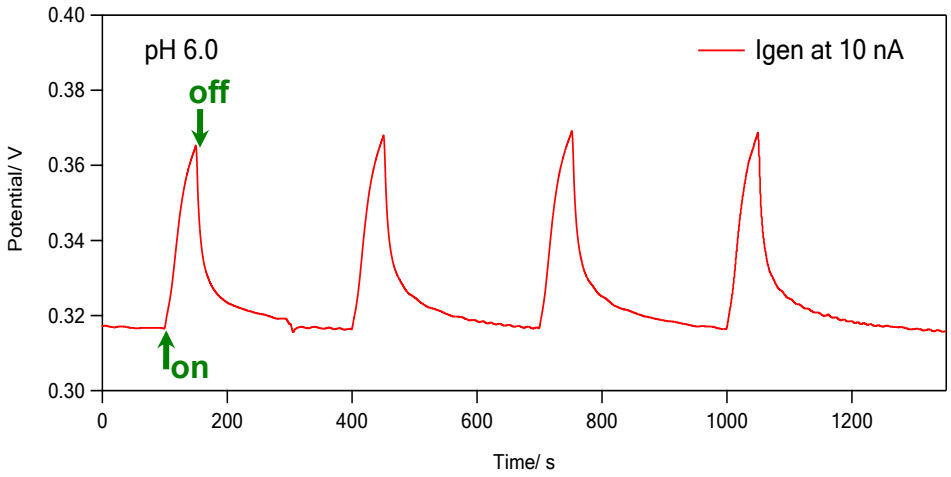

Figure 4.11 Graph of potential change at disc pH sensor caused by H^+ generation at the ring. Solution: 10 mM HEPES pH 6.0, current: 10 nA.

The ring generator-disc pH sensor was then applied on the titratable acidity by H^+ generation at different constant currents in 10 mM HEPES at pH 6.0, conditions as in Figure 4.12. I_{gen} mode (5, 10, 20, 40 and 80 nA) were applied while the potential of the disc pH sensor was simultaneously monitored. The increase in potential were observed for all constant applied currents. This is expected due to the increase in generated H^+ near the disc pH sensor proximity. Higher value of applied constant currents give higher

flux of H^+, hence larger change in the disc potential is observed. As shown in Figure 4.12, I_{gen} of 80 nA shows the sharpest increase in the disc potential and highest value of local pH before the H^+ generation ends. Rise of potentials are different under change in applied currents. Larger potential rate change is consistent with higher applied currents. The can imply that our sensor is promising to monitor changes H^+ under different rate of H^+ generation.

At fixed pH (pH 6), different currents were applied and initial rates of potential changes were calculated. Higher I_{gen} applied, faster potential changes were observed. Change in pH at the effective area also depends on the rate of H^+ titration by base species (A^-).

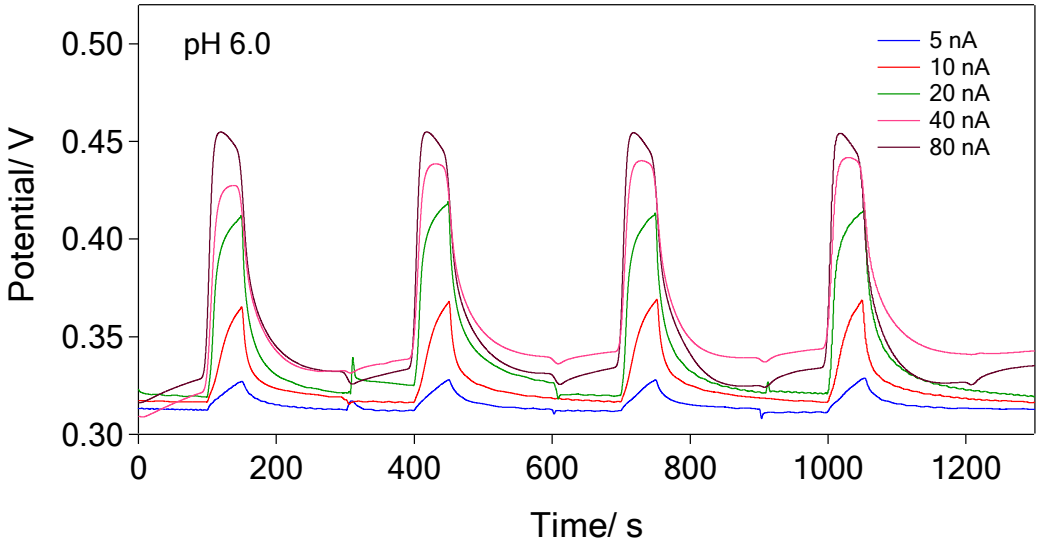

Figure 4.12 Potential change from disc pH sensor while H^+ generation at the ring with different applied currents. Solution: 10 mM HEPES pH 6.0, applied current: 5, 10, 20, 40 and 80 nA.

Different buffer capacity of HEPES buffer was further investigated under the system of ring generator-disc pH sensor detection. The titratable acidity by fixed generation current at 10 nA under different pH of 10 mM HEPES solutions was monitored. Higher buffer capacity (at pH closer to pK_a) gives smaller change of disc potential, due to greater buffer resistant to H^+ perturbation. As shown in Figure 4.13, at pH 7.55 (pK_a of HEPES), change of the disc potential is smallest which is consistent to its highest buffer capacity.

Rate of potential change were calculated and plotted versus I_{gen} for pH 5.55 to pH 7.55 (pK_a). Larger differences in the rate of potential change between each pH were obtained with higher generation of H^+ flux (or I_{gen}). At pH where the buffer capacity is low, the rate of potential change is noticeably higher at the same flux of titrated H^+. With this titration system, we are able to estimate the buffer capacity for unknown buffer by monitoring the change in pH at any given H^+ flux.

At fixed I_{gen} (10 nA), the rate of potential change decreases with the decrease in buffer incapacity (away from pK_a).

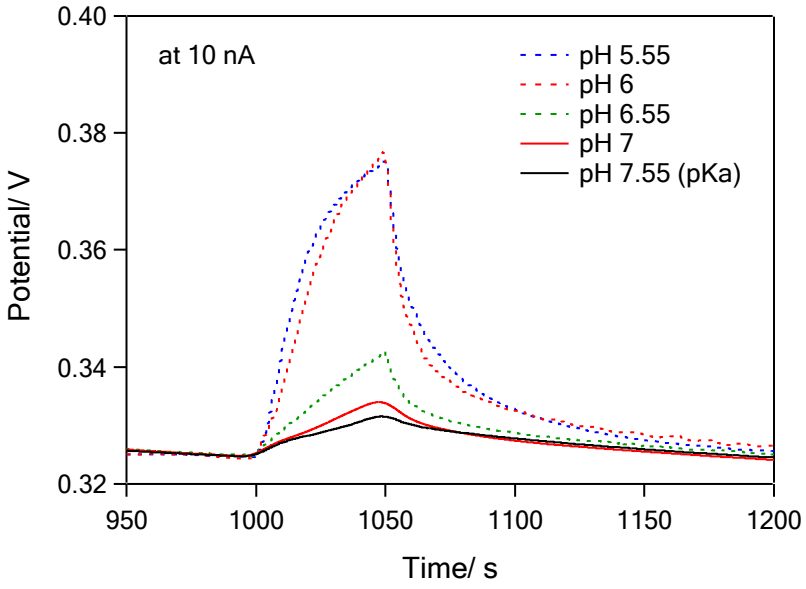

Figure 4.13 Potential change at disc pH sensor on the H^+ generation at the ring at different pH. Solution: 10 mM HEPES pH 5.55 to 7.55, applied current: 10 nA.

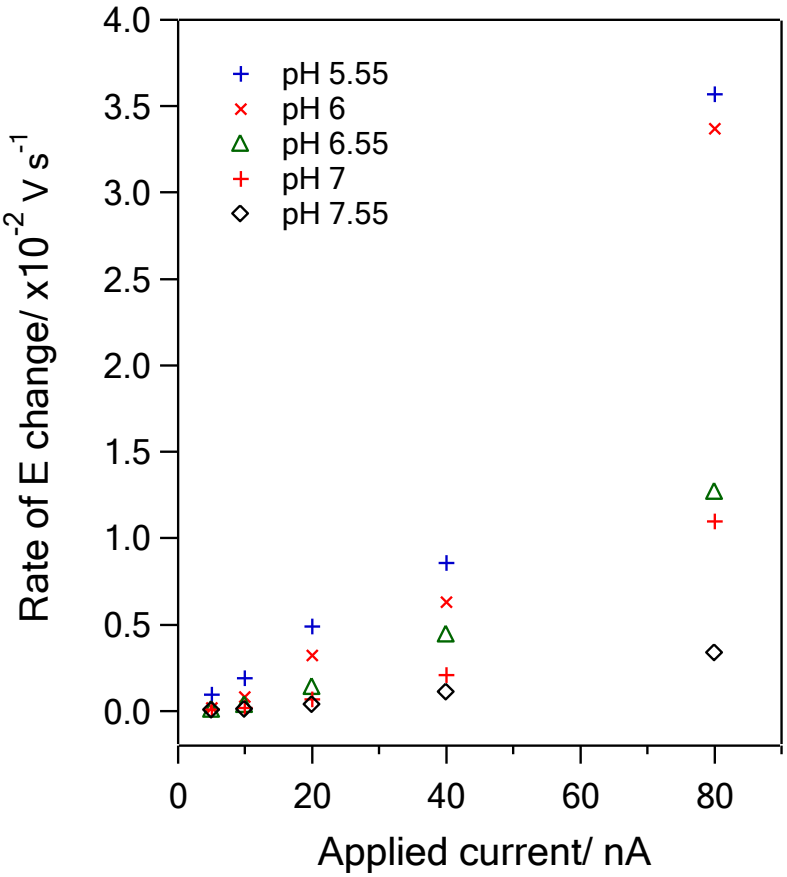

Figure 4.14 Plot of initial rate of potential change with applied current for 10 mM HEPES buffers pH 5.55 to 7.55 (pK_a), (n=5).

4.5.3 Steady state measurement

Steady potential can be reached for all I_{gen}. Higher I_{gen} gives shorter time to reach the equilibrium. For I_{gen} at 40 and 80 nA, intial rates are too high compared to the diffusion rate of A^- into sampling volume, and the amount of conjugated based (A^-) were titrated quickly resulting in sharp potential change (pH change). pH gradually decreases until it reaches to equilibrium.

At steady potential, rate of H^+ generation is equal to rate of A^- diffusion (and the reaction rate of titration is very fast). We can estimate the amount of base species for the buffer if the effective sampling is determined. With known base concentration, buffer capacity can be predicted.

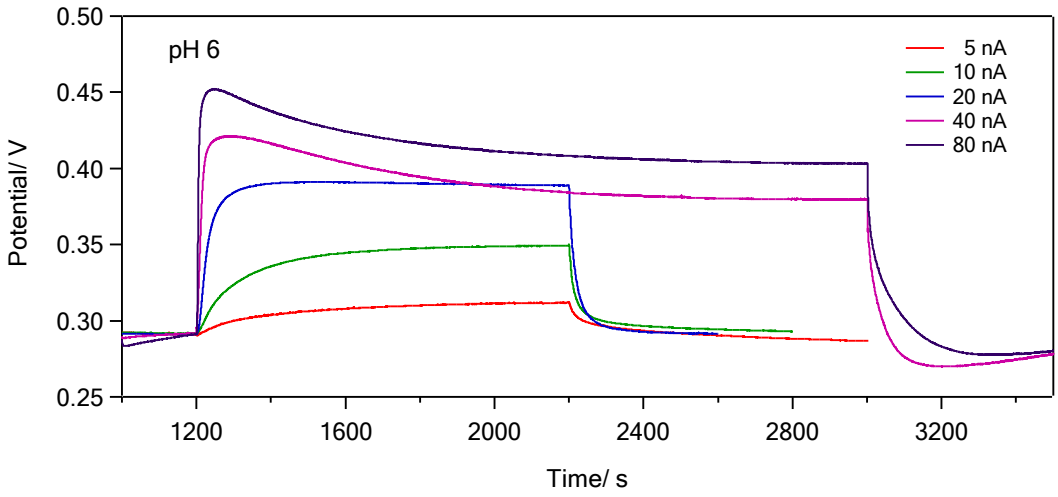

Figure 4.15 Change for disc potential with different applied currents for 10 mM HEPES buffers pH 6. Applied currents were stopped after reaching the steady potential.

4.5.4 Test with bicarbonate (HCO_3^-) system

Bicarbonate is of interest because it plays an important role for controlling pH of blood in our body. The pK_a for bicarbonate buffer in blood system is about 6.1. Please be note that the amount of CO_2 is

$$H_2O(l) + CO_2(g) \rightarrow H_2CO_3(aq) \rightarrow H^+(aq) + HCO_3^-(aq) \quad ; pK_a\ 6.1$$

Normal blood pH is in range 7.35 – 7.45 which is away from pK_a value. Small change of pH can cause a severe health problem (acidosis or alkalosis). Determination of buffer capacity in blood can indicate how good and robust of your blood to pH change is and we can help to prevent the causes of acidosis or alkalosis in time.

Experimental section

25 mM HCO_3^- samples were prepared by diluting a stock solution of 250 mM $NaHCO_3$ and adjusted to desired pH by adding appropriate amount of diluted phosphoric acid. All other experimental details are as previously reported unless otherwise stated.

Result and discussion

Bicarbonate buffer pH 7.4 which is close to the blood pH was selected. Different applied currents were tested and shown in figure 8. The observed potential change is larger with higher I_{gen}. Steady potential can be reached when longer I_{gen} is performed (as seen in the last transient). Another set of experiments with pH 7.5 was done in order to compare the rate of potential change and steady potential when the pH difference is extremely small (~0.1 unit).

As shown in Figure 4.16 (bottom), the steady potentials obtained from the same applied current are quite different. It took longer to reach to equilibrium for pH 7.4. This could be related to the differences in buffer capacity.

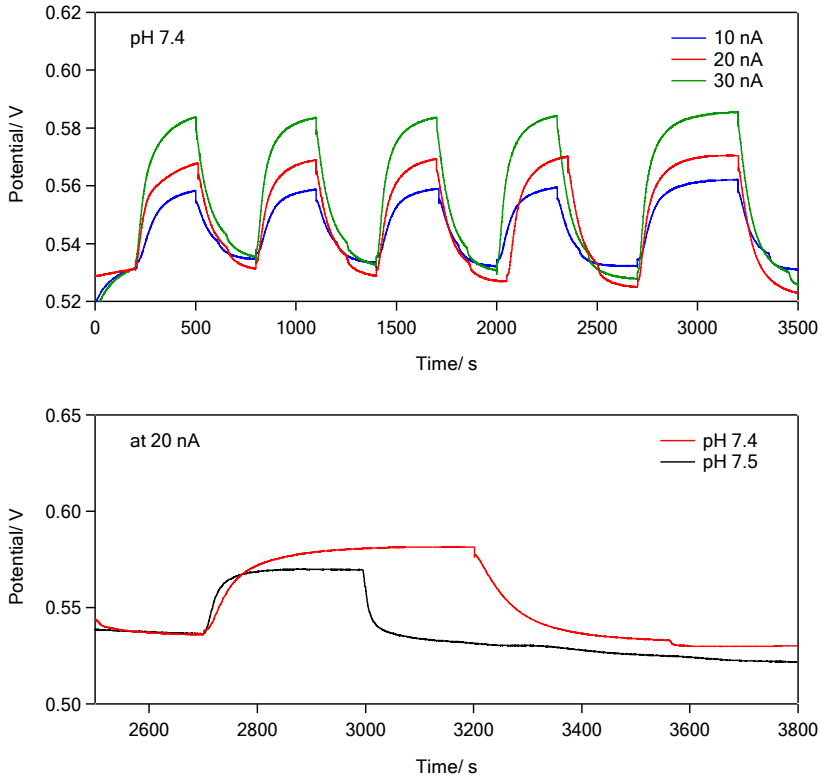

Figure 4.16 Change of disc potential with different applied currents for 25 mM HCO_3^- buffer at pH 7.4 (top). A comparison of the transients between pH 7.4 and 7.5 (bottom) at 20 nA.

Initial rates of potential change were plotted and showed small difference between pH 7.4 and 7.5 for each H^+ flux (figure 4.17). These differences could indicate and differentiate the buffer capacity of the normal status from risk status in real applications. However, more experimental data are required. Titratable acidity in bicarbonate system is in progress.

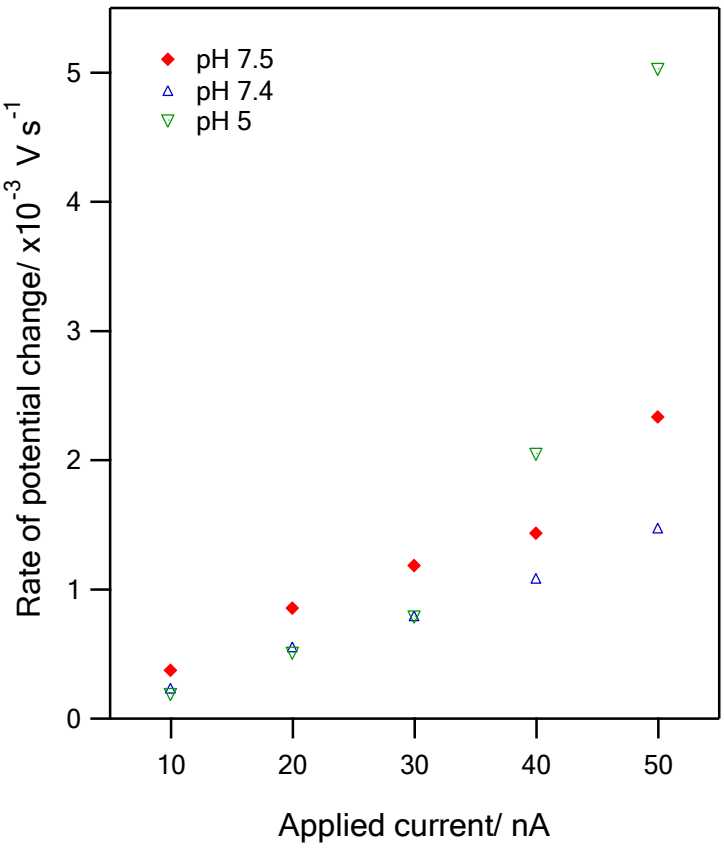

Figure 4.17 Plot of initial rate of potential change with applied current for 25 mM HCO_3^- buffers pH 5, 7.4 and 7.5 (n=5).

4.6 Conclusion

The ring – disc microelectrode configuration is a promising device for generation – collection detection. Detection of pH change can be achieved using fabricated ring – disc microelectrode under the mode of H^+ generation – transient detection. Transient detection is carried out using the modified pH electrode with iridium oxide film on the disc while the constant current generation is applied on the ring electrode. Sensor calibration under Britton-Robinson buffer in the pH range of 2 to10 was satisfied with high sensitivity and good linearity. Super Nerstian response with the sensitivity up to 73.7 mV/pH was obtained from the fabricated disc pH electrode. The pH electrodes exhibit consistent performance under pH 2 to 10 with r^2 up to 0.9995.

Titratable acidity was performed under the ring generation-disc pH detection with HEPES buffer. This system provides significant change in monitored H^+ titration for both transient and steady state current mode. Data from the sensor showed capability to monitor changes H^+ under different rate of H^+ generation (different flux of H^+ generation). The rate of pH change was extracted from transient signal. Lower rate of pH change belongs to higher buffer capacity solution. Steady state current stands for equal rates of proton generation and titration. This is encourage that local proton concentration can be theoretically estimated and the information of buffer capacity in the solution can be determined [15].

References

1. Davenport HW: **The ABC of Acid—Base Chemistry: the elements of physiological blood-gas Chemistry for medical students and physicians.,** 5th edn: The University of Chicago Press; 1969.
2. Ellison G, V Straumfjord J, P Hummel J: **Buffer capacities of human blood and plasma**. 1959, **4**(6):452-461.
3. Kellum JA: **Determinants of blood pH in health and disease**. *Critical Care* 2000, **4**(1):6-14.
4. A. SD, M. WD, James. HF: **Analytical chemistry : an introduction**, 7th edn. Fort Worth ; London: Saunders College; 2000.
5. A. SD, James. HF, R. CS: **Principles of instrumental analysis**, 6th edn. Pacific Grove, Calif. : Brooks/Cole ; London: Thomson Learning; 2007.
6. Vanderschoot B, Bergveld P: **An ISFET-based microliter titrator - integration of a chemical sensor actuator system**. *Sensors and Actuators* 1985, **8**(1):11-22.
7. Głab S, Hulanicki A, Edwall G, Ingman F: **Metal-Metal Oxide and Metal Oxide Electrodes as pH Sensors**. *Critical Reviews in Analytical Chemistry* 1989, **21**(1):29-47.
8. Kurzweil P: **Metal Oxides and Ion-Exchanging Surfaces as pH Sensors in Liquids: State-of-the-Art and Outlook**. *Sensors* 2009, **9**(6):4955.
9. Bitziou E, O'Hare D, Patel BA: **Simultaneous detection of pH changes and histamine release from oxyntic glands in isolated stomach**. *Anal Chem* 2008, **80**(22):8733-8740.
10. Bitziou E, O'Hare D, Patel BA: **Spatial changes in acid secretion from isolated stomach tissue using a pH-histamine sensing microarray**. *Analyst* 2010, **135**(3):482-487.
11. Kazusuke Y: **Anodically Electrodeposited Iridium Oxide Films (AEIROF) from Alkaline Solutions for Electrochromic Display Devices**. *Japanese Journal of Applied Physics* 1989, **28**(4R):632.
12. Yamanaka K: **The Electrochemical Behavior of Anodically Electrodeposited Iridium Oxide Films and the Reliability of Transmittance Variable Cells**. 1991, **30**(6):1285-1289.
13. Bezbaruah AN, Zhang TC: **Fabrication of Anodically Electrodeposited Iridium Oxide Film pH Microelectrodes for Microenvironmental Studies**. *Analytical Chemistry* 2002, **74**(22):5726-5733.
14. Wang M, Yao S, Madou M: **A long-term stable iridium oxide pH electrode**. *Sens Actuator B-Chem* 2002, **81**(2-3):313-315.
15. Bell CG, Seelanan P, O'Hare D: **Microelectrode generator-collector systems for electrolytic titration: theoretical and practical considerations**. *Analyst* 2017, **142**(21):4048-4057.

Chapter 5:
Generation – Collection Processes for Dual Electrode System

5. Generation – Collection Processes for Dual Electrode System

5.1 Overview of Generation-Collection Electrode System

A generation-collection electrode system is considered as two working electrodes, generator and collector. The generator is used for oxidation or reduction the analyte which then diffuses to where it can be detected at the collector. In voltammetric or amperometric operation, the collector will be set at a potential to electrochemically transform the generated species to original species or more generally consumed in an electrode reaction. In the case of passive potentiometic detection the concentration of the generated tracer can be logged as a function of mass transport and reaction. General reactions of generation-collection system are presented in equation 5.1. It should be noted that the product of the reaction at collector can be a different species from the starting material depending on a chemical reaction of an intermediate or by product that could occur. A schematic of a generation-collection system is presented in Figure 3.2.

$$\begin{aligned} &\text{at generator:} \quad A \pm e^- \leftrightarrow B \\ &\text{at collector:} \quad B \pm e^- \leftrightarrow A \ (or\ other\ species) \end{aligned} \qquad (5.1)$$

The generation-collection process is the collection efficiency, CE, which calculated from the ratio of the current at collector (I_{col}) to the current at the generator (I_{gen}) as shown in equation 5.2, below:

$$CE = \left|\frac{I_{col}}{I_{gen}}\right| \qquad (5.2)$$

Typically, the CE is aimed to be highest for each examined system or for maximum sensitivity to couple homogeneous chemistry or mass transport. This can be achieved by the system of generator electrode which is completely surrounded by the collector, allowing less of the generated species diffuses away into the bulk solution and for independence of CE on direction of any hydrodynamic bulk flow. Ring-disc electrode is ideal system for generation-collection process. Besides, forcing the generated species to the collector either by convection or limiting the diffusion of generated species to a fixed direction can decrease the losses. Another important factor is electrode distance:

a small distance between generator and collector will maximise the number of generated species to be collected thus enhancing the CE, though possibly at the cost of reducing sensitivity to local mass transport or coupled chemistry. Several generator-collector systems have been reported [1]. Different electrode geometries and method of transport between generator and collector have been varied. Developed by Frumkin *et al.* [2], the rotating ring-disc electrode (RRDE) is applied with electrodes of a rotating disc and a concentric ring separated by a gap of insulation. To operate the RRDE, the central disc will be rotated (at fixed or varied speed) and induce convective flow onto electrode. The flow moves radially onto the surface and outward to the ring collector. A schematic diagram of RRDE system is shown in Figure 5.1. Albery *et al.* further investigated ring-disc geometry and published a number of articles based on RRDE [3-9]. One of the works similar to RRDE is the use of wall jet ring-disc electrode (WJRDE). In WJRDE, analyte is transported from the nozzle toward the centre of the disc electrode, creating a similar flow profile that occurs in RRDE system [3, 4], though without the analytical advantage of uniform hydrodynamic boundary layer observed at the RDE. This has however proved to be a useful technique for flow analysis with end column detection. Applications of WJRDE include identification and determination of proteins [5, 6], organic and inorganic compounds [7-9]. Schematic picture for WJRDE is presented in figure 5.2. Other studies have used a micro ring-disc electrode which is adapted for scanning electrochemical microscopy (SECM) to investigate a mechanism of processes from the conductive surface and insulation. Theory and applications of micro ring-disc electrode in SECM have been reviewed [10, 11]. With this approach, simultaneous monitoring of two near co-located species using a steady-state measurement is also possible.

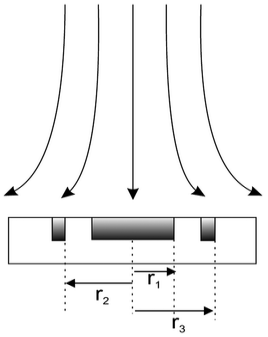

Figure 5.1 Schematic diagram of cross-sectional view of RRDE system under the convective flow, where r_1, r_2 and r_3 represent the disc, inner ring and outer ring radii, adapted from [12].

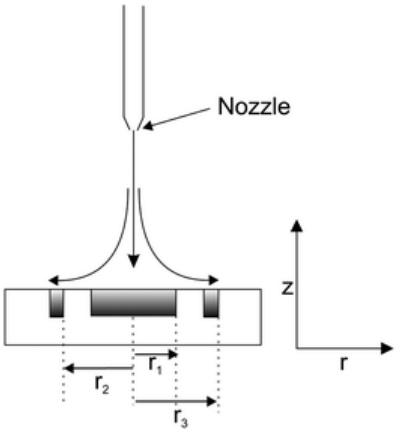

Figure 5.2 Schematic diagram of cross-sectional view of WJRDE system under the impinging jet flow, where r_1, r_2 and r_3 represent the the disc, inner ring and outer ring radii, adapted from [12].

Steady state operation in SECM simplifies the theoretical treatment and can reduce the problems associated with double layer charging [10]. A common mode of operation is disk-generation/ring-collection. Conceptually, a redox mediator reacts under diffusion-controlled conditions at the disc and is regenerated at the ring electrode. Ring-disc SECM shows potential for monitoring of spontaneous reactions, partitioning across interfaces and detection of reaction intermediates [11].

Another double electrode system is the dual band device which consists of two planar parallel microband electrodes fabricated inside the flow channel. In this system, analyte flows over the generator and then detected at a downstream collector, as schematically shown in Figure 5.3. Theoretical treatment and applications of dual band electrode are extensively reported for electrochemical titration [13-16]. In electrochemical titration, the electrogenerated species is reacted with target analyte in solution; less collection occurs at the collector and thus CE reduces. In terms of sensitivity and multireaction versatility, a further advance system from the dual band electrode is the multi-electrode system.

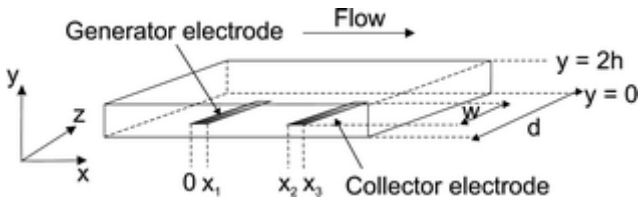

Figure 5.3 Schematic diagram of in-channel dual electrode system, adapted from [12].

Interdigitated array (IDA) electrodes have been developed and applied for the electroanalytical determination of various species [17-19] including experiments under flow environment as well [20-22]. A thin-film microsystem based on the planar interdigitated array electrode is shown in Figure 5.4. The IDA electrode was fabricated using photolithography with typical band gap in the lower micrometre range. Metal and carbon arrays have been manufactured.

As seen from Figure 5.4, small of electrode distances can be produced. This can result in an overlap of the diffusion layer for the generator and collector bands. Feedback current is expected as the regenerated species from the collector can rapidly diffuse back to the generator. The feedback can enhance the generator current and gives better sensitivity. Enhancement of sensitivity is a common application of IDAs. Arrays of disc electrodes and ring-disc electrodes have been generated and investigated in theory and biological application [23-25]. It was agreed that the array of generation-collection electrode is a promising device for detection of unstable intermediates and provide higher currents compared to single discs in the array [18, 22, 23]. Electrode arrays are well developed and likely to find more widespread application.

In our work, the generation-collection processes at a dual disc device will be the focus of interest. Where possible, performances in both steady state and transient mode will be compared with numerical and analytical models.

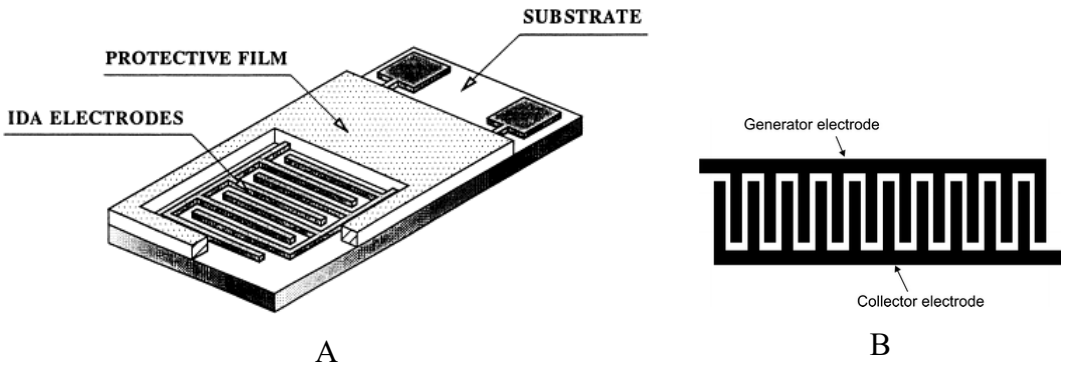

Figure 5.4 Schematic picture of IDA electrode system (A) and its operation (B), adapted from [19]

5.2 Dual Disc Electrode

Electrodes with generator-collector properties can be successfully used to study electrochemical reaction mechanisms [26-28]. Most of them are based on the well-known features associated with electrodes with at least one dimension in the range of micrometers. Dual disc electrode is made of two microdiscs in close vicinity to one another. With small distance between two electrodes and sufficient amount of supporting electrolyte, the transport of generated species will be largely by diffusion [29]. Schematic pictures of dual disc electrode and the hemisphere of each disc electrode can be illustrated in Figure 5.5. The dual disc electrode is easy to fabricate and polishing of the electrode is facile. Moreover, measurements can be performed without sophisticated equipment; for example, rotating device or flow. The dual disc device also provides excellent voltammetric features when used in stationary solution [30]. In many experiments, the dual disc microelectrode is a viable alternative to the RRDE. However, in terms of kinetic studies on homogeneous reactions of intermediates, use of disc microelectrode is limited due to the electrode spacing.

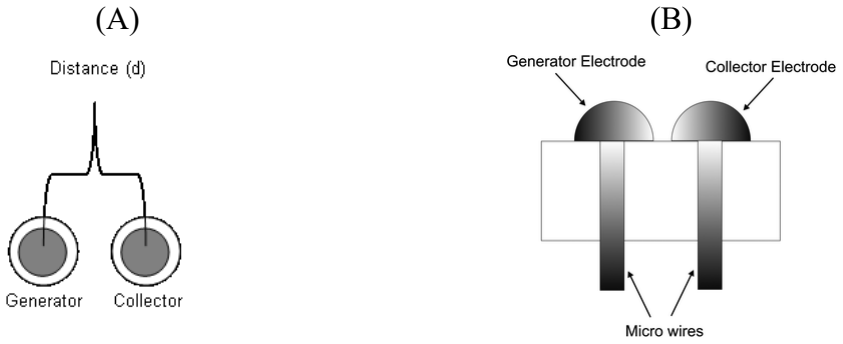

Figure 5.5 Schematic picture of an inlaid dual disc electrode (A) and cross section of a dual hemisphere system (B), adapted from [12, 30]

5.3 Electrode Behaviour of Single Electrode on Inlaid Dual Disc

In practice, all working electrodes were electrochemically characterised prior to each experiment, as previously described in Chapter 2. Steady state voltammograms and capacitance extracted from voltammetric data of the electrode were used to characterise electrode properties in terms of size and structure. For the same sensor, the electrode behaviour was compared to different electroactive species. Additionally, the feedback effect was investigated for the self-fabricated sensor by comparison of separate scan of single disc to simultaneous scans of both discs.

Method and Materials

Three redox species with different diffusion coefficients were chosen for steady state voltammetry. Solutions of 10 mM ruthenium hexaammine ($Ru(NH_3)_6^{2+/3+}$), 1.5 mM ferrocene carboxylate (ferrocene) and 10 mM potassium ferrocyanide ($Fe(CN)_6^{4-}$) were prepared in 1 M KCl. All reagents were obtained from Sigma-Aldrich and prepared using MilliQ water with resistivity of at least 10^{15} Ω cm. Standard solutions were bubbled for at least 5 mins with argon gas in order to remove dissolved oxygen prior to the experiment.

The multichannel potentiostat CHI model 1030 (CH Instruments Inc., Texas) was operated to control the potential at the disc in an electrochemical cell containing Pt mesh as a counter electrode and Ag|AgCl reference electrode (3 M KCl (aq)). A 75 μm dual disc sensor was used as working electrode. The distance (d) from centre-to-centre

of the discs is 355 μm, measured from an SEM micrograph (see Section 2.3.3). Prior to each experiment, the dual disc microelectrode was sonicated sequentially in diluted detergent solution (Decon), warm water, methanol, and then warm water in a ultrasonic bath. Steady state currents were obtained by separate potential scan at each disc electrode with each species. Feedback effects were checked by a simultaneous scan of both electrodes and compared by separate scan.

Results and discussion

Estimation of current is based on voltammetric conditions as described in the mass transport theory (see Chapter 1). The mechanism contributing to the transport of electroactive species in the solution layer is only diffusion (given by Fick's law) and that charge transferred at the electrodes is reversible. Plots of i versus V obtained from DG1 and DG2 are shown in Figure 5.6. Please note that only forward scans are displayed for comparison. Observed current from each disc agrees well with theoretical estimation with less than 5% of difference. Slightly lower steady state currents for ferrocene were observed even with slow scan rate of 5 mV s^{-1}, reason behind this is not clear. Again, all plots of steady current curves of three electroactive species are consistent with well-behaved and straightforward electrode behaviour. A feedback effect is also observed, but not greatly enhance the limiting current of each disc because of the large distance between generator and collector. Comparison of each disc current obtained from separate and simultaneous scans were shown in Figure 5.7. Generation-collection process was performed by applying a fixed potential at collector while the potential of the generator was scanned. Only standard $Ru(NH_3)_6^{3+}$ was presented in this thesis, since this is a rapid electrode reaction with simple outer sphere electron transfer. Plots of i-V from generation-collection process are displayed in Figure 5.8, from where CE data is extracted. From the test, the collector current (I_{col}) gradually increased while forward scan is progressed at the generator. Once reaction at generator reaches to its limit, I_{col} reaches a maximum value. The I_{col} from reversed scan keeps increased as the existing $Ru(NH_3)_6^{2+}$ ions are being oxidised at fixed potential while the generated $Ru(NH_3)_6^{3+}$ions diffuse away into bulk solution. Only 5 % CE was observed. Another way to increase the CE is smaller gap between dual discs. However, with simple fabrication method where precise electrode distance is hard to control, studies focused on steady current and transient generation-collection at a fixed distance.

Electrode	DG1	DG2
$Ru(NH_3)_6^{3+}$	$i\ (\times\ 10^{-9})$ A 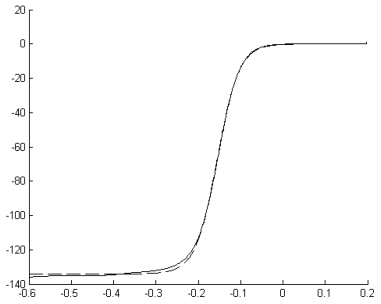 $E\ (V)$	$i\ (\times\ 10^{-9})$ A 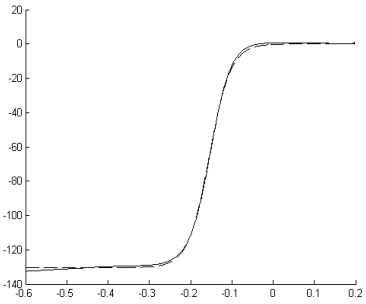 $E\ (V)$
$Fe(CN)_6^{4-}$	$i\ (\times\ 10^{-9})$ A 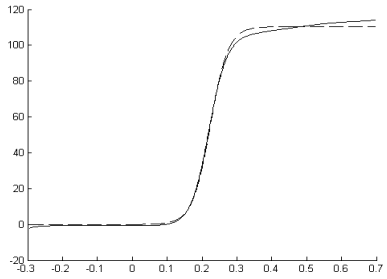 $E\ (V)$	$i\ (\times\ 10^{-9})$ A 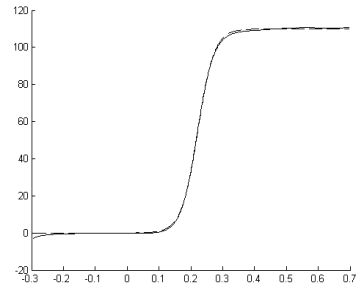 $E\ (V)$
Ferrocene	$i\ (\times\ 10^{-9})$ A 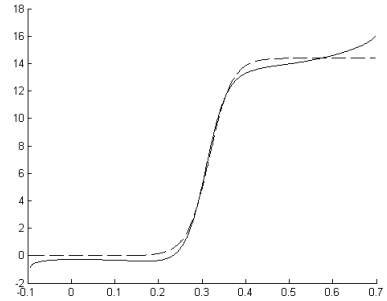 $E\ (V)$	$i\ (\times\ 10^{-9})$ A 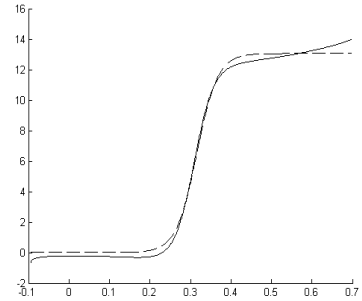 $E\ (V)$

Figure 5.6 i-V plots for single disc calibration of DG1 and DG2 obtained from theoretical model $(\cdots)$ and experiment $(-)$ of 10 mM $Ru(NH_3)_6^{3+}$, 10 mM $Fe(CN)_6^{4-}$ and 1.5 mM Ferrocene. 75 μm dual disc sensor was used, with scan rate 5 mV/s.

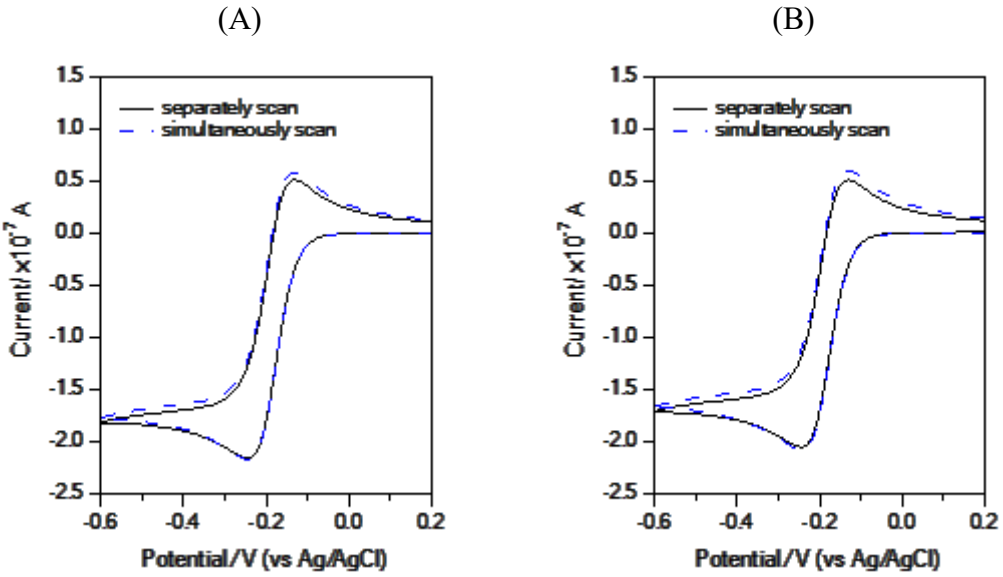

Figure 5.7 i-V plots of DG1 (A) and DG2 (B) obtained from simultaneous (⋯) and separate (-) scan using 10 mM $Ru(NH_3)_6^{3+}$ in 1.0 M KCl, scan rate 50 mV/s.

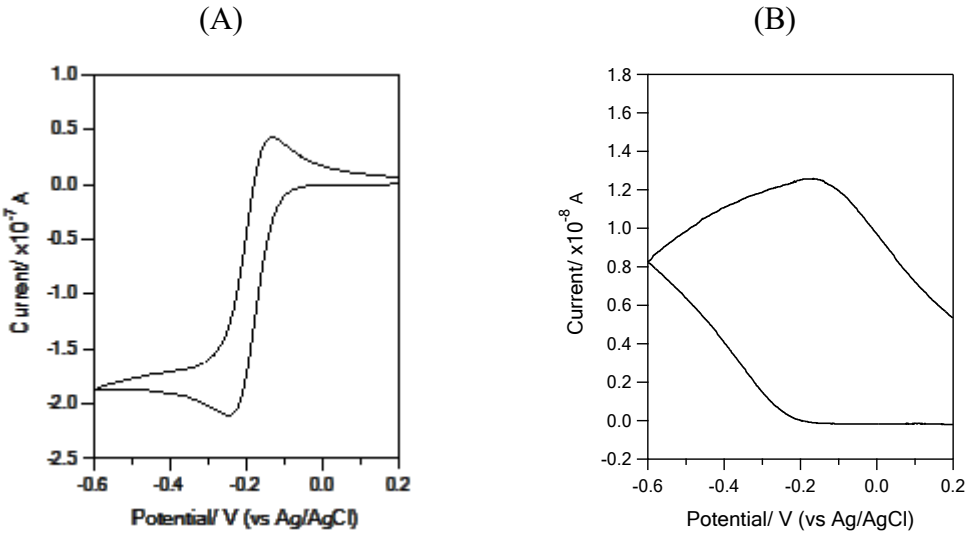

Figure 5.8 Test of generation-collection process by potential scanning of generator DG1 (A) and holding collector potential at DG2 (B) using 10 mM $Ru(NH_3)_6^{3+}$ in 1.0 M KCl, scan rate 50 mV/s.

5.4 Generation-Collection Detection on Dual Disc Sensor

Effective simulation of the response of a redox couple provides a basis for more complex and three-dimensional orientations and has the potential to enable insight into the key parameters for optimized operation in any given experiment or application. In this work, the theory of voltammetric processes at a diffusion controlled dual microelectrode system is attempted by redox processes of species over two electrodes [12, 31, 32]. Systems of two disc electrodes enclosed in the insulator within micrometre distance are examined [33, 34]. Analyte is considered to diffuse within the simulation space where effects of migration and convection are negligible. It can be assumed that the concentration distributions in the solution between dual discs depend only on the separation distance. The concentration profile is simulated and compared to the observed data.

5.4.1 Constant Current Generation – Passive Collection System

In this mode, analyte is generated at the generator where the potential across the collector is monitored. This process is similar to buffer capacity measurement which pH sensor selectively senses the ions of interest, H^+ surrounding collector surface. Constant current generation provides constant flux of ions generated at electrode surface. Since the collector surface is non-modified, a reversible redox couple with known concentration is applied and detection is based on the relationship of Nernst's equation.

Method and Materials

The redox couple of ferri/ferro cyanide was chosen as preparation of different concentration ratios is easy and its electrochemical properties and physico-chemical parameters are well known. Standard ferri/ferro solutions with concentration ratio of 1:1 and 1:10 dissolved in 1 M KCl were prepared. All standard chemicals were obtained from Sigma-Aldrich and dissolved in the MilliQ water. Precision current source Keithley model 6220 (Keithley Instruments, Inc., Ohio) was operated to control the

current at the disc generator in the electrochemical cell containing a large Pt mesh as a counter electrode. The collector was equipped with the multichannel potentiostat CHI model 1030 (CH Instruments Inc., Texas) using open circuit potential (OCP) mode. The 75 μm dual disc sensor with *d* of 355 μm was used as working electrode connected with Pt counter electrode and Ag/AgCl reference electrode. Prior to each experiment, the dual disc microelectrode was sonicated under diluted cleaning solution (Decon), warm water, methanol, and then warm water under ultrasonic bath, respectively.

Results and discussion

Steady state current was performed for both concentration ratio of ferri/ferrocyanide. Limiting currents of 1:1 and 1:10 ferri/ferrocyanide concentration were achieved by separate scan of each disc using 25 µm platinum (DPt) and 75 µm gold (DG) dual sensors, the *d* between each system is of 195 µm and 355 µm, respectively. This is to limit the range of potential where we can observe the steady potential at the collector following to mass transport controlled reaction. Reversible process of ferri/ferrocyanide can be expressed as follow,

$$Fe(CN)_6{}^{3-}(aq) + e^- \leftrightarrow Fe(CN)_6{}^{4-}(aq) \qquad (5.3)$$

with E^0 0.25 V (vs Ag|AgCl).

Applying to Nernst equation, the equilibrium potential follows to equation 5.4, shown below,

$$E = E^0 - \frac{RT}{nF} ln \frac{[Fe(CN)_6{}^{3-}]}{[Fe(CN)_6{}^{4-}]} \qquad (5.4)$$

where E^0 is formal potential, *R* is the gas constant, *F* is Faraday's constant, *n* is electron number and *T* is temperature.

In practical, generation starts after 100 s of collector response to get a stable baseline. Observed steady potentials of each ratio of different ferri/ferrocyanide concentration were taken after transient change in the first 300 to 400 s. It can conclude that steady

potential is attainable after a period of time allowing generated species to reach the collector, as shown in figure 5.9. The changes of potential over time were recorded when DPt2 acted as collector (Figure 5.9A), whereas the plots in figure 5.9B were obtained by operating the switching mode of dual disc. Negative current was applied to explore the change of reverse reaction; generation-collection process is also feasible. Like in the measurement of buffer capacity, potential at the collector were resumed back to the initial value since the solution composition turn into its equilibrium.

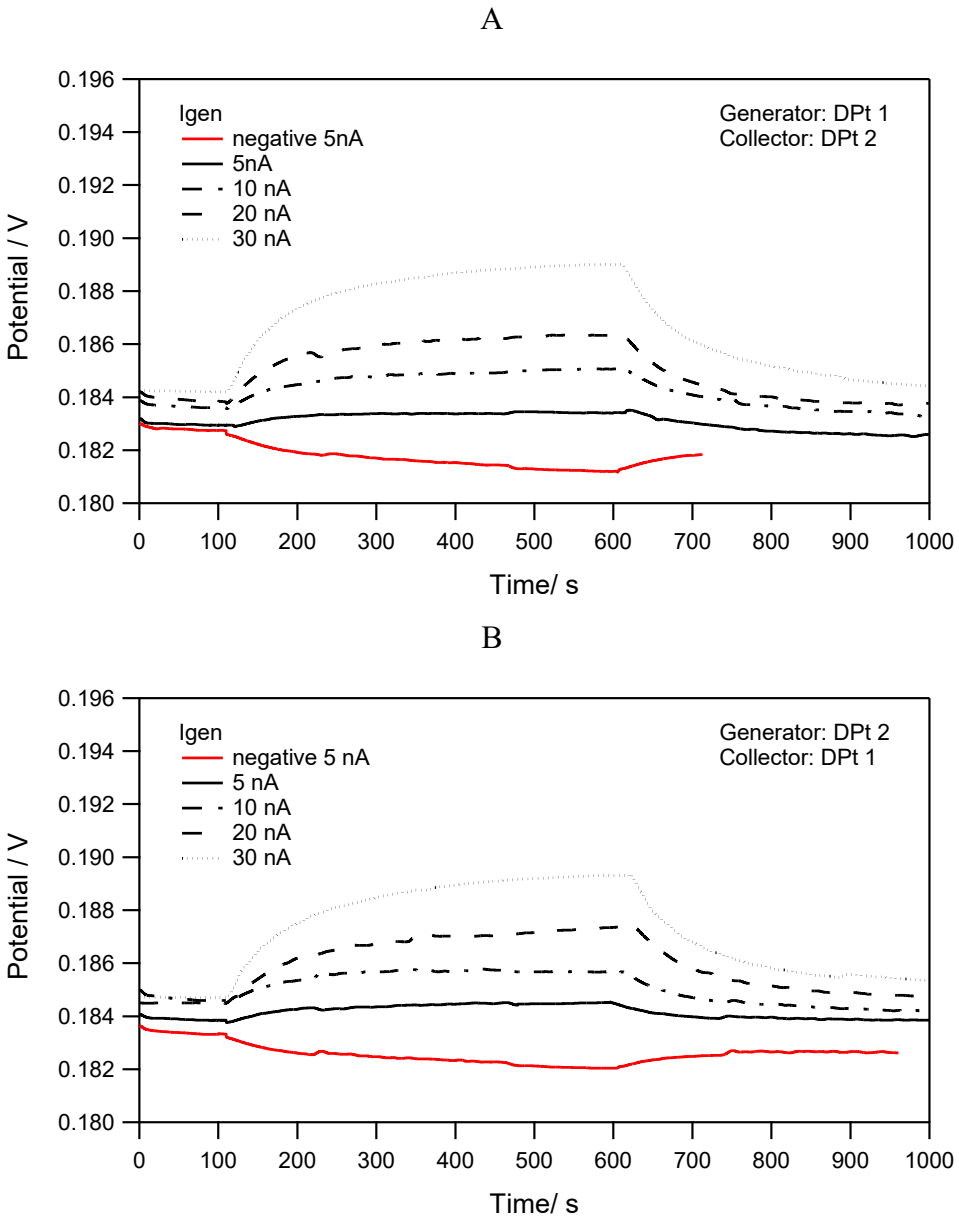

Figure 5.9 Plots of potential (E) versus time (t) observed from the constant potential generation – passive collection mode of 1 mM $Fe(CN)_6^{3-}$ and 10 mM $Fe(CN)_6^{4-}$ in 1 M KCl using a 25 μm dual disc sensor.

Passive detection with constant current generation was further investigated using 1:1 ferri/ferrocyanide concentration ratio. With 10 mM $Fe(CN)_6^{3-}$ and 10 mM $Fe(CN)_6^{4-}$ solution, limiting current of reduction reaction was high as equal as the oxidative current due to equivalent flux of active species; therefore, a wide range of negative current can be applied. Steady potentials were recorded and shown in Figure 5.10. Distance plays an important factor under the same experimental conditions. A theoretical model of passive detection has been studied in our group and compared to the experimental data [35]. Steady potential is solved within inlaid disc condition and local concentration at collector disc can be approximated, details are not shown here. In our test, observed potentials are broadly consistent with the model. We have found that simple method of electrode fabrication with controllable and precise distance is problematic. However, this passive detection system can be used as a primary test for the examination of non-modified surface dual disc sensor.

A

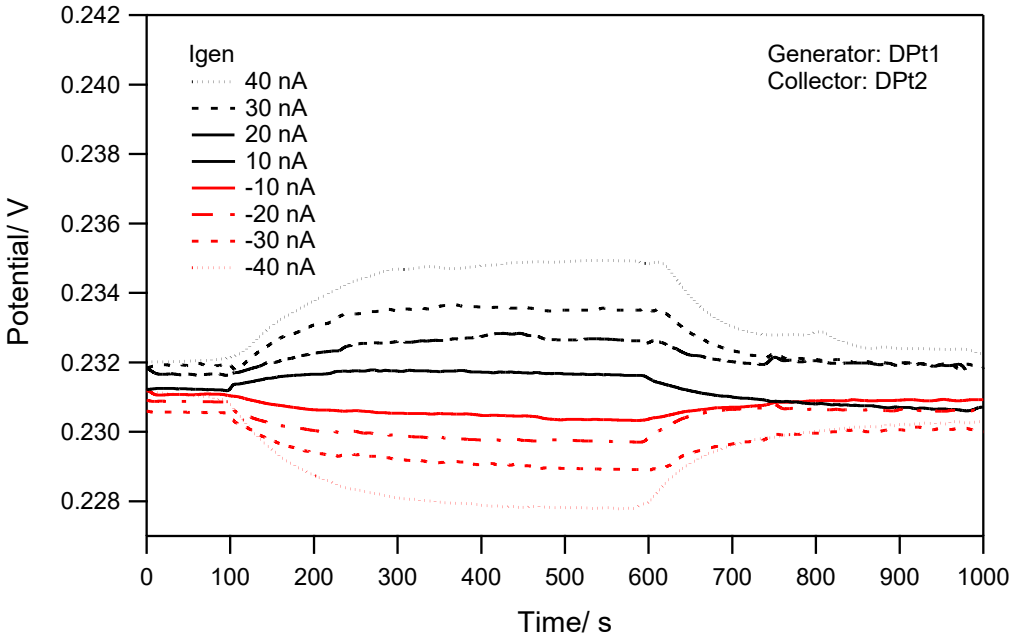

B

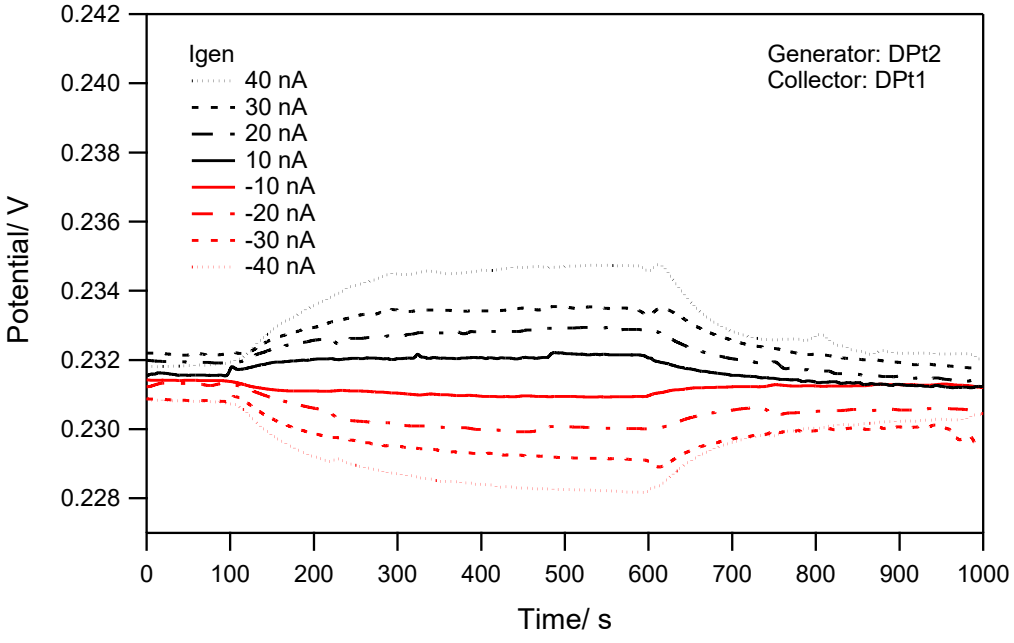

Figure 5.10 Plots of potential (E) versus time (t) observed from the constant potential generation – passive collection mode of 10 mM $Fe(CN)_6^{3-}$ and 10 mM $Fe(CN)_6^{4-}$ in 1M KCl using 25 μm dual disc sensor.

5.4.2 Constant Potential Generation – Constant Potential Collection System

In this section, we will work on the regenerating of target species to examine the CE of our dual disc system. To explore the efficiency of dual disc electrode, three redox species with known diffusion coefficient, *D*, were carried out. Ruthenium hexaammine (D 7.70×10^{-10} m^2s^{1-}), potassium ferrocyanide (D 6.50×10^{-10} m^2s^{1-}) and ferrocene carboxylate (D 5.73×10^{-10} m^2s^{1-}) are employed; each D was as reported in the literature [28, 36]. Constant potential was operated at the disc as a generator. As the rate of ions generation over the solution layer are constant, this effects to the transient detection.

Method and Materials

Standard 10 mM ruthenium hexaammine ($Ru(NH_3)_6^{3+}$), 1.5 mM ferrocene carboxylate (Ferrocene) and 20 mM potassium ferrocyanide ($Fe(CN)_6^{4-}$) were prepared as previously described in section 5.3. Prior to the experiment, standard solutions were bubbled for at least 5 mins with argon gas in order to remove dissolved oxygen. The multichannel potentiostat CHI model 1030 (CH Instruments Inc., Texas) was operated to control the voltage in an electrochemical cell containing Pt mesh counter electrode and Ag/AgCl reference electrode.75 μm dual disc sensor with *d* of 355 μm was operated as working electrode. Electrode cleaning and characterisation were regularly done before each test, as previously mentioned in section 5.3.

Results and discussion

- **Ruthenium hexaammine (III) system, $Ru(NH_3)_6^{3+}$**

Constant potentials were applied to both disc electrodes (generator and collector). Generation-collection processes are as followed.

Disc 1

Generator: $Ru(NH_3)_6^{3+} + e^- \rightarrow Ru(NH_3)_6^{2+}$; const. E (start at 50 s, for 500 s)

Disc 2

Collector: $Ru(NH_3)_6^{2+} \rightarrow Ru(NH_3)_6^{3+} + e^-$; const. E

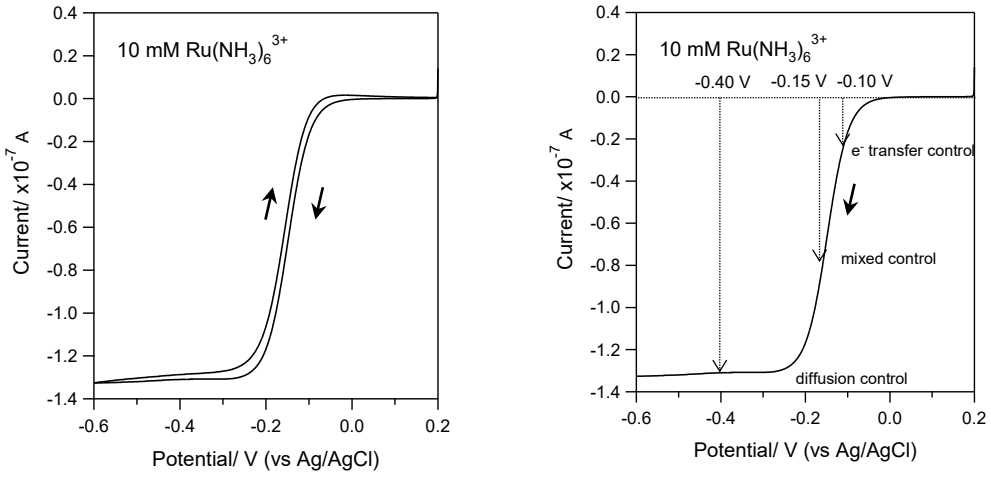

Figure 5.11 i-V curve of 10 mM $Ru(NH_3)_6^{3+}$ in 1M KCl from 75 μm dual disc sensor; one cycle scan (A) and the indicated generator potential at different region (B).

With fixed potential at the collector, the applied potentials of the generator were varied among the e^- transfer, mixed and the diffusion dominant region. Steady state current and different regions of collection potentials were obtained from i-V curve as illustrated in figure 5.11. Generation was started after few second of recording on the collector, and then stopped once it reaches to steady state value. At collective potential of 0 V where reverse reaction current is limited, steady currents obtained from more negative potential (closed to diffusion limit) is higher, implied to higher mass transport to the electrode surface.

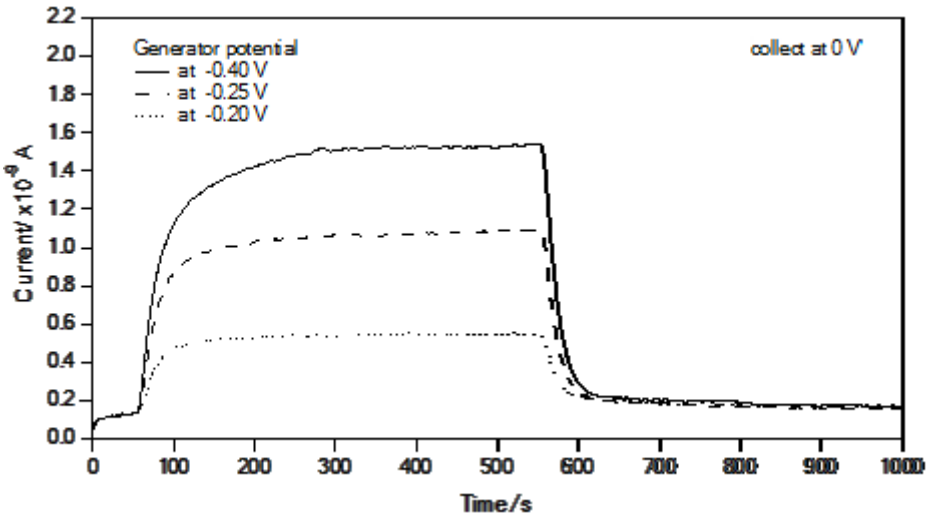

Figure 5.12 i-t curve obtained from generation-collection process under constant potential mode using 75 μm dual disc sensor with 10 mM $Ru(NH_3)_6^{3+}$ in 1M KCl.

The results of constant potential mode of $Ru(NH_3)_6^{3+}$ system show steady current after 300 s for all applied generation potential. Plot of i-t curve obtained from generation-collection process under different potentials are shown in Figure 5.12. However, the switching mode cannot be achieved at the time of testing, comparison of collection responses from both discs is lacking for this system. Like in passive detection, the observed currents are comparable to the estimation. The transient reveals faster change which is inferred to higher rate of mass transport. Prediction of transient is more interesting as it provides shorter analysis time. Change of transient is currently investigated using theoretical model developed by our group.

- **Ferrocynanide system, $Fe(CN)_6^{4-}$**

Dual disc electrode system was examined using potassium ferrocyanide, $K_4Fe(CN)_6$ (represented as $Fe(CN)_6^{4-/3-}$ redox couples). i-V curve of 20 mM $K_4Fe(CN)_6$ in 1 M KCl with 5 mVs^{-1} scan rate is shown in Figure 5.13. The reason for using higher concentration compared to previous experiment is to increase the sensitivity. Generation-collection process was performed as reversed to $Ru(NH_3)_6^{3+}$ system, the starting material undergoes oxidation reaction at generator while the collector potential is fixed for reduction. Therefore, sign of collective current was opposite to $Ru(NH_3)_6^{3+}$ system. Results from generation-collection process with switching mode of electrode function are shown in Figure 5.14.

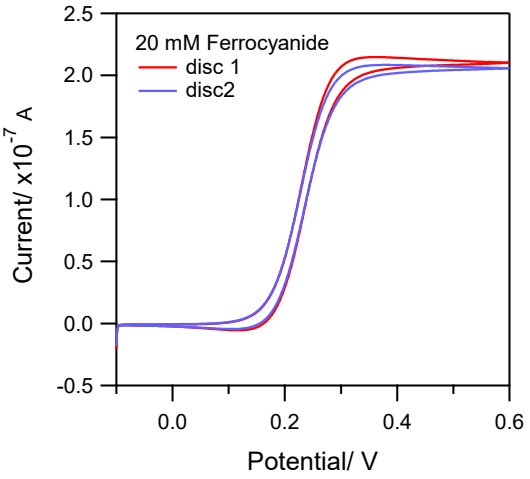

Figure 5.13 i-V curve of 20 mM $Fe(CN)_6^{4-}$ in 1M KCl from separate scan of 75 μm dual disc sensor under scan rate 5 mVs^{-1}.

Although steady currents were observed, equilibrium took longer time to reach in comparison with $Ru(NH_3)_6^{3+}$ system. This is due to smaller diffusion coefficient of ferrocyanide ion. Smaller changes of transient were also consistent with prediction.

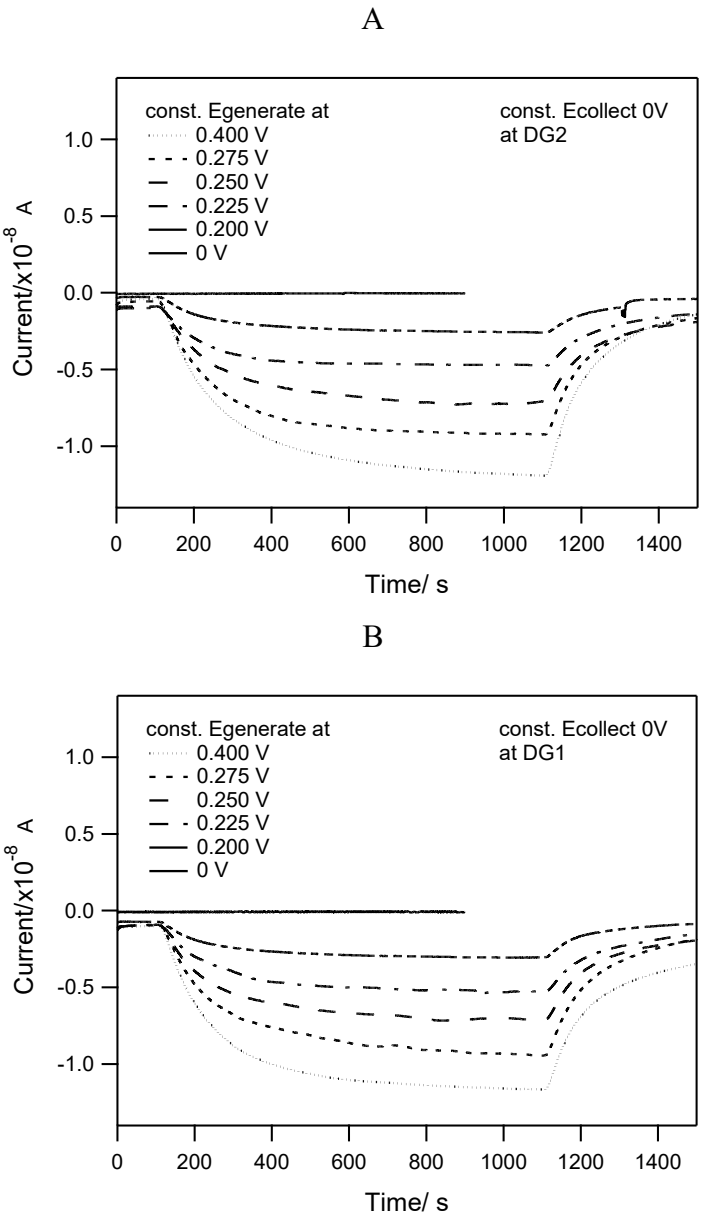

Figure 5.14 i-t curve obtained from generation-collection process under constant potential mode using 75 μm dual disc sensor with 20 mM $Fe(CN)_6^{4-}$ in 1M KCl.

- **Ferrocene monocaboxylate system, Ferrocene**

Ferrocene redox is another interesting couple as it has been used on many bioanalytical applications. The most drawback of ferrocene is its low solubility. i-V curve of 1.5 mM ferrocene in 1 M KCl with 5 mVs^{-1} scan rate is shown in figure 5.15. Sensitivity was low, but acceptable for 75 μm electrode. Generation-collection process was performed as similar to $Fe(CN)_6^{4-}$ system. Results from generation-collection process with switching mode of electrode function are shown in figure 5.16. As seen in the changes of transient response of ferrocene species, steady state currents were hard to reach among three tested redox species. The diffusion coefficients of these ions are reasonably responsible for changes in transient response. With the use of dual electrode system and efficient theoretical model, generation-collection process is able to estimate diffusion coefficient of analyte for particular electrochemical conditions as well as determine analyte concentration of the system.

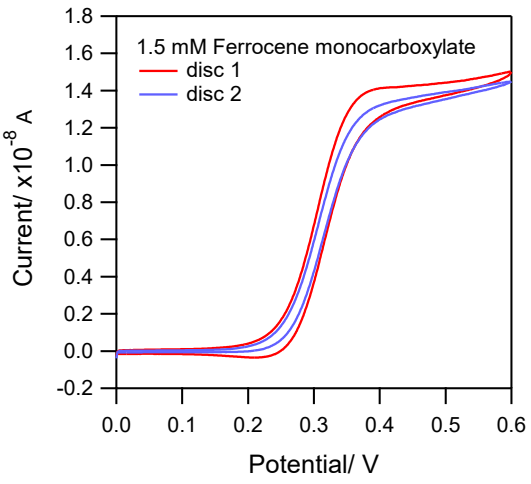

Figure 5.15 i-V curve of 1.5 mM ferrocene in 1 M KCl obtained from separate scan of 75 μm dual disc sensor under scan rate 5 mVs^{-1}.

A

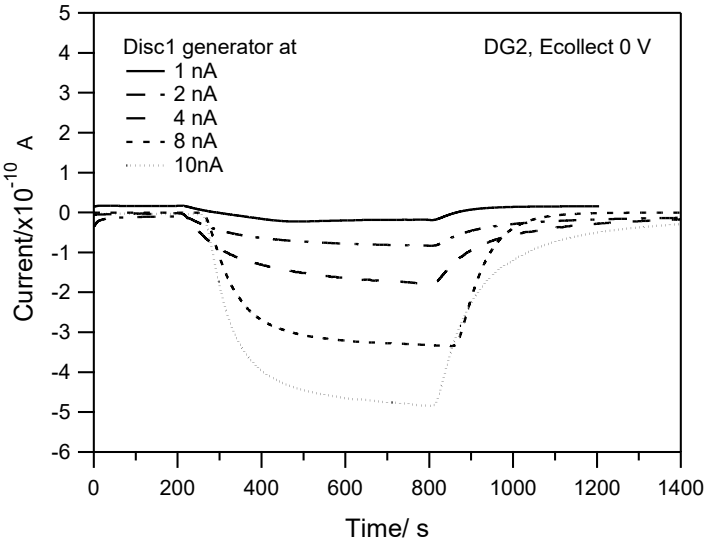

B

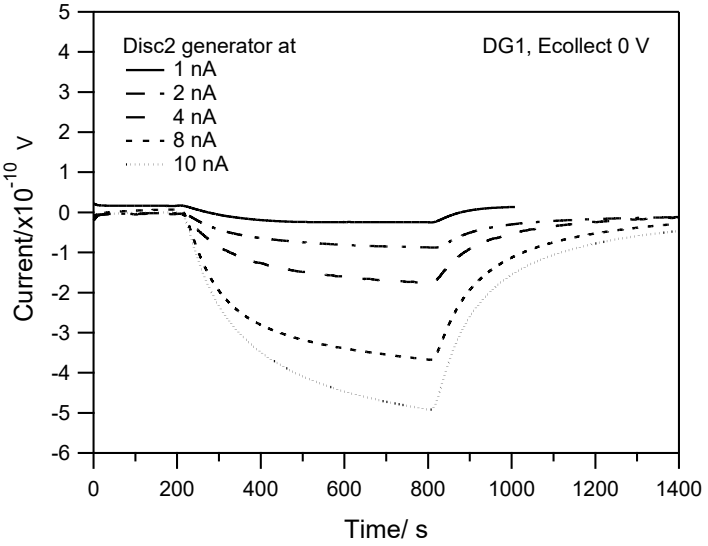

Figure 5.16 i-t curve obtained from generation-collection process under constant potential mode using 75 μm dual disc sensor with 1.5 mM ferrocene in 1 M KCl.

5.5 Conclusion

Generation – Collection processes for dual electrode system were investigated under co planar dual disc electrode. Dual disc electrode were used as a constant current generator at one disc and passive detection collector on the other disc. Chemically reversible reactions of selected redox species which are ruthenium hexaammine ($Ru(NH_3)_6^{2+/3+}$), ferrocene carboxylate (ferrocene) and potassium ferrocyanide ($Fe(CN)_6^{4-}$) were applied since their well-characterised behaviours and differences in diffusion coefficient of each species.

Electrode behaviour of single electrode on inlaid dual disc studied on cyclic voltammetry (CV) of each analyte showed good agreements with the theory. It was found that the steady state currents for all selected redox species were satisfied to the expected value for our dual disc electrode system. Less feedback was observed based on the comparison of simultaneously CV scan of both discs versus separate single disc CV scan. This can be emphasized of the characterisation of self-fabricated electrode to practical steady state performance is obtainable and suitable for further generation – collection experiment.

In generation – collection experiment, analyte is to diffuse within the distance of two-disc electrodes where the concentration distributions in the solution between the discs depend only on the separation distance. Constant current generation – passive collection mode investigated under 1:1 and 1:10 ferri/ferrocyanide concentration, similar to buffer capacity measurement which pH sensor selectively senses the H^+ surrounding collector surface (see Chapter 4). Steady potential is achievable after a period of generation time, allowing generated species to reach the collector. The application of current for reverse reaction was applied and showed that the generation-collection process can be succeed. These results encourage for the use of the dual sensor for more applications involving in different species apart from H^+. Change of potential at the collector are noticeably closed by both positive and negative currents applied at the generator, so the distance plays an important factor under the same experimental conditions. Steady potential is being solved within inlaid disc condition and local concentration at collector disc can be approximated which are moderately consistent with the theoretical model of passive detection in our group [35].

The efficiency of dual disc electrode explored under constant potential generation – constant potential collection system showed consistent responses to three tested redox species of known diffusion coefficients. The system of constant potential at the collector were similarly resulted in steady current results when applied potential is closed to diffusion limit. Faster change in transient is inferred to higher rate of mass transport to the electrode surface. The observed currents are comparable to the estimation passive detection. Change of transient can be predicted under theoretical model developed by our group [35]. Among three tested redox species, the diffusion coefficients of these ions are reasonably responsible for changes in transient response. Smaller diffusion coefficient of ions took longer time to reach in the equilibrium. Smaller changes of transient were also consistent with prediction.

As of the experimental studied with comparison to our proposed theoretical model, dual disc electrode system demonstrated a practical generation – collection device based on the application of different mode for each electrode in the system. Generation – collection processes under dual disc electrode for tested redox species, ruthenium hexaammine, ferrocene carboxylate and potassium ferrocyanide, can be accomplished and further used as supporting information for theoretical model for an inlaid coplanar disc-disc electrode. With the efficient theoretical model, generation-collection process under our dual electrode system will be able to estimate diffusion coefficient of analyte for particular electrochemical conditions as well as determine analyte concentration of the system.

References

1. Barnes EO, Lewis GE, Dale SE, Marken F, Compton RG: **Generator-collector double electrode systems: a review**. *Analyst* 2012, **137**(5):1068-1081.
2. Frumkin A, Nekrasov L, Levich B, Ivanov J: **Die anwendung der rotierenden scheibenelektrode mit einem ringe zur untersuchung von zwischenprodukten elektrochemischer reaktionen**. *Journal of Electroanalytical Chemistry (1959)* 1959, **1**(1):84-90.
3. Albery WJ, Brett CMA: **The Wall-Jet Ring-Disc Electrode .1. Theory**. *Journal of Electroanalytical Chemistry* 1983, **148**(2):201-210.
4. Albery WJ, Brett CMA: **The Wall-Jet Ring-Disc Electrode .2. Collection Efficiency, Titration Curves and Anodic-Stripping Voltammetry**. *Journal of Electroanalytical Chemistry* 1983, **148**(2):211-220.
5. Albery WJ, Svanberg LR, Wood P: **The Estimation and Identification of Proteins by Ring-Disc Titration .1. Titration and Identification**. *Journal of Electroanalytical Chemistry* 1984, **162**(1-2):29-43.
6. Albery WJ, Svanberg LR, Wood P: **The Estimation and Identification of Proteins by Ring-Disc Titration .2. Application to Liquid-Chromatography**. *Journal of Electroanalytical Chemistry* 1984, **162**(1-2):45-53.
7. Albery WJ, Haggett BGD, Jones CP, Pritchard MJ, Svanberg LR: **The Packed-Bed Wall-Jet Electrode and the Determination of No3**. *Journal of Electroanalytical Chemistry* 1985, **188**(1-2):257-263.
8. Albery WJ, Bartlett PN, Cass AEG, Craston DH, Haggett BGD: **Electrochemical Sensors - Theory and Experiment**. *Journal of the Chemical Society-Faraday Transactions I* 1986, **82**:1033-1050.
9. Albery WJ, Haggett BGD, Svanberg LR: **The Development of Sensors for Hydroponics**. *Biosensors* 1985, **1**(4):369-397.
10. Liljeroth P, Johans C, Slevin CJ, Quinn BM, Kontturi K: **Disk-generation/ring-collection scanning electrochemical microscopy: Theory and application**. *Analytical Chemistry* 2002, **74**(9):1972-1978.
11. Liljeroth P, Johans C, Slevin CJ, Quinn BM, Kontturi K: **Micro ring-disk electrode probes for scanning electrochemical microscopy**. *Electrochemistry Communications* 2002, **4**(1):67-71.
12. Barnes EO, Lewis GEM, Dale SEC, Marken F, Compton RG: **Generator-collector double electrode systems: A review**. *Analyst* 2012, **137**(5):1068-1081.
13. Svir IB, Oleinick AI, Compton RG: **Dual microband electrodes: current distributions and diffusion layer 'titrations'. Implications for electroanalytical measurements**. *Journal of Electroanalytical Chemistry* 2003, **560**(2):117-126.
14. Rajantie H, Strutwolf J, Williams DE: **Theory and practice of electrochemical titrations with dual microband electrodes**. *Journal of Electroanalytical Chemistry* 2001, **500**(1-2):108-120.
15. Rajantie H, Williams DE: **Potentiometric titrations using dual microband electrodes**. *Analyst* 2001, **126**(11):1882-1887.

16. Rajantie H, Williams DE: **Electrochemical titrations of thiosulfate, sulfite, dichromate and permanganate using dual microband electrodes**. *Analyst* 2001, **126**(1):86-90.
17. Tomcik P, Jursa S, Mesaros S, Bustin D: **Titration of As(III) with electrogenerated iodine in the diffusion layer of an interdigitated microelectrode array**. *Journal of Electroanalytical Chemistry* 1997, **423**(1-2):115-118.
18. Niwa O, Morita M: **Carbon film-based interdigitated ring array electrodes as detectors in radial flow cells**. *Analytical Chemistry* 1996, **68**(2):355-359.
19. Tomcik P, Mesaros S, Bustin D: **Titrations with electrogenerated hypobromite in the diffusion layer of interdigitated microelectrode array**. *Analytica Chimica Acta* 1998, **374**(2-3):283-289.
20. Takahashi M, Morita M, Niwa O, Tabei H: **Highly sensitive detection of catecholamine with interdigitated array microelectrodes in HPLC**. *Sensors and Actuators B: Chemical* 1993, **13**(1–3):336-339.
21. Niwa O, Tabei H, Solomon BP, Xie F, Kissinger PT: **Improved detection limit for catecholamines using liquid chromatography-electrochemistry with a carbon interdigitated array microelectrode**. *Journal of Chromatography B: Biomedical Sciences and Applications* 1995, **670**(1):21-28.
22. Liu ZM, Niwa O, Kurita R, Horiuchi T: **Carbon film-based interdigitated array microelectrode used in capillary electrophoresis with electrochemical detection**. *Analytical Chemistry* 2000, **72**(6):1315-1321.
23. Menshykau D, O'Mahony AM, Javier del Campo F, Munz FX, Compton RG: **Microarrays of Ring-Recessed Disk Electrodes in Transient Generator-Collector Mode: Theory and Experiment**. *Analytical Chemistry* 2009, **81**(22):9372.
24. Kim LTT, Girard A, Griscom L, Razan F, Griveau S, Bedioui F: **Micro-ring disc ultramicroelectrodes array for direct detection of NO-release from S-nitrosoglutathione**. *Electrochemistry Communications* 2011, **13**(7):681-684.
25. Menshykau D, Cortina-Puig M, del Campo FJ, Muñoz FX, Compton RG: **Plane-recessed disk electrodes and their arrays in transient generator–collector mode: The measurement of the rate of the chemical reaction of electrochemically generated species**. *Journal of Electroanalytical Chemistry* 2010, **648**(1):28-35.
26. Anderson LB, Reilley CN: **Thin-layer electrochemistry: use of twin working electrodes for the study of chemical kinetics**. *Journal of Electroanalytical Chemistry (1959)* 1965, **10**(5–6):538-552.
27. Anderson LB, McDuffie B, Reilley CN: **Diagnostic criteria for the study of chemical and physical processes by twin-electrode thin-layer electrochemistry**. *Journal of Electroanalytical Chemistry (1959)* 1966, **12**(5–6):477-494.
28. Konopka SJ, McDuffie B: **Diffusion coefficients of ferri- and ferrocyanide ions in aqueous media, using twin-electrode thin-layer electrochemistry**. *Analytical Chemistry* 1970, **42**(14):1741-1746.

29. Cutress IJ, Wang Y, Limon-Petersen JG, Dale SEC, Rassaei L, Marken F, Compton RG: **Dual-microdisk electrodes in transient generator-collector mode: Experiment and theory**. *Journal of Electroanalytical Chemistry* 2011, **655**(2):147-153.
30. Matysik F-M: **Voltammetric characterization of a dual-disc microelectrode in stationary solution**. *Electrochimica Acta* 1997, **42**(20-22):3113-3116.
31. Harvey SLR, Parker KH, O'Hare D: **Theoretical evaluation of the collection efficiency at ring-disc microelectrodes**. *Journal of Electroanalytical Chemistry* 2007, **610**(2):122-130.
32. Bitziou E, Snowden ME, Joseph MB, Leigh SJ, Covington JA, Macpherson JV, Unwin PR: **Dual electrode micro-channel flow cell for redox titrations: Kinetics and analysis of homogeneous ascorbic acid oxidation**. *Journal of Electroanalytical Chemistry* 2013, **692**:72-79.
33. Rahman ARA, Guiseppi-Elie A: **Design considerations in the development and application of microdisc electrode arrays (MDEAs) for implantable biosensors**. *Biomedical Microdevices* 2009, **11**(3):701-710.
34. Bell CG, Howell PD, Stone HA: **Time-dependent chronoamperometric response of dual inlaid disk electrodes**. *Journal of Electroanalytical Chemistry* 2013, **689**:303-313.
35. Bell CG, Seelanan P, O'Hare D: **Microelectrode generator-collector systems for electrolytic titration: theoretical and practical considerations**. *Analyst* 2017, **142**(21):4048-4057.
36. Bard AJ, Faulkner LR: **Electrochemical Methods: Fundamentals and Applications**, 2nd edn. New York; Chichester Wiley; 2000.

Chapter 6: Summary and Future Work

6. Summary and Future Work

Our work has been focused on development of electrochemical generation-collection sensor for bioanalysis. In terms of bioanalysis application, in terms of biomolecule detection, bioanalytical titration and buffer capacity measurement are preliminary focused in order to perform the direct and/or indirect detection via the fabricated sensors.

Generation-collection mode is applicable and applied to our biomolecule detection such as amino acid and peptide (Chapter 3). Generation-collection sensors of interest are ring-disc and dual disc electrode. Ring-disc electrode offers well characterised generation-collection behavior and it is similar to rotating ring-disc electrode system. However, fabrication of ring-disc sensor is complicated and challenging. This work continues using a novel fabrication technique of PVD employed with inverted hollow cylindrical sputter coater to deposit platinum layer onto the platinum insulated wire (Chapter 2). In comparison with available techniques, this novel method gives an improvement of ring fabrication and electrode distance depends on the insulation thickness. From both SEM and electrochemical characterisations, the metal deposition is uniform and the sensors were electrochemically validated. Simple ring-disc electrode fabrication were accomplished; however, electrode behaviors were not consistent and well performed under the application of generation-collection mode.

Dual disc electrode was simply made by sealing two insulated wire with resin inside a tip. Simple fabrication and easy handling are the major benefits. However, distance between two discs is randomized within the size of micron. Characterisation of ring-disc and dual disc electrodes are satisfied with theory. However, collection efficiency at stationary and flow environment are not well improved.

Ring-disc microelectrode showed a versatile applicability as both standalone device and as part of flow analysis. Promising results for amino acid detection was observed by using Pt/Pt ring-disc (Chapter 3). Sensor fouling is major factor producing more complex behavior of Pt/Pt ring-disc sensor than has been reported for macro electrode under similar system. Less improvement in sensitivity than anticipated from literature results was observed with the generation-collection mode using electrochemical biuret

system for small molecule and peptide detection. In conclusion, our self-fabricated ring-disc electrode can be miniaturised and has the advantage of uniform flux in generation-collection process; nevertheless, sensitivity, repeatability and robustness are in needs for practical use in real sample.

Buffer capacity measurement device was proposed by modification of disc electrode to proton sensitive surface. Disc electrode becomes pH sensor where the ring generate proton and alter the acid-base equilibrium in solution. Electrode surface was modified and deposited with iridium oxide film using anodically electrodeposited iridium oxide film (AEIROF). Our disc pH sensor was calibrated under the standard buffers with pH range from acidic to basic solution (pH 2 to 10), a super Nernstian response up to 70 mV/pH was obtained. Generation-collection detection was performed based on the H^+ generation at generator and passive detection on Iridium oxide pH electrode at the disc (Chapter 4). Under different pH value of buffer solutions, change of local pH can be related to solution buffer strength. The benefits of this device include miniaturization, portability and real time monitoring. Fabricated pH sensors exhibit excellent sensitivity and stability. However, durable proton generator is required as platinum ring electrode is easily damage and not suitable for long term use. It was found that response and behavior on Pt ring was unpleasant after being operated for a long period or with a number of experiments.

The dual disc electrode was extensively studied for generation-collection process. Different modes of active and passive collections were examined (Chapter 5). Three redox couples were selected and studied as a model under generation-collection detection with our fabricated dual sensors. Dual sensors showed a promising behavior among three model species, a ruthenium complex, ferrocene monocarboxylic acid and ferricyanide. The overall results show that generation-collection processes are strongly dependent on the size and distance.

In future work, generation-collection sensors will be developed for robust and use to help in pH monitoring with the real sample such as blood or biological fluid under the novel sensor fabrication and practical method of characterisation. To enhance of sensitivity, small distance between each electrode is preferred.

More work of interest would be applying numerical model that can determine analyte concentration on the collector. This will provide a good noteworthy method for general or specific application. Mathematical and numerical model solutions will be proposed and evaluated to progress the fabricated sensor in order to determine local concentration and change under the environment for titration reactions. Good agreement between theoretical model and experimental result can validate and enhance the generation-collection sensor for various purpose of bioanalytical application and medical use in advance.

- Appendix

a. List of Figures

Figure	Description	Page
1.1	A schematic picture of human blood composition, a common biological sample, adapted from Raven PH et al [4].	11
1.2	Chemical structure of amino acid (left) where R is the substituent group and primary protein structure (right), adapted from [22].	14
1.3	A schematic picture of spectrophotometer for UV detection using diode array detector, adapted from [24].	17
1.4	A schematic picture of mass spectrometric detection, adapted from [39].	17
1.5	A general electrode reaction pathway, adapted from Bard A.J. [41]	19
1.6	Potential waveform and cyclic voltammogram, where E_1 is initial potential, E_2 is final potential and i_p peak current, adapted from Fisher A. C. [42]	25
1.7	Potential waveform and cyclic voltammogram, where E_i is initial potential, E_r is reversible potential, E_p^{red} and E_p^{ox} are the peak potentials of reduction and oxidation reactions, adapted from Fisher A. C. [42]	26
1.8	Potential waveform and current – voltage curve, where E_i is initial potential, E_r is reversible potential and i_d limited current, adapted from Zoski C. G. [45]	30
2.1	Set up of PVD showing pictures from outside (A) and inside (B) of the chamber with schematic diagram of inverted hollow cylindrical sputter coater (C) used for deposition of Pt layer on insulated Pt wire, adapted from Harvey *et al.* 2008 [16].	41
2.2	A schematic picture illustrated the fabrication of Pt/Pt ring – disc sensor.	42
2.3	A schematic picture illustrated the fabrication of C/C ring – disc sensor.	43
2.4	A schematic of the fabrication process for the dual disc sensor.	44
2.5	SEM images of Pt/Pt ring-disc sensor obtained from 50 µm Pt disc with a cross sectional view (A), magnified ring thickness (B) and perpendicular view (C).	47
2.6	Schematic picture and limiting current equations for disc (i_{disc}) and ring (i_{ring}) electrode summarised from [19-20, 22].	48
2.7	i-V curves separately measured on 50 µm Pt disc (red) and Pt ring (blue) using 10 mM $Ru(NH_3)_6Cl_3$ in 1 M KCl from 0.2 to -0.6 V versus Ag/AgCl reference electrode at a scan rate 50 mV/s. Solid lines in blue and red represent ring and disc current, respectively. Inset table shows observed and calculated currents based on theoretical prediction (n=5).	49

Figure	Description	Page
2.8	Cyclic voltammogram from 125 μm Pt electrode in 0.5 M H_2SO_4 at scan rate of 100 mVs^{-1} (versus Ag/AgCl reference electrode), adapted from [23,24].	49
2.9	Cyclic voltammograms of different size of Pt/Pt ring-disc microelectrodes in 0.5 M H_2SO_4 at 100 mVs^{-1} scan rate from 1.2 V to -0.4 V (versus Ag/AgCl reference electrode).	50
2.10	SEM images of C/C ring – disc sensor obtained from 30 μm carbon fibre and ring layer of carbon paint.	53
2.11	**Figure 2.11** i-V curves separately measured from 30 μm C disc (red) and C-paint ring (blue) using 10 mM $Ru(NH_3)_6Cl_3$ in 1 M KCl from 0.2 to -0.6 V versus Ag/AgCl reference electrode at scan rate 50 mV/s. Solid line in blue and red represent ring and disc current, respectively. Inset table shows observed and calculated currents based on theoretical prediction (n=5).	54
2.12	SEM image of dual disc sensor obtained from 75 μm insulated gold wires	55
2.13	SEM image of dual disc sensor obtained from 25 μm insulated platinum wires.	55
2.14	i-V curves separately measured from dual disc sensor where DG1 (red) and DG2 (blue) using 10 mM $Ru(NH_3)_6Cl_3$ in 1 M KCl at 5 mV/s scan rate (quasi-steady). Inset table shows observed and calculated currents based on theoretical prediction (n=6).	56
2.15	**Figure 2.15** i-V curves separately measured from dual disc sensor where DPt1 (red) and DPt2 (blue) using 10 mM $Ru(NH_3)_6Cl_3$ in 1 M KCl under 5 mV/s scan rate. Inset table shows observed and calculated currents based on theoretical prediction (n=6).	57
2.16	Diagram illustrating disc generation – ring collection process using $Ru(NH_3)_6^{2+/3+}$ redox couples.	58
2.17	i-V curves of generation – collection process using 10 mM $Ru(NH_3)_6Cl_3$ in 1 M KCl from Pt/Pt ring – disc sensor. Potential was scanned (A) from 0.2 to -0.6 V at disc (red) under 50 mV/s scan rate where 0.2 V was fixed for ring (blue). In (B), disc and ring potentials were fixed at -0.6 and 0.2 V, respectively (B).	59
2.18	Schematic diagram of flow analysis and the setup using PDMS flow cell probed with three-electrode system; Ag/AgCl reference electrode, stainless steel counter electrode and Pt/Pt ring – disc electrode, connected to a controlled potential source.	60
2.19	Schematic diagram of flow profile in the tube (a) and the effect of impinging flow onto surface which is centred (b) and eccentric to sensor, adapted from [24].	61

Figure	Description	Page
2.20	Effect of flow on generation current (A), collection currents (B) and collection efficiency (C) tested with 10 mM $Ru(NH_3)_6Cl_3$ in 1 M KCl using disc generation–ring collection mode. The potential was set at -0.4 V for disc and 0.2 V for ring electrode. Experiments were obtained from 50 µm Pt/Pt ring – disc sensor.	62
2.21	Comparison between numerical and experimental data of %CE with applied flow rate, measured by 50 µm Pt/Pt ring–disc electrode with 10 mM $Ru(NH_3)_6Cl_3$ in 1 M KCl under disc generation-ring collection mode (n=4). Solid line refers to numerical data [24].	63
2.22	i-V curves of generation–collection process using 10 mM $Ru(NH_3)_6Cl_3$ in 1 M KCl from C/C ring–disc sensor under 50 mV/s scan rate. A), Potential was scanned from 0.2 to -0.6 V at C disc (red) where 0.2 V was fixed for C ring (blue). In B), both disc and ring potentials were fixed at -0.6 and 0.2 V, respectively.	64
2.23	i-V curves of generation–collection process using 10 mM $Ru(NH_3)_6Cl_3$ in 1M KCl from dual gold sensor under 10 mV/s scan rate of both electrodes (A) and collector DG2 alone (B). Potential was scanned from 0.2 to -0.6 V at DG1 (red) where 0.2 V was fixed	66
3.1	A schematic picture of standard amino acid structures, adapted from [14].	73
3.2	A schematic picture of the titration process where target analyte (A) is titrated with the generated titrant (T). The excess amount of T will be collected and turn to initial reactant (R) after titration is completed.	74
3.3	A schematic picture of the titration process on the ring-disc electrode	75
3.4	Reactions of amino acid titration with electrogenerated bromine in acidic and basic condition, adapted from Albery *et al.* [9].	76
3.5	Cyclic voltamograms of 0.5 M KBr in 25 mM borate buffer pH 9.2.	78
3.6	Detection of 1.0 mM methionine in 0.5 M KBr and 25 mM borate buffer; flow rate 1 ml/min. Disc generator-ring collector mode, E_{disc} 0.85 V and E_{ring} 0.50 V.	79
3.7	Amperometric detection of 10 mM $Ru(NH_3)_6Cl_3$ in 1 M KCl with different flow rates (after amino acid titration). The potentials of disc generator mode were set at -0.4 V for disc and 0.1 V for ring electrode versus Ag/AgCl. Experiments were obtained from 50 µm Pt disc/Pt ring sensor.	81
3.8	Successive runs of 100 cycles CV with 0.5 M KBr in 25 mM borate buffer, pH 9.2 using 50 µm Pt/Pt ring-disc sensor. The potential of disc was scanned from 0.5 to 1.0 V and fixed at 0.5 V for ring electrode. Data shown were selected and exported from the first and last cycles, represented the generating current (A) and collecting current (B) with time. CVs of generator and collector were shown (C).	82

Figure	Description	Page
3.9	Schematic picture and reactions of MnO_4^- titration with electrogenerated Fe^{2+} on ring-disc electrode, adapted from [29].	83
3.10	i-V curves of 50 mM $NH_4Fe(SO_4)_2$ in 0.5 M H_2SO_4 obtained from scanning of disc potential from 0.8 to -0.2 V and a fixed ring potential at 0.8 V using 50 mm Pt/Pt ring-disc electrode.	84
3.11	Plots of %CE versus time obtained from 10 µl injections of 10 mM $KMnO_4$ with the system of 50 mM $NH_4Fe(SO_4)_2$ in 0.5 M H_2SO_4 under flow rate 0.5 ml/min (A) and with 1.0 ml/min (B). Disc and ring potentials were fixed at -0.2 V and 0.8 V, respectively. Detection sensor is 50 µm Pt disc/Pt ring electrode.	85
3.12	A schematic picture of Cu(II)-peptide complex, where n is the number of peptide bonds.	86
3.13	A schematic picture illustrating the reaction of G_3-biuret complex, adapted from [36].	89
3.14	Cyclic voltamograms of G_3 – biuret complex with concentration of 2 mM G_3 using 2.5 mm glassy carbon (GC), 2 mm Pt, 30 µm C-fibre and 25 µm Pt microelectrode. Ratio of G_3:Cu^{2+}:tartrate concentration is 1:5:15.	90
3.15	Cyclic voltamograms of G_3 – biuret complex from G_3 concentration of 0, 1, 2, 5 and 10 mM using 2.5 mm glassy carbon (GC), 2 mm Pt, 30 µm C-fibre and 25 µm Pt microelectrode. Selected currents from the forward scans were shown.	91
3.16	Cyclic voltammograms of 0, 1, 2, 5 and 10 mM G_3-biuret complex obtained from 30 µm C-disc (A) and C-ring (B) electrodes. Plots between G_3-biuret complex concentrations and oxidative current, monitored at 0.65 V (C).	93
3.17	i-t curves showing the collection efficiency obtained from disc generator-ring collector mode with biuret solution, 1 mM and 10 mM G_3-biuret complexes. Disc potential was set at 0.65 V, ring potential was fixed at 0.2 V (vs Ag/ÁgCl).	94
4.1	Titration curve of 0.5 M acetic acid (pK_a 4.75) with 0.5 M NaOH.	101
4.2	Plots of buffer capacity, β, versus solution pH of 0.1 and 0.2 M acetic acid (HAC), adapted from [1].	102
4.3	Diagram of relationship between buffer composition of the blood and acid-base homeostasis [1].	104
4.4	A schematic picture of potentiometric system including the ion-selective electrode (red line) [4].	107
4.5	A commercial pH device of Mettler (A) and internal diagram of glass pH electrode (B), adapt from [5].	110
4.6	Pictures of develop product of ISFET (A), bare ISFET chip (B) and a cross-sectional view of ISFET (C).	111

Figure	Description	Page
4.7	CV of 0.5 M sulphuric acid, pre- (blue line) and post-deposition (red line) with iridium oxide film.	114
4.8	Calibration data obtained from pH sensor fabricated on Pt disc by a stepwise increase in pH using the series of Britton-Robinson buffers in the pH range of 2 to10 (A) and calibration plot (B).	116
4.9	A schematic picture representing the iridium oxide/disc and Pt/ring electrode and water oxidation process at the ring.	117
4.10	Schematic of experimental set up (Pt-ring generates H^+, IrO_2/Pt-disc is pH detector).	118
4.11	Graph of potential change at disc pH sensor caused by H^+ generation at the ring. Solution: 10 mM HEPES pH 6.0, current: 10 nA.	119
4.12	Potential change from disc pH sensor while H^+ generation at the ring with different applied currents. Solution: 10 mM HEPES pH 6.0, applied current: 5, 10, 20, 40 and 80 nA.	120
4.13	Potential change at disc pH sensor on the H^+ generation at the ring at different pH. Solution: 10 mM HEPES pH 5.55 to 7.55, applied current: 10 nA.	121
4.14	Plot of initial rate of potential change with applied current for 10 mM HEPES buffers pH 5.55 to 7.55 (pK_a), (n=5).	122
4.15	Change for disc potential with different applied currents for 10 mM HEPES buffers pH 6. Applied currents were stopped after reaching the steady potential.	123
4.16	Change of disc potential with different applied currents for 25 mM HCO_3^- buffer at pH 7.4 (top). A comparison of the transients between pH 7.4 and 7.5 (bottom) at 20 nA.	124
4.17	Plot of initial rate of potential change with applied current for 25 mM HCO_3^- buffers pH 5, 7.4 and 7.5 (n=5).	125
5.1	Schematic diagram of cross-sectional view of RRDE system under the convective flow, where r_1, r_2 and r_3 represent the disc, inner ring and outer ring radii, adapted from [12].	130
5.2	Schematic diagram of cross-sectional view of WJRDE system under the impinging jet flow, where r_1, r_2 and r_3 represent the the disc, inner ring and outer ring radii, adapted from [12].	131
5.3	Schematic diagram of in-channel dual electrode system, adapted from [12].	132
5.4	Schematic picture of IDA electrode system (A) and its operation (B), adapted from [19].	133
5.5	Schematic picture of an inlaid dual disc electrode (A) and cross section of a dual hemisphere system (B), adapted from [12, 30]	134

Figure	Description	Page
5.6	i-V plots for single disc calibration of DG1 and DG2 obtained from theoretical model (⋯) and experiment (−) of 10 mM $Ru(NH_3)_6^{3+}$, 10 mM $Fe(CN)_6^{4-}$ and 1.5 mM Ferrocene. 75 μm dual disc sensor was used, with scan rate 5 mV/s.	136
5.7	i-V plots of DG1 (A) and DG2 (B) obtained from simultaneous (⋯) and separate (-) scan using 10 mM $Ru(NH_3)_6^{3+}$ in 1 M KCl, scan rate 50 mV/s.	137
5.8	Test of generation-collection process by potential scanning of generator DG1 (A) and holding collector potential at DG2 (B) using 10 mM $Ru(NH_3)_6^{3+}$ in 1 M KCl, scan rate 50 mV/s.	137
5.9	Plots of potential (E) versus time (t) observed from the constant potential generation – passive collection mode of 1 mM $Fe(CN)_6^{3-}$ and 10 mM $Fe(CN)_6^{4-}$ in 1M KCl using a 25 μm dual disc sensor.	140
5.10	Plots of potential (E) versus time (t) observed from the constant potential generation – passive collection mode of 10 mM $Fe(CN)_6^{3-}$ and 10 mM $Fe(CN)_6^{4-}$ in 1M KCl using 25 μm dual disc sensor.	142
5.11	i-V curve of 10 mM $Ru(NH_3)_6^{3+}$ in 1M KCl from 75 μm dual disc sensor; one cycle scan (A) and the indicated generator potential at different region (B).	144
5.12	i-t curve obtained from generation-collection process under constant potential mode using 75 μm dual disc sensor with 10 mM $Ru(NH_3)_6^{3+}$ in 1M KCl.	144
5.13	i-V curve of 20 mM $Fe(CN)_6^{4-}$ in 1M KCl from separate scan of 75 μm dual disc sensor under scan rate 5 mVs^{-1}.	145
5.14	i-t curve obtained from generation-collection process under constant potential mode using 75 μm dual disc sensor with 20 mM $Fe(CN)_6^{4-}$ in 1M KCl.	146
5.15	i-V curve of 1.5 mM ferrocene in 1 M KCl obtained from separate scan of 75 μm dual disc sensor under scan rate 5 mVs^{-1}.	147
5.16	i-t curve obtained from generation-collection process under constant potential mode using 75 μm dual disc sensor with 1.5 mM ferrocene in 1 M KCl.	148

b. List of Tables

Table	Description	Page
1.1	The ∇^2 forms for different types of electrode geometry, obtained from Bard A. J. [41]	22
2.1	Capacitance values obtained from 0.5 M H_2SO_4 cyclic voltammograms of disc and ring electrode taken at 0.75 V (see figure 2.9).	51